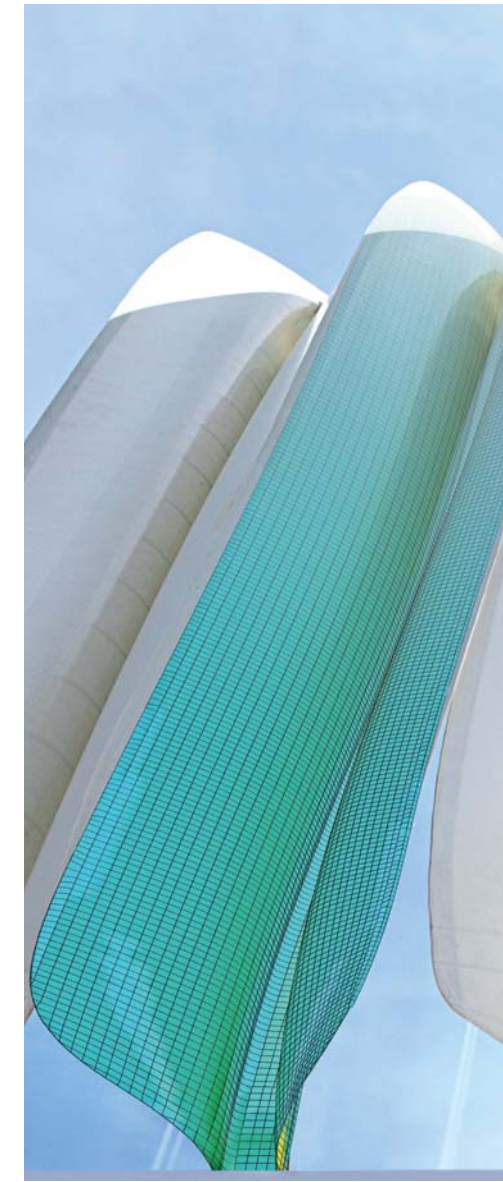




Julian Lienhard
Bending-Active Structures

Form-finding strategies
using elastic deformation in static and kinematic
systems and the structural potentials therein





Forschungsberichte

itke

aus dem Institut für Tragkonstruktionen
und Konstruktives Entwerfen,
Universität Stuttgart

Herausgeber:
Professor Dr.-Ing. Jan Knippers

Bending-Active Structures

Form-finding strategies using elastic deformation
in static and kinetic systems and the structural potentials therein

von der Fakultät Architektur und Stadtplanung der Universität Stuttgart
zur Erlangung der Würde eines Doktor-Ingenieurs
(Dr.-Ing.) genehmigte Abhandlung

Institut für Tragkonstruktionen und Konstruktives Entwerfen:
Forschungsbericht 36

Julian Lienhard:
Bending-Active Structures
Form-finding strategies using elastic deformation in static
and kinetic systems and the structural potentials

Stuttgart, Juli 2014

ISBN 978-3-922302-36-0

D 93

© Institut für Tragkonstruktionen
und Konstruktives Entwerfen
Universität Stuttgart
Keplerstraße 11
D-70174 Stuttgart



Alle Rechte, insbesondere der Übersetzung, bleiben
vorbehalten. Vervielfältigung jeglicher Art, auch auszugs-
weise, ist nicht gestattet.

Vorgelegt von
Julian Lienhard
aus Hamburg

Hauptberichter: Prof. Dr.-Ing. Jan Knippers
Mitberichter: Prof. Achim Menges
Mitberichter: Prof. Dr.-Ing. Kai Uwe Bletzinger

Tag der mündlichen Prüfung 11. April 2014

Institut für Tragkonstruktionen und Konstruktives Entwerfen der
Universität Stuttgart, 2014

Abstract

This thesis aims to provide general insight into form-finding and structural analysis of bending-active structures. The work is based on a case study approach, in which findings from prototypes and commercial building structures become the basis for generalised theoretical investigations. Information is continuously fed back from these case study structures into theoretical research, which creates the basis for overall working methods.

The behaviour of five investigated structures is found to be independent of clearly predictable load bearing categories. Their load bearing mechanisms are largely dependent on the boundless variety of topologies and geometrical expressions that may be generated. The work therefore understands active bending as an approach to generating new structural forms, in which common load bearing behaviour is found due to the structures inherently large elasticity and inner stress state.

Based on engineering and historical background, methodological, mechanical and material fundamentals of active-bending are discussed in Chapter B and C. The case study structures introduced in Chapter D open a wide field of active-bending applications, in lightweight building structures. Whether the conclusions drawn from case studies, are generally viable for bending-active structures is then discussed in the core of the work presented in two chapters on Form-Finding (Chapter E) and Structural Behaviour (Chapter F). The chapter on form-finding introduces the working methods and modelling environments developed for the present work. The chapter on structural behaviour is concerned with the influence of residual bending stress on the stiffness, scaling and stability of bending-active structures.

Based on these findings, generalised design rules for bending-active structures are highlighted in a concluding chapter.

*'Perfection is achieved, not when there is nothing left to add,
but when there is nothing left to remove'* Antoine de Saint-Exupéry

Kurzfassung

Die vorliegende Arbeit beschäftigt sich mit der Formfindung und den mechanischen Eigenschaften biegeaktiver Tragstrukturen. Die aus dieser Arbeit gewonnenen Erkenntnisse dienen einem verallgemeinerten Verständnis der Formgebung und des Tragverhaltens als Entwurfshilfe bei der Entwicklung von biegeaktiven Tragstrukturen.

Biegeaktiv

„Biegeaktive Tragwerke sind gekrümmte Tragwerke, deren Geometrie und Systemsteifigkeit durch elastisches Verformen des Tragelements erzeugt werden. Das Grundprinzip solcher biegeaktiver Tragwerke basiert auf der Formgebung durch Biegung. So entstehen z. B. Gitterschalen, die aus einem ebenen Stabgitter in eine doppelt gekrümmte Schalenform gebogen werden oder Schalenformen, die sich durch gekrümmte, in der Fläche liegende Falten ergeben. Der Vorteil dieses Prinzips liegt in der Möglichkeit, komplexe gekrümmte Formen aus einfachen geradlinigen oder ebenen Bauteilen zu erzeugen. Ausreichend dünne Bauteildicken ermöglichen auch sehr kleine Biegeradien und gleichzeitig lassen sich die eingeprägten Biegespannungen auf einem niedrigen Niveau mit ausreichender Resttragfähigkeit halten. Die notwendige Steifigkeit wird durch das Koppeln mehrerer Biegelemente und deren Biegevorspannung hergestellt.“ (Definition des Autors im Atlas Kunststoffe und Membranen [Knippers et.al. 2010])

Elastische Biegung kann demnach dazu genutzt werden, komplexe räumlich gekrümmte Tragsysteme aus ursprünglich geradlinigen oder ebenen Tragelementen zu erzeugen. Sowohl die Kopplung von Stab- und Flächenelementen als auch die Integration biegeaktiver Tragelemente in Membrankonstruktionen stellen potentielle Anwendungsbereiche der biegeaktiven Tragsysteme dar.

In dem Formgebungsprozess biegeaktiver Tragsysteme bleiben die Verformungen im linear elastischen Bereich. Aus der elastischen Verformung entstehen somit Rückstellkräfte, welche das System unter Vorspannung setzen.

Der Begriff „biegeaktiv“ beschreibt somit die Vorspannung des Tragsystems durch Biegung, welche aktiv im Tragwerk eingebracht wird, um neben der Formgebung idealerweise auch dessen Systemsteifigkeit zu erhöhen.

Aufbau der Arbeit

Nach einer allgemeinen Einleitung der begrifflichen und relevanten mechanischen sowie werkstofftechnischen Grundlagen werden historische und aktuelle gebaute Beispiele biegeaktiver Tragstrukturen vorgestellt.

In der vorliegenden Dissertation werden die besonderen Eigenschaften dieser Tragwerke anhand von fünf Fallbeispielen erforscht. Daraus abgeleitete Erkenntnisse werden anhand von Abstraktionsmodellen auf ihre Allgemeingültigkeit überprüft. Diese fünf Fallbeispiele sind unter Anleitung und Mitwirken des Autors im Zeitraum der Dissertation entstanden. Die Arbeiten werden in dem zentralen Kapitel D zunächst allgemein vorgestellt, um dann in den folgenden Analysen der Formfindungsansätze und mechanischen Eigenschaften immer wieder Bezug auf detaillierte Eigenschaften dieser gebauten Strukturen zu nehmen.

Das Kapitel E beschäftigt sich mit physikalischen und numerischen Formfindungsansätzen für biegeaktive Tragsysteme, sowie mit Hybriden im Zusammenwirken mit mechanisch vorgespannten Membranflächen. Neben Modellbau und analytischen Ansätzen werden insbesondere die eigens programmierten Algorithmen für die inkrementell iterative Simulation großer elastischer Verformungen mit Hilfe der Finiten Elemente Methode vorgestellt.

Das zentrale Thema der Dissertation beschäftigt sich mit dem Einfluss eingeprägter Biegespannungen auf das Tragverhalten biegeaktiver Tragkonstruktionen. Im Kapitel F werden dafür zwei Themenfelder behandelt. In einer ersten Betrachtung wird der Einfluss eingeprägter Biegespannungen auf Steifigkeit und Stabilität des Tragwerks analysiert. In einem zweiten Abschnitt wird die Skalierbarkeit biegeaktiver Tragstrukturen überprüft. In beiden Betrachtungen werden zunächst Vergleichsstudien an abstrakten Grundformen durchgeführt, um dann mit den kom-

plexen Systemen aus den Fallbeispielen zu zeigen, inwieweit die Erkenntnisse verallgemeinert werden können.

Die verallgemeinerten Erkenntnisse aus den Kapiteln E und F werden am Ende der Arbeit durch eine Zusammenfassung der Ergebnisse und einen Ausblick nochmals verdeutlicht.

Erkenntnisse

In der Arbeit mit biegeaktiven Tragstrukturen zeigt sich, dass der Formgebungsansatz durch elastische Biegung die Entwicklung hocheffizienter Tragsysteme ermöglicht, welche - frei von traditionellen typologischen Ansätzen der Tragwerkslehre - allein aus dem Kurzschließen von Rückstellkräften entstehen.

Trotz großer typologische Unterschiede in den betrachteten Tragstrukturen lässt sich ein gemeinsames Tragverhalten feststellen. Dieses leitet sich aus der den biegeaktiven Tragwerken inhärent hohen Flexibilität ab, welche insbesondere in Bezug auf die Stabilität zu dem meist maßgebenden Versagensfall des Durchschlagens führt. Eine wichtige Erkenntnis der Arbeit bezieht sich demnach auf die Möglichkeit, Systemsteifigkeit durch geschicktes Einstellen der Eigenspannungszustände zu erhöhen.

Preface

This thesis was developed between 2007 and 2013 where I was engaged in research and teaching at the Institute of Building Structures and Structural Design University of Stuttgart.

To my supervisor Prof. Dr.-Ing. Jan Knippers I would like to express my gratefulness for providing a unique working environment where motivation and inspiration are nourished by trust and freedom. His expertise and open guidance have been of substantial importance for the development of this dissertation.

The thesis committee also included Prof. Dr.-Ing. Kai-Uwe Bletzinger and Professor Achim Menges, whom I thank for their helpful suggestions and valuable advice in the wider subject matter. Prof. Bletzinger provided his profound knowledge in understanding structural mechanisms and thereby developing an extensive understanding for the complex load bearing behaviour of bending active structures. Prof. Menges's methodological approach to computational design in Architecture became an integral part of the case study projects carried out in collaboration with the Institute for Computational Design.

I thank Prof. Dr. Thomas Speck with Dr. Simon Poppinga from PBG Freiburg and Dr. Markus Millwich with Lena Müller from ITV Denkendorf for the great collaboration and essential exchange in our research project on 'Flexible surface structures on the basis of biomimetic principles'.

I would like to acknowledge Prof. Dr.- Ing. Manfred Bischoff for his relevant contributions in interpreting stiffness in actively bent systems.

I want to extend genuine gratitude to Prof. Dr.-Ing. Christoph Gengnagel for our great collaboration in the IASS working group on active-bending, the work on the Review of bending-active structures and the many intense and inspiring discussions.

To my colleagues at the Institute of Building Structures and Structural Design, I owe the recognition for providing a pleasant and fun working environment, with special thanks to Petra Heim for the organisational support. At the Institute I shared an influ-

ential collaboration in the work on Flectofin® and the research pavilion 2010 with my colleague Simon Schleicher. Our fruitful exchange and teamwork were inspiring and led to very valuable results.

Much appreciation to the Diploma students David Sommer, Antonis Galanis and Kay Unterer for their insightful contributions coming out of their research. To David Sommer I owe the recognition for the first correction of the final draft. I also thank Daiana Mesoras and Elena Vlasceanu for the precise graphics and model building. Special thanks to Caleigh Freeze for her text and graphical work.

I am grateful to Prof. Sean Ahlquist for our excellent collaboration during the M1 project and countless insightful and influential discussions on textile hybrids.

Genuine gratitude to Falko Dieringer and Benedikt Philip from TU München for sharing their knowledge and interest in our intense working sessions on understanding load bearing mechanisms in bending-active structures.

Special thanks to Dr. Alexander Michalski helping me keep my thoughts straight in the crucial moments of finding an outline for my work as well as drawing clear conclusions!

I would like to express my deepest gratitude to my mother and father who have supported me in every step I have ever taken.

My deepest gratitude goes to my beloved wife Marie, for her love and support during this and our journey. Beyond her patience, moral and family support during this seemingly endless endeavour, our fruitful intellectual exchange brought this work the aesthetics an engineer may only find with the help of an artist. Last but not least she contributed to this thesis with English corrections and hands on help in the realisation of the case studies. And finally I am addressing my brilliant sons Fynn and Léo; always interested and enthusiastically involved in the building site experiences during the realisation of the case study projects!

Stuttgart, June 2014, Julian Lienhard

A Marie, ma femme

Contents

(main headings only)

A	Introduction	2
B	Fundamentals	8
B1	Bending-active Structures and the Framework of Structural Systems	8
B2	Basics of Mechanical Behaviour	15
B3	Precedence of Elastic Materials for Bending-active Structures	33
C	Active Bending in Building Structures	45
C1	Material-driven Form	46
C2	Categorisation	49
C3	Review of Active Bending in Building Structures	52
D	Introduction of Case Studies	66
D1	Temporary Static Structure: ICD/ITKE Research Pavilion 2010	66
D2	Permanent Textile Hybrid Structure: Umbrella for Marrakech	72
D3	Temporary Textile Hybrid Structure: M1	78
D4	Permanent Adaptive Structure: Softhouse	84
D5	Elastic Kinetic Research Demonstrator: Flectofin®	90
D6	Reflection on the Role of FEM in the Design Processes	98
D7	Reflection on Structural Typologies Presented by the Case Study Structures	101
E	Form-finding and Simulation	104
E1	Variables of the Form-Finding Process	104
E2	Form Development	106
E3	Analytical Approximation	113
E4	Computational Form-finding	118
E5	Validation of FE Simulation	130
F	Structural Behaviour of Bending-active Structures	140
F1	Stiffness and Stability	141
F2	Scaling and Stability	166
G	Conclusions and Future Trends	182
Appendix		189
Bibliography		198

Nomenclature

Geometric

b	width of a cross section [mm]
h	height of a cross section [mm]
L	span [mm]
l	length of a deformed element [mm]
f	rise of an arc / sag of a cable [mm]
r	radius [mm]

Mechanic

dl	dead load [N/mm ³]
E	modulus of Elasticity [N/mm ²]
I _y	moment of Inertia [mm ⁴]
N	axial force [N]
q _w	wind load [kN/m ²] (perpendicular to element)
q _z	line load [N/mm]
U _{x,y,z}	deflection in global direction [mm]
U _{zz}	deflection in local direction [mm]
W _y	section modulus [mm ³]
K	Stiffness matrix
M	Mass matrix
F	Force [kN]
P	Pre-tension [kN] / Pre-stress [kN/m]
ρ	density [N/mm ³]
σ _M	bending stress [N/mm]
λ	Eigenvalue [-]
ω	Frequency [1/s]

Numeric

n	factor (integer) [-]
λ	load factor [-]
s	scale factor [-]

Abbreviations

GFRP:	Glass Fibre-Reinforced Polymer
FRP:	Fibre Reinforced Polymer
NFRP:	Natural Fibre Reinforced Polymer
FEM:	Finite Element Modelling
FEA:	Finite Element Analysis
Geo. nonl.:	geometric nonlinear
Ref. geo.:	reference geometry

A Introduction

A Introduction

The research on bending-active structures focuses on imposed force and form interaction. In this inseparable relationship, the disciplines of architecture and structural engineering are equally addressed. Starting with form-finding as a common denominator, it focuses on engineering in terms of the theoretical description of structural behaviour and addresses architecture through the formulation of design rules for applications.

The focus lies on the structural advantages that may be generated by active elastic bending; based on the form-finding and design strategies that are necessary to develop such structures. The approach therein is based on a practical understanding of the task. In order to generate a comprehensive understanding of these potentials, the research is based on findings from five case study projects. The prerequisites for such an approach are existing basic research. Each aspect of the work is therefore introduced with a review of existing work, creating the scientific framework this research is based upon.

Motivation

Various empiric construction methods known from vernacular architecture make use of the available building materials elastic behaviour. However, only few such examples are to be found in 20th century architecture. Here elastic deformation is mainly utilised as an economic construction method; for double curved shell structures which are mostly form-found based on hanging models or simplified analytical approaches. Recent developments in simulation techniques now render it possible to form-find and analyse structures, that derive their complex curved geometry solely from erection processes in which they are elastically deformed. This has formed the basis for various explorations that include new types of surface- and gridshells and membranes with elastically bent battens as well as various types of adaptive and elastic kinetic structures. Even though these examples may differ in their construction type, they all share the approach of creating curved geometries based on straight or planar building elements by means of elastic bending. On a structural level, they are curved structures influenced by residual stresses in their

load bearing behaviour and structural capacities. The common motivation for employing active bending lies in the simplicity of producing curved elements. In the past, the lack of alternative manufacturing techniques for curved building components or entire structures, made active bending a widely spread and recognised building technique. Today, economic reasons such as advantages in transportation and the assembling process, as well as the performance and adaptability of structures, support the use of active bending. The advantages of bending-active structures lie however, not only in the possibility of generating complex curved geometries for static structures, but also in the shape adaptation possibilities, and furthermore, in kinetics, which are entirely based on reversible elastic deformation.

Providing enough elasticity for the erection or shape adaptation can contradict the stability and load bearing capacity of the structure. In this dissertation, focus will be placed on studying the structural performance of bending-active structures in order to generate form-finding and design strategies, that help develop sufficient load bearing capacity and stability. In order to develop a comprehensive understanding of the potentials therein, the research is based on feedback from real size prototypes that show various types of static and kinetic systems.

Structural Aspects

It is found that the behaviour of the investigated bending-active structures do not fall into clearly predictable categories, their load bearing is largely dependent on the variety of topologies and geometrical expressions that may be generated. Similarly to membrane structures, the geometry must be form-found, in this case simulating the elastic bending deformation. In contrast to membrane structures, however, the form-finding result does not automatically define a structurally optimised geometry. This dissertation aims to provide key information on the structural behaviour of various types of bending-active structures. The discussion on structural behaviour focuses on aspects of stiffness and scaling in connection with stability that are linked to the residual stress, low material stiffness and slenderness of the profiles used.

The influence and active use of geometric nonlinearities, such as stress stiffening effects on the performance of large bending-active structures, are specifically investigated. The effects investigated are particularly important for elastic kinetics, i.e. compliant mechanisms. The study of various types of bending-active structures, which include surface- and gridshells and membranes with elastically bent battens, may therefore lead to a more fundamental understanding of the structural behaviour that is found in the more complex behaviour of adaptive and elastic kinetic structures exposed to external loads.

Similarity of static and kinetic systems

Static as well as adaptive and kinetic bending-active structures are discussed in this dissertation. This seemingly wide field of study shares a distinct common ground when considering aspects of form-finding and structural behaviour. Form-finding in this case refers to the numerical simulation of the deformed state. Apparent differences in these systems are found in the design process, detailing and materialisation. It may be concluded that, providing the right material properties and a reversible erection process, bending-active structures can become adaptive and even kinetic without a change of topology or degree of static determinacy. This leads to the hypothesis that bending-active structures and elastic kinetics are comparable on a structural level. The study of bending-active structures may therefore become a vehicle for development of large scale elastic kinetic systems.

Exclusions

Next to single element bending-active systems, there is always the option of increasing stiffness by combining several individual actively bent elements into a combined section. A stacking of elements, much like curved glue lam timber beams, allows control of any kind of predefined shape and leads to known predictable load bearing mechanisms. This case is not analysed in this work since focus is set on defining the practical boundaries of structures composed of individual bending-active elements, whose form and load bearing behaviour is largely influenced by its form defining inner stress state.

An important assumption underlying this research lies in the constant mechanical properties of material assigned to the struc-

tural analysis. Long term behaviour resulting from creep, relaxation and fatigue had to be excluded from the investigation on structural behaviour in order to enable a larger scan of basic structural characteristics.

Objective

It is not possible to approach bending-active structures with a single or a general theoretical concept. Here, the study of successful structures will identify the performative regions in the given discontinuous design space. Based on such findings, the scattered knowledge and experiences in the work with bending-active structures aim to be set into relation and thereby broaden the design space. Following the central argument that elastic deformation can actively be used to permanently or temporarily shape curvature in load bearing elements, the dissertation will be built up in three main parts.

A-C. These general chapters set the framework and historical background. In chapter D, five case study projects which the author was involved in during this research are introduced in several investigations on form-finding and structural behaviour.

E. Because the geometry of bending-active structures has to be determined by means of experimental or computational form-finding, in this chapter various form-finding and design strategies that were developed and used in this research are introduced and discussed.

F. The structural behaviour of various types of bending-active structures are analysed, based on the experience gained through the case studies as well as further abstracted analysis models that allow more generalised conclusions.

Selected findings out of this dissertation have been pre-published in accordance with §2.4 of the University Stuttgart Dissertation regulations. These papers are listed in the bibliography with indications in the corresponding text passages.



B Fundamentals

B1	Bending-active Structures and the Framework of Structural Systems	8
B 1.1	Structural Action	9
B 1.2	Elastic Kinetics and Compliant Mechanisms	15
B2	Basics of Mechanical Behaviour	15
B 2.1	Nonlinearity	15
B 2.2	Pre-stress	21
B 2.3	Eigenvalues	24
B 2.4	Theory of Bending	26
B3	Precedence of Elastic Materials for Bending-active Structures	33
B 3.1	Material Overview	33
B 3.2	Design Codes and Guidelines for FRP	36

B Fundamentals

The chapter on fundamentals introduces the conceptual, structural and mechanical background this thesis is based upon. The sections on mechanical behaviour and material properties are especially limited to a review of aspects that will be of importance for this thesis.

B1 Bending-active Structures and the Framework of Structural Systems

The categorisation of basic structural systems has played an important part in developing analytical calculation techniques that help analyse structures on the basis of abstract static systems. What was a great achievement at the time meant that the logic of structural typologies was largely influenced by the restricted capacities of analytical calculation methods. In today's engineering praxis, analytical calculation methods are still an important basis for initial approximations and simplified check calculations of complex computational analysis models. However, there is no longer a need to design a structure to suit exclusively analytical calculation methods. The advances in computational mechanics, leading to a general availability of Spatial-Framework and Finite Element Modelling (FEM) programs, offers new degrees of complexity and efficiency in the design of structures. Knippers (2013) links the fact, that such potentials have not yet been fully explored in building construction, with typology based model thinking:

"Engineers are trained in 'model thinking', in knowing all these typologies and then choosing and applying the most appropriate one for a given design task...The introduction of computational design offers the potential to break through these barriers of model thinking (thinking in discrete typologies) in structural engineering."

[Knippers 2013: 77]

The prospect of using FEM software environment to break free from traded expressions of structure is starting to unfold in what Bollinger et. al (2010) refer to as nonlinear structures:

KNIPPERS, J. (2013): *From Model Thinking to Process Design*.

BOLLINGER, K., GROHMANN, M. and TESSMANN, O. (2010) *Structured Becoming: Evolutionary Processes in Design Engineering*.

ENGEL, H. (1999) *Tragsysteme – Structure Systems*.

"The finite element method (FEM) allows the examination of structures beneath the scale of parts that dissolves traditional structural engineering typological building blocks. Structural behaviour relies more on a network of interconnected elements than on simple structural typologies. (...) Analysis data is fed back into the generative model and serves as a design driver rather than the basis for mere post-rationalisation"
[Bollinger et. al 2010: 21]

This potential also brings new questions to the role of structural engineers and their working methods: if everything is possible, what are the criterion for developing a functional and efficient structural system? Current trends of including physical behaviour in computational parametric design tools are starting to develop new methodologies that may also contribute to the unveiling of new potentials in structural design. The capacity and accuracy of analysing physical behaviour with Finite Element Modelling reaches much further than typical physics-based modelling environments. However, it is in parts still too elaborate and still not interactive enough to be included easily in a design process. How can physical-based computational modelling and Finite Element Modelling be combined in a design methodology without the limitations of one hindering the other?

Bending-active structures do not present an answer to these far-reaching questions, but may contribute to the current discourse in their particular approach to developing various types of structural systems based on the physical behaviour of elastic bending. They may not be circumscribed with the abstract and restrictive concept of typology, as formal and topological diversity is the essence of these structures. Additionally, due to a system inherent residual stress state and elasticity, their load bearing behaviour is characterised by nonlinearities which can both be stabilising, as well as destabilising, for the structure. This supports the understanding that bending-activation, as an approach, cannot be circumscribed by a single type of structural system.

B 1.1 Structural Action

Among the many different methods of categorising structures, the one by Heino Engel sticks out [Engel 1999]. Engel defines abstract 'families' of structural action, each of which is subdivided

into 'types', and finally 'structure singles'. Connecting bending-active structures to this logic is not so much intended to make them fit into a frame work, but seeks above all to show how they may evolve into many different types by placing them on the first and most abstract level of Engels definition in the context of structural action.

Structural action describes the process of receiving, transferring and transmitting a load. In the load transfer of bending-active structures, the residual bending stresses play an important role, which makes them unique from the other families of structural action described by Engel.

Figure B.1 shows different types of load bearing structures categorised according to structural action. In contrast to Engels further differentiation into 'types' and 'singles', it is chosen to show the various shapes and abstract topological arrangements of the structural elements for each type of structural action. This is an attempt at a relatively open typological interpretation of structures showing the broad potential application of bending-active structures. A previous version of this graph was published by the author in Knippers et al (2011: 135) in which the following definitions are based upon.

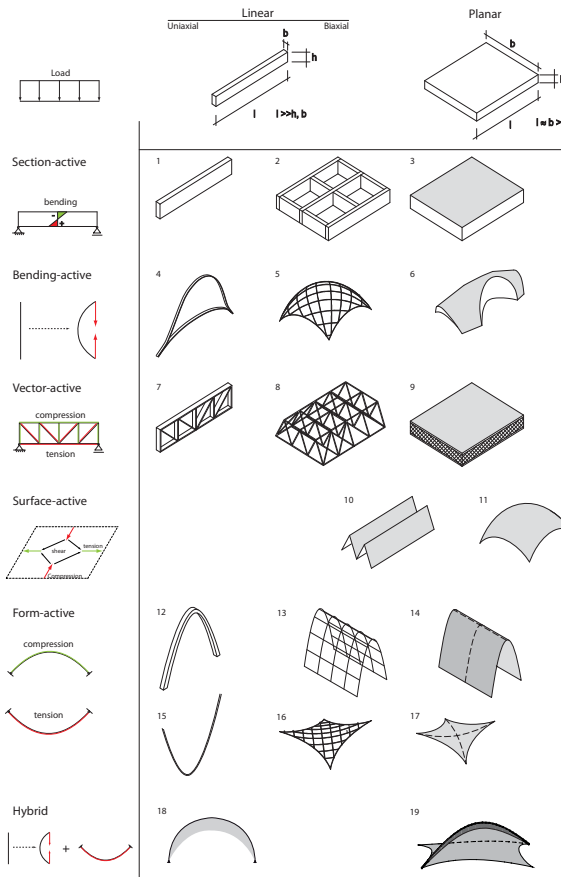
Section-active structures

Load-bearing structures that carry external loads primarily by way of bending moments are referred to as section-active. This is due to the definition of the bending moment as an internal effect imposed on a section through the structural member.

Typical section-active structures include: beams, frames, grillage and plates.

Vector-active structures

Connecting straight trusses to form a triangulated framework with hinged joints produces a stable structural system in which every component is loaded in either tension or compression. Such systems are referred to as vector-active, where the forces carried by the straight members are following the force vectors exclusively in the form of normal (axial) forces.



Typical vector-active structures include: plane and curved trusses and spatial frameworks.

Surface-active structures

Plate and shell structures that carry external loads via a combination of surface tension, compression, and shear stresses without significant bending components are referred to as surface-active structures. Aligning the surface along the flow of forces makes it possible to activate pure membrane stress states.

Fig B.1 Different types of load bearing structures categorised according to structural action. Based on Knippers et al (2011: 135)

Typical surface-active structures include: shells, plates carrying in-plane loads and folded plates.

Form-active structures

The characteristic feature of form-active structures is that they carry external loads by pure tension (cables, membranes) or pure compression (arches) without shear forces or bending moments. In order to achieve this, it is necessary to match the geometry of the load bearing structure to the flow of forces. With varying external loads such as wind or snow, the geometry must be able to change and deform as well.

Typical form-active structures include: cable structures, membrane structures as well as catenary arches and shells.

Height-active structures

Engel's definition of a structural type that is characterised by rigid elements in predominantly vertical extension is height-active. As they transfer forces from section-, vector-, surface- and form-active structures, they are not classified as an indigenous working mechanism and therefore not listed in Figure B.1.

Typical height-active structures include: towers and high-rise buildings.

Bending-active

The term "bending-active" is introduced by the author to describe curved beam and surface structures that base their geometry on the elastic deformation of initially straight or planar elements [Knippers et al 2011: 134]. Active bending in this context is understood to be a form defining strategy based on systemized elastic deformation, i.e. bending. In general, bending-active structures are understood to be an approach rather than a distinct structural type. The path of forces, as a yardstick for the efficiency of a structure, cannot be generalised in terms of an all inherent mechanism for bending-active structures. Their common denominator is therefore not a circumscribed load bearing behaviour or geometrical definition, but a formation process during which they are elastically bent.

As the load bearing includes a combination of bending and nor-

mal forces, bending-active structures can be understood as a sub-category of section-active structures. The capacity of bending-active structures to develop real arch or shell properties in their final deformed state makes their load bearing behaviour similar to that of form- and surface-active structures. A key feature of bending-active structures is their potential for structural integration and heterogeneity, leaving the limits of strictly categorised building structures by accumulating different load bearing strategies in hybrid systems. This leads to the following definition of bending-active structures:

Bending-active structures are structural systems that include curved beam or shell elements which base their geometry on the elastic deformation from an initially straight or planar configuration.

The pre-stressing of bending-active structures is generated through large nodal displacements in statically indeterminate structures. As a result, individual building elements are largely deformed and therefore exposed to a constant bending stress, i.e. pre-stress. The element stiffness is chosen so that the induced bending stress never reaches the elastic limit of the used materials. Therefore, a linear material law (Hooke's Law) is always used for the subsequent investigations. As a consequence to the large deformations of bending-active structures, the calculations generally must be performed geometrically non-linear.

Bending-active in structural terms: constrained statically indeterminate structures with residual bending stress.

The main motivation for active-bending lies in the simplicity of producing complexly curved elements, leading to the overall understanding.

Bending-active structures are understood to be an approach rather than a distinct structural type!

Hybrid structures

The principal mechanisms of load transfer introduced above in praxis often appear in combined form, acting simultaneously in a structural system and even within one structural element. The intentional combination of load transfer mechanisms is referred

to as a hybrid structure. In general, hybrid structure systems result from the linkage of two parental systems of dissimilar internal load transmission into a coupled system. If the parental systems are equipotent in terms of their structural capacity, their coupling to a hybrid system may be in favour of the two when reciprocal stress compensation and/or additional rigidity through opposite system deflection are actively enabled.

Typical hybrid structures involve:

- Superposition and/ or coupling of section- and form-active structures.
- Superposition of vector- and surface-active structures

Textile Hybrid

The interdependence of form and force of mechanically pre-stressed textile membranes and bending-active fibre-reinforced polymers is suggested by the author to be classified as a *Textile Hybrid*. The flexibility and lightness inherent to bending-active structures integrates well with the pre-stressed membrane structures that are themselves flexible and adjust to applied loads. Their particular reciprocal dependency of mechanical properties, pre-stress and form makes them a particularly interesting field of application for bending-active structures which will be included in some of the studies of the following chapters.

Functionally, the integration of elastic beams within a pre-stressed membrane surface offers the possibility of short-cutting tension forces and creating free corner points. The system is stabilised solely by the elastic beams which, in turn, are restrained by the membrane surface. Since buckling of the beam is prevented, slender profiles may be used. The combination of pre-stressed membranes with elastically deformed beams furthermore offers advantages in the homogeneous utilisation of the beam's cross-section. Without the pre-stressing of the membrane, the elastic beam will take on a parabolic shape where the end segments are straightened out and the apex is bent into a tighter radius of curvature. Set into an interactive equilibrium with the pre-stressed membrane, there can be substantially less variation in curvature of the elastic beam.

B 1.2 Elastic Kinetics and Compliant Mechanisms

The study of forces on a stationary rigid body is generally circumscribed by the field of *statics*. *Dynamics* describes the forces on a rigid body in motion, whereas *Kinematics* is the consideration of motion without its causes and *Kinetics* is the study of motion including mass and the forces. If a system undergoes elastic deformation as a cause of its motion, it cannot be described by kinematics only because motion and deformation are interdependent with the mechanical properties of the system and the forces causing the motion. It is therefore suggested that a system which transfers input force or displacement to another point through elastic body deformation falls under the category of *Kinetics*, or more precisely: *Elastic Kinetics*. In mechanical engineering, such systems are called *compliant mechanisms*;

'A compliant mechanism also transfers or transforms motion, force, or energy. Unlike rigid-link mechanisms, however, compliant mechanisms gain at least some of their mobility from the deflection of flexible members rather than from moveable joints only.' [Howell 2001]

In contrast to kinematical rigid-link mechanisms and similar to bending-active structures, compliant mechanisms are always statically indeterminate (Figure B.2 and B.3). In conclusion, we may consider that elastic kinetics and compliant mechanisms are bending-active structures that allow reversible erection.

Kinematics:
- statically determinate
- rigid-link mechanism

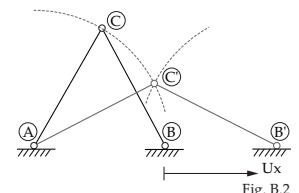


Fig. B.2

Elastic Kinetics:
- statically indeterminate
- compliant mechanism

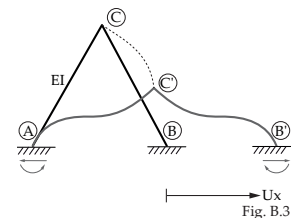


Fig. B.3

B2 Basics of Mechanical Behaviour

Without any claim of giving a complete summary of structural mechanics, this chapter describes some basics of mechanical behaviour which is referred to in the core of this work.

B 2.1 Nonlinearity

A system of equations is considered nonlinear when system equations cannot be written as a linear combination of system variables. Applied to the equations of static equilibrium this implies: if the external forces of a linear system are multiplied by

Fig B.2 Deformation of a kinematical rigid-link mechanism.

Fig B.3 Deformation of a compliant mechanism.

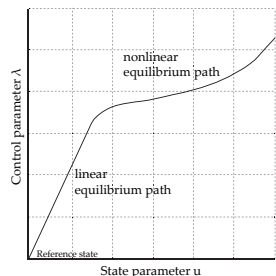


Fig. B.4

a factor n , the displacements and internal stresses also change with the factor n . Systems that behave differently are classified as *nonlinear*. In the analysis of structural systems, several aspects of nonlinearity can be differentiated:

- Nonlinear material behaviour: plastic deformation (not considered in bending-active structures).
- Nonlinear boundary conditions: change of supporting condition under deformation (may be considered in bending-active structures, where large deflections lead to additional supporting points and contact between initially separate elements).
- Geometric nonlinearity: nonlinear relationship of external forces and deflection (must be considered in all bending-active structures).

Equilibrium Path

The equilibrium path is a graphical representation of structural behaviour in the form of a response diagram, most commonly plotting the equilibrium relation of external load and internal reaction forces or deflections in a continuous curve, i.e. path. Load deflection response diagrams represent a key to the analysis of nonlinear structural behaviour. The degree of nonlinearity of a load deflection curve directly expresses the nonlinearity of structural behaviour. So-called critical points mark the magnitude of a load where the structure loses stability, i.e. equilibrium becomes indifferent or unstable in which the structure deflects without external work.

- *Limit points* mark the beginning of a secondary equilibrium path, characterised by a horizontal tangent: snap-through buckling.
- *Bifurcation points* mark a point at which multiple equilibrium paths cross: bifurcation buckling.

A general load deflection diagram is given in Figure B.4 with the load factor λ on the vertical axis and deflection U on the horizontal axis. This type of diagram will be used extensively in the analysis of structural behaviour of bending-active structures in section F.

Fig B.4 General load deflection diagram

In elastic kinetics we are actively tracking every stable point of the equilibrium paths and thereby describe the geometrical variability of the system.

Aspects of nonlinear Finite Element Analysis

In static linear Finite Element Analysis (FEA), the basic formulation of equilibrium is given by the linear equation (1_B) with the force vector F , the quadratic stiffness Matrix K and the unknown displacement vector u . Linearity of the system is given if the equation of equilibrium can be formulated on the undeformed structure and a multiplication of the force Vector F with the factor n leads to multiplication of the resultant displacement vector u with the same factor n , given in equation (2_B). In this case, the stiffness matrix K is constant. For a nonlinear system behaviour, equilibrium is only fulfilled in the deformed configuration where the stiffness matrix is no longer constant and updated based on the actual deflections: $K(u)$ (3_B). Here, an n times larger force vector leads to an m times larger deflection, with n unlike and disproportionate to m (4_B). This phenomenon is generally referred to as geometric nonlinearity.

Linear:

$$\underline{\underline{K}} \cdot \underline{\underline{u}} = \underline{\underline{F}}$$

$$\underline{F} \cdot n = \underline{\underline{K}} \cdot \underline{\underline{u}} \cdot n$$

Nonlinear:

$$\underline{\underline{K}}(\underline{\underline{u}}) \cdot \underline{\underline{u}} = \underline{\underline{F}}$$

$$\underline{F} \cdot n = \underline{\underline{K}}(\underline{\underline{u}}) \cdot \underline{\underline{u}} \cdot m$$

with $n \neq m$

Geometric nonlinearity

In contrast to geometric linear theory, geometric nonlinear theory considers the static equilibrium on the deformed system. Through this consideration, the resulting reaction forces are composed from a linear proportion and a deformation-dependent non-linear proportion. This consideration of the equilibrium on the deformed system leads to a change of the element stiffness matrix. The imposed stresses which are existent in the deformed state of the structure lead to the formulation of geometric stiffness, also known as initial stress-stiffness. Even though the term ‘initial stress’ describes this phenomenon better than the term

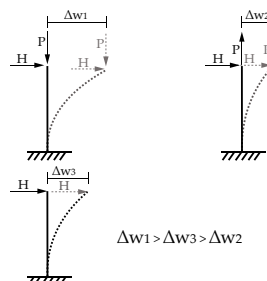


Fig. B.5

'geometric', the latter will be used here because it corresponds to the direct translation of the German terminology.

Geometric stiffness

Geometric stiffness is dependent on the initial load and geometry of a structure. It is largely influenced by normal forces within a structure. In general, a tensile normal force causes an increase of stiffness in a building structure. A compressive normal force causes a decrease in stiffness. This effect is well illustrated by a mast with clamped support (Figure B.5). Here, it becomes clear that the fixed end moment and system deformation is dependent on the direction of the point load P . If P is a compression force to the beam, the horizontal deformation caused by H increases. P therefore has an increasing eccentricity to the support and hence, adds to the fixing moment. P acting in the opposite direction (i.e. in tension) would straighten the mast and thereby reduce the fixing moment. This is, academically, often just an example to describe what is known as the P-Delta effect, which is only considered in second order theory and nonlinear analysis. More generally, the P-Delta effect is described as a bending moment that occurs from eccentricities which appear in the equilibrium conditions of nonlinear analysis and typically is the dominating effect of second order theory.

In geometric nonlinear analysis, the stiffness matrix is general referred to as *tangent stiffness* matrix K_t , which can be split into the elastic stiffness matrix K_e , the initial displacement stiffness matrix K_u and the geometric stiffness matrix K_g , which is computed based on the stress state of the previous equilibrium iteration.

$$(K_e + K_u + K_g) \cdot u = F \quad (5_B)$$

The development of the three stiffness components for the snap-through buckling problem of a three hinged triangular frame is given in Figure B.6. With the individual and combined development against the different deformation states of snap-through buckling it becomes visible how the elastic stiffness remains constant, the initial displacement stiffness is directly related to the deformation of the system and the geometric system to the normal force with a noticeably destabilising effect from compression. After snap-through the truss is in tension, leading to a

Fig B.5 P-delta effect of mast with clamped support.

Fig B.6 Development of the three stiffness components for the snap-through buckling problem of a three hinged triangular frame. Based on Bischoff (2011).

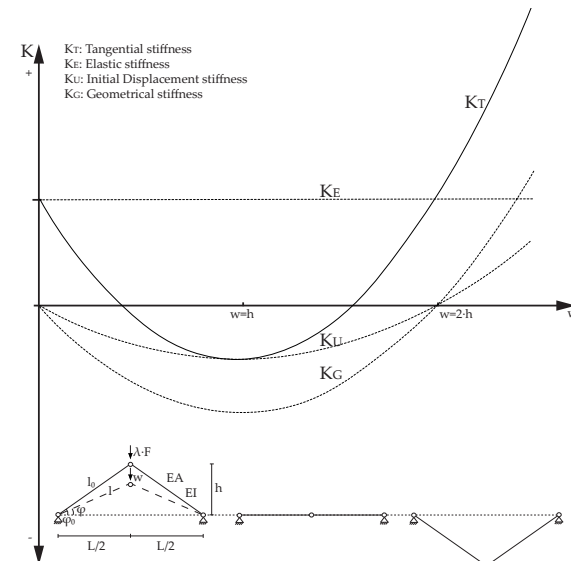


Fig. B.6

regain in geometric stiffness. This analysis is based on Bischoff (2012).

Formulations for geometric stiffness matrices of truss and beam elements usually factor out a quotient that includes normal force divided by element length. A typical formulation for the geometric stiffness matrix of a truss element is given in (6_B) [Werkle 2008: 483]. Similarly, the geometric stiffness matrix of a beam element with consideration of the P-Delta effect and cubic consideration of displacement is given in (8_B) [Przemieniecki 1968]. The general problem in modelling beam elements lies in considering large and independent rotations; therefore numerous formulations of stiffness matrices exist with varying degrees of freedom at the nodes and increasing complexity in the consideration of nonlinear phenomena. The formulation in (8_B) represents a simple second order theory beam, where interpretation of the variables included is still easily possible. Other very recent formulations consider higher degrees of freedom. For example, the TL Plane Beam in (9_B) (Appendix A) uses total Lagrangian (TL) kinematics to derive the equations for a two node Timoshenko beam ele-

ment. Interestingly, this approach factors out not only normal force N , but also shear force V in the formulation of geometric stiffness matrix [NFEM: 10-21]. For simplified second order plate and shell elements, the geometric stiffness matrix can be split into the components of membrane-stress as given in (10_B) (Appendix B). Similar to the truss and beam elements, the membrane stress is factored out of the matrix [Werkele 2008: 504]. More complex plate and shell elements will not allow the splitting of membrane and bending forces leading to numerous complex formulations for various specific fields of application.

It can be generalised that in nonlinear analysis, the geometric element stiffness, and hence, in composition the entire structure, is influenced by the strains and stresses within the structural elements. As an example we can analyse a simple truss element with tension pre-stress P_x from (6_B). When setting $EA=0$ and multiplying the geometric stiffness matrix with the displacement vector we can derive (7_B). Here it becomes apparent that the pre-stress terms only appear in combination with the perpendicular v direction and not with the longitudinal direction u . The normal force P_x adds stiffness in the v direction because it is pulling the system straight, an effect also known as stress-stiffening effect.

$$\left(\frac{EA}{l} \cdot \begin{bmatrix} 1 & 0 & -1 & 0 \\ 0 & 0 & 0 & 0 \\ -1 & 0 & 1 & 0 \\ 0 & 0 & 0 & 0 \end{bmatrix} + \frac{P_x}{l} \cdot \begin{bmatrix} 0 & 0 & 0 & 0 \\ 0 & 1 & 0 & -1 \\ 0 & 0 & 0 & 0 \\ 0 & -1 & 0 & 1 \end{bmatrix} \right) \cdot \begin{bmatrix} u_1 \\ v_1 \\ u_2 \\ v_2 \end{bmatrix} = \begin{bmatrix} F_{x1} \\ F_{y1} \\ F_{x2} \\ F_{y2} \end{bmatrix} \quad (6_B)$$

$$\begin{bmatrix} 0 \\ \frac{P_x \cdot v_1 - P_x \cdot v_2}{l} \\ 0 \\ -\frac{P_x \cdot v_1 + P_x \cdot v_2}{l} \end{bmatrix} = \begin{bmatrix} 0 \\ F_{y1} \\ 0 \\ F_{y2} \end{bmatrix} \quad \text{for } EA = 0 \quad (7_B)$$

$$K_G = \frac{P_x}{l} \cdot \begin{bmatrix} 0 & & & \\ 0 & \frac{6}{5} & & \\ 0 & \frac{1}{10}l & \frac{2}{15}l^2 & \\ 0 & 0 & 0 & 0 \\ 0 & -\frac{6}{5} & -\frac{1}{10}l & 0 & \frac{6}{5} \\ 0 & \frac{1}{10}l & -\frac{1}{30}l^2 & 0 & -\frac{1}{10}l & \frac{2}{15}l^2 \end{bmatrix} \quad (8_B)$$

Stress stiffening

Stress- or more precisely tension-stiffening is referred to as the stiffening effect of tension normal forces or stresses on the geometric stiffness matrix (see above). Others refer to this effect as geometric stiffening, incremental stiffening, initial stress stiffening, or differential stiffening. The inclusion of such effects in structural analysis is only provided in fully nonlinear analysis and is still subject of today's research, e.g. in the formulation of nonlinear beam elements. Commercial Finite Element Modelling software such as Ansys® or the here-used Sofistik® offer the full consideration of stress stiffening in nonlinear analysis of truss, beam and shell elements. As this stiffening effect is only visible for systems with low elastic stiffness, it is usually only considered for slender structures with small bending stiffness compared to axial stiffness, such as cables, thin beams, and shells. The geometric nonlinearities that are inherent to bending-active structures may lead to stress stiffening effects that work in favour of the structural performance. This influence on the system stiffness will be of importance in the analysis of structural behaviour in section F and is further explained by its relation to Eigenfrequencies in B2.3.

B 2.2 Pre-stress

Pre-stressing or pre-tensioning is used in various scenarios to increase the stiffness of a structure based on the above introduced geometric nonlinear consideration of stress stiffening. Pre-stress generally introduces internal stresses into structural elements to counteract the stresses that will result from external loads. Since these forces are introduced prior to external and dead loads, we refer to them as "pre"-stress or -tension. Generally, pre-stressing of a structure may only increase its stiffness but not its load bearing capacity. As shown above, pre-stress with positive algebraic sign (tension) appears as an increasing factor to the geometric stiffness matrix and thereby increases element stiffness (compare (6_B)). For lightweight structures in particular, this potential for increasing stiffness in an entire structural system is often the key to their feasibility. This may have led the engineer Jörg Schlaich to his understanding of pre-stressing being "one of the most ingenious and effective tricks a structural engineer may use" [Brinkmann and Blum 1990: 91].

For linear elements such as cables, we generally use the term *pre-tension*, whereas planar elements, such as slabs and membranes, are referred to as being *pre-stressed*. The most common uses of pre-stressing in building structures are found in the following table:

Construction type	Cause	Effect
Trussed beam	External cable pre-tension	Counteracting dead load deformation
Pre-stressed concrete slab	Internal pre-stressing	Pre-compression of concrete.
	tendons	Counteracting dead load deformation
Tempered safety glass	Thermal or chemical pre-stress	Crumbles into small granular chunks when broken. Surface flaws are pressed closed by the residual compression forces leading to increased strength.
Pre-tensioned cable net	Tensioning cables against external supports	Increase in geometrical stiffness
Pre-stressed membrane	Mechanical: Tensioning against stiff or cable edges Pneumatic: Tension due to differential air pressure	Increase in geometrical stiffness. Avoiding compression-stress in „tension only“ materials

Tab. B.7

Within these examples three main effects can be observed:

- Amplifying beneficial material behaviour.
Concrete: pre-tensioned tendons - constant compression stress
Membrane: pre-stress of membrane - constant tension stress
- Counteracting external loads: Pre-stress induced deformation works in opposite direction of dead load or governing load case deformation.
- Increase in geometrical stiffness of flexible structures.

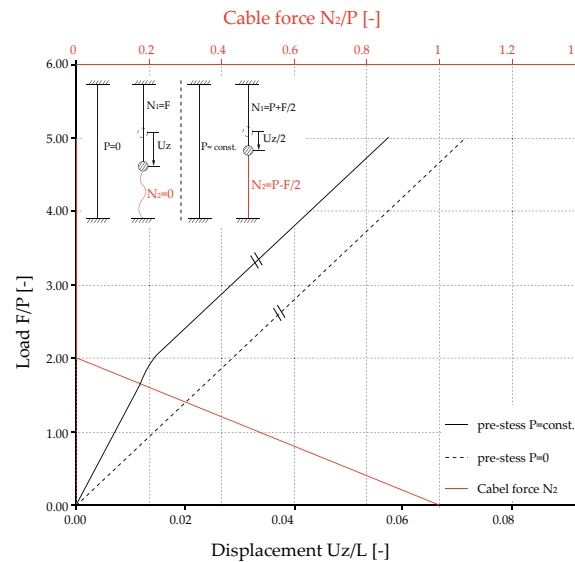


Fig. B.8

Cable pre-tension

A classic example for understanding the effects of a pre-tensioned cable is given by Schlaich in Brinkmann and Blum (1990: 91). (see Figure B.8). This example of a vertically tensioned cable shows the effect of a pre-tensioned cable bearing compression forces. Interestingly, the achieved increase in stiffness is stored in the system even after the compression force has exceeded the pre-tension of the cable. This effect can be seen in Figure B.8 where the load deflection diagram of a cable is compared including pre-tension and without pre-tension; both are loaded with a normal point load in the middle of the cable. The two curves become parallel when the cable tension on the unloaded side is zero, indicated by the red line of the lower cable force N_2 . The higher stiffness of the pre-tensioned cable even after $N_2=0$ is due to its initially shorter length. Schlaich notes that a pre-tensioned cable “does not forget its history”.

Membrane pre-stress

A shell element can include pre-stress in two perpendicular directions. This so-called *biaxial* pre-stress state can be of same magnitude.

tude in the two directions, i.e. *isotropic* or of different magnitude, i.e. *orthotropic*. The effect of membrane pre-stress is similar to that of a cable and therefore sometimes discretised by a cable mesh (force density method). In Finite Element Analysis, pre-stressing effects are considered by nonlinear shell elements with the possibility of assigning special membrane properties such as the loss of stiffness under compression.

Structurally, one distinguishes between *mechanical* pre-stress induced by displacement loads and *pneumatic* pre-stress induced by pressure difference.

Residual stress

Residual stresses are generally referred to as stresses that are induced before external loading which remain in the structure after their original cause is removed. As such, they include pre-stress but also permanent stress states from elastic bending, heat gradients, etc.

Nominally identical structures may differ in structural behaviour due to residual stress states. Residual stress may have an influence on the following characteristics of a structure:

- Statics: Stiffness, Stability
- Dynamics: Eigenfrequencies

B 2.3 Eigenvalues

Mathematically, an Eigenvalue is characterised by equation (11_B), in which A is a quadratic matrix, λ the Eigenvalue and x the Eigenvector. For small matrices the eigenvalues are found by solving singular equation (12_B), with the unit matrix E . [Werle 2008: 14]

$$\underline{\underline{A}}\underline{x} = \lambda \underline{x} \quad (11_B)$$

$$\det(\underline{\underline{A}} - \lambda \underline{\underline{E}}) = 0 \quad (12_B)$$

Apparently for larger matrices the determination of Eigenvalues becomes more complicated, thus special iterative algorithms are used.

In structural dynamics the analysis of Eigenvalues is used to determine the *Natural frequencies* of a given system, also referred to as *Eigenfrequencies*. The linearised Eigenproblem is given in (13_B), in which K is the stiffness and M the mass matrix. The square root of the Eigenvalue λ defines the frequency of vibration ω . The *Eigenvectors* x of the linearised eigenproblem describe the resultant shapes of the vibration modes: the *mode shapes* [Humar 1990: 422].

$$\underline{\underline{K}} \cdot \underline{x} = \lambda \cdot \underline{\underline{M}} \cdot \underline{x} \quad \text{with } \lambda = \omega^2 \quad (13_B)$$

Dynamic Eigenvalues are also linked to the stability of structures; Rayleigh (1877) found a relation between the axial load and natural frequency of a column. This effect is related to geometric stiffness and it was found that the first eigenfrequency of a column under compression becomes zero when instability is reached, known as the Euler critical buckling load. Stability problems in nonlinear structural analysis is therefore characterised by equation (14_B).

$$(\underline{\underline{K}_e} + \lambda \cdot \underline{\underline{K}_g}) \cdot \underline{u} = 0 \quad (14_B)$$

Stiffness and Eigenfrequency

Equation (13_B) suggests that both stiffness and mass have an influence on the Eigenfrequency of a system. For a given system with constant mass one can therefore describe a reciprocal dependency between pre-stress (stiffness) and Eigenfrequency, as well as span (mass and stiffness) and Eigenfrequency. This phenomenon is well explained by the example of a guitar string. Tensioning of the string leads to a higher Eigenfrequency which corresponds to a higher note. Likewise, shortening the span of the string by pressing a chord will increase the Eigenfrequency and thereby the note (Figure B.9). In Figure B.10 the eigenfrequency of the first, fifth and tenth Eigenmode are plotted for various degrees of pre-tension in a cable with 3 m span. Figure B.11 correspondingly shows the change in Eigenfrequency between the first ten Eigenmodes for four levels of cable pre-tension, highlighting the vertical oscillations. This analysis shows a nonlinear relation between pre-tension and Eigenfrequency, yet clearly indicates the increase in Eigenfrequency with increasing pre-tension.



Fig. B.9

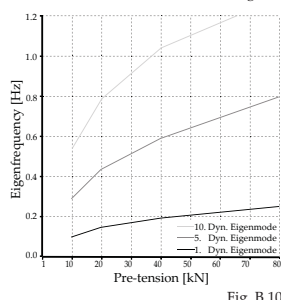


Fig. B.10

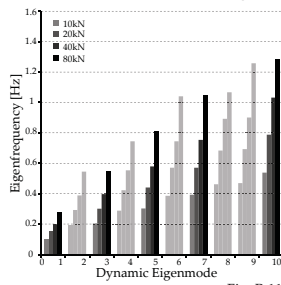


Fig. B.11

Fig B.9 Eigenfrequency, span and pre-tension relation shown on the example of a guitar.

Fig B.10 Eigenfrequency of the first, fifth and tenth Eigenmode plotted for various degrees of pre-tension in a cable.

Fig B.11 change in Eigenfrequency between the first ten Eigenmodes for various degrees of cable pre-tension. Highlighting the vertical oscillations.

In return, the study of Eigenfrequency of a system, will give an indication of its stiffness. This offers a unique tool to globally measure the change in system stiffness of two nominally identical structures with differing inner stress states. This approach has, for example, been used to measure the change in stiffness of annealed steel plates [Lieven and Greening 2001]. The relation of Eigenfrequency and geometric stiffness will be of importance in the analysis of structural behaviour in section F.

B 2.4 Theory of Bending

The basics of bending are introduced in reference to the analysis of beams; the basic relations also apply to the bending of plates and shells.

B 2.4.1 Nonlinear beam theory

The most common mathematical models for beams in structural mechanics are the *Bernoulli-Euler* (BE) model and the *Timoshenko* model.

The Bernoulli-Euler (BE) Model, also known as the *classical beam theory* or *engineering beam theory*, covers elementary mechanics. The model assumes that plane sections remain plane and normal to the axis of the beam. Based on these assumptions the simplified differential equation of bending is formulated:

$$w''(x) = \frac{M(x)}{EI} \quad (15_B)$$

For linear cases integration of (15_B) leads to the formulation of curvature $\varphi(x)$ and deflection $w(x)$. In Figure B.12 the well known solution for the differential equation is given and illustrated for a single span beam with line load $q(x)$.

Timoshenko assumes that cross sections remain plane and rotate about the same neutral axis. In contrast to Bernoulli-Euler theory, the cross sections do not remain normal to the deformed longitudinal axis. The model thereby considers first-order shear deformations based on the deviation from normality. This assumption is especially more precise than the Bernoulli-Euler beam when analysing non-slender beams. For beams and plates in bending-

LIEVEN, N. AJ. and GREENING, P. (2001) *Effect of experimental pre-stress and residual stress on modal behaviour*.

FERTIS, D. G. (2006) *Nonlinear Structural Engineering. With Unique Theories and Methods to Solve Effectively Complex Nonlinear Problems*.

active structures, the height is kept significantly smaller than the length; therefore, both beam models may be valid for the form-finding and analysis of bending-active structures. Additionally, in context with FEM the Timoshenko Model may exhibit shear locking phenomena for large deformations of very thin sections if the modelling approach is not chosen correctly (see Chapter E4.2).

The Bernoulli-Euler law also formulates a second order nonlinear differential equation for larger nonlinear deformations. This becomes far more complex and does not offer simple solutions as illustrated above. The equation, given in (16_B), also states that bending moment is always proportional to the change in curvature produced by the action of the load [Fertis 2006: 9]:

$$\frac{1}{r(x)} = \frac{w''(x)}{[1+(w'(x))^2]^{2/3}} = -\frac{M(x)}{EI} \quad (16_B)$$

Solutions of (16_B) involve elliptic integrals and lead to the theory of *elastica curves* introduced below.

B 2.4.2 Elastica

The geometry of curves described by a beam's elastic deformation in its post buckled shape has fascinated scientist for centuries. First attempts at finding a closed solution are traced back to James Bernoulli in 1691, who publishes a first solution in 1694. In 1742 this work is picked up again by Daniel Bernoulli in a letter to Euler. In 1744 Euler publishes the first completely characterised family of Elastica curves based on variational techniques (see Figure B.13) [Euler 1744]. The problem of the Elastica has been approached from many different angles, including mechanical equilibrium, the calculus of variations and elliptical integrals. It has been a driving force in the general development of these mathematical models and is an important field of development of mathematical splines still today. This brief historical summary is based on the very elaborate research by Levien (2009: 67ff).

Based on the understanding of structural mechanics, the Elastica may be described as:

- Post-buckling curve (Figure B15. - B19 are valid equilibrium

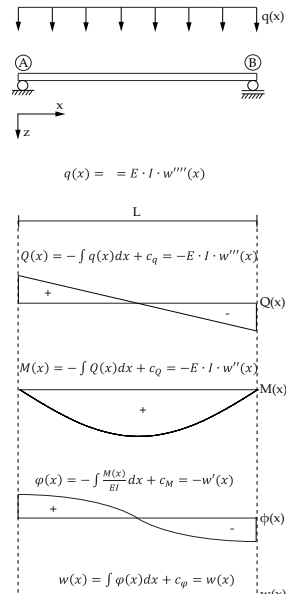


Fig. B.12

EULER, L. (1744) *Methodus Inveniendi Lineas Curvas.*

FERTIS, D. G. (2006) *Nonlinear Structural Engineering. With Unique Theories and Methods to Solve Effectively Complex Nonlinear Problems*.

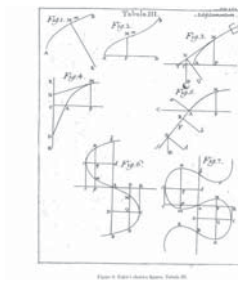


Fig. B.13

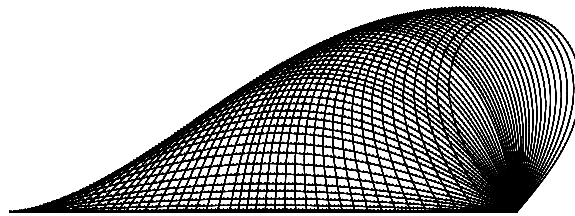


Fig. B.14

states after passing a critical point on the load deflection curve)

- Moment progression in a static system (16_B) curve that generates a minimum of potential bending energy in the overall system
- Equilibrium of forces in a static system.
(Finite Element Approach)

The two first approaches involve complex mathematical methods to develop closed form solutions. The understanding that the Elastica is a curve that generates a minimum of potential bending energy in a constrained system describes best the inseparable interdependency of mechanical behaviour and form present in all bending-active structures. Here, the Elastica is characterized by the local curvature along its arch length. The curvature is described by the local derivative of the tangent angle Θ . Elastic bending of the beam produces potential energy in the system which, according to the elasticity theory, behaves proportionately to the square of the local curvature $\kappa(x_0)$. The total amount of the potential bending energy of a beam is therefore described by (17_B):

Fig B.13 completely characterised family of Elastica curves by Euler (1744).

Fig B.14 Evolution of the elastica curve simulated for a single span beam from straight to maximum deformed configuration.

LEVIEN, R. L. (2009) *From spiral to spline*.

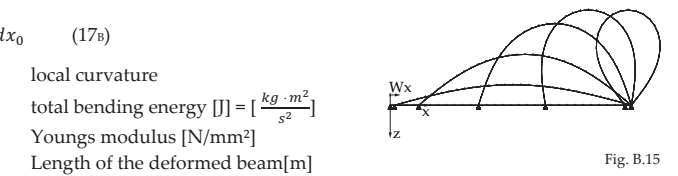
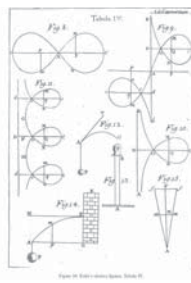


Fig. B.15

Fig. B.16

$$\tilde{E}[\kappa(x_0)] = \frac{1}{2} \int_0^l EI \cdot \kappa(x_0)^2 dx_0 \quad (17_B)$$

$\kappa(x_0)$

local curvature

\tilde{E}

total bending energy [J] = [$\frac{kg \cdot m^2}{s^2}$]

E

Youngs modulus [N/mm²]

l

Length of the deformed beam[m]

When completely unconstrained, the Elastica will assume the shape of a straight line, in which the curvature everywhere is zero, and thus, the total bending energy is also zero. When constrained, the bending energy will tend to be the minimum possible under the constraints [Levién 2009: 17]. The solution to this mathematical problem involves calculus of variations which is not followed up here, since the limited and purely geometric description of the Elastica is not practical for the design of bending-active structures. Here, the Finite Element Approach based on the equilibrium of forces will be used by applying nonlinear Finite Element Analysis to the problem of form-finding “minimum potential energy constraint bending curves”.

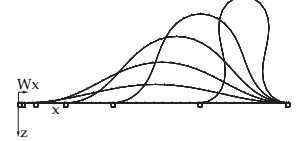


Fig. B.17

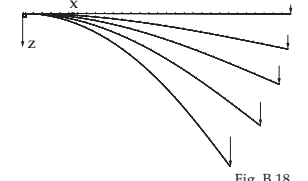


Fig. B.18

B 2.4.3 Deriving the moment curvature relation

Independent of beam theory, a relationship between local bending curvature and bending moment can be formulated at a differential segment. Figure B.20 shows the geometrical relations in a largely deflected beam. Looking at the differential segment we can derive the following relation using the interception theorem:

$$\frac{r(x_0)}{dx} = \frac{t}{\Delta dx} \quad (18_B)$$

by putting t in a relation to r and introducing Hook's Law we can derive:

$$\frac{t}{r(x_0)} = \frac{\Delta dx}{dx} = \varepsilon = \frac{\sigma}{E} = \frac{M(x_0) \cdot t}{E \cdot I} \quad (19_B)$$

This leads to the following bending stress – curvature relation at the differential segment.

$$\frac{1}{r(x_0)} = - \frac{M(x_0)}{E \cdot I} \quad (16_B)$$

$$\sigma(x_0) = \frac{E \cdot t}{2 \cdot r(x_0)} \quad (20_B)$$

And finally, to the formulation of the minimal bending radius for a given permissible stress σ_{RD} :

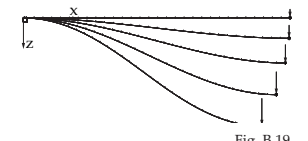


Fig. B.19

Fig B.15 -19 various basic elastica curves based on the Euler cases of buckling.

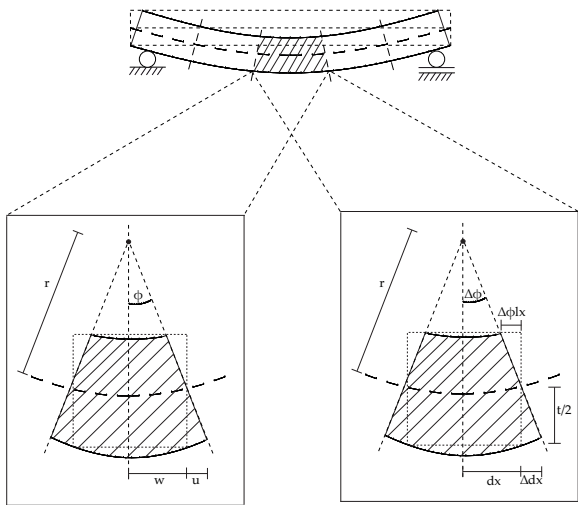


Fig. B.20

$$r_{min}(x_0) = \frac{E \cdot t}{2 \cdot \sigma_{Rd}} \quad (21_B)$$

The same relationship can be derived from the strain of the outer fibre in a curved segment with ideally planar sections: The arc length is proportional to the radius.

$$L = \frac{\alpha \cdot \pi \cdot r}{180} \quad (22_B)$$

Therefore the strain can be described by (compare figure B.21):

$$\epsilon = \frac{\Delta L}{L} = \frac{\frac{t}{2}}{r} = \frac{t}{2 \cdot r} \quad (23_B)$$

Again, introducing Hook law leads us back to equation (20_B). Equation (20_B) was compared to the result of a Finite Element simulation for the system shown in Figure B.22 which is deformed by a moment force introduced at either end of the beam. Measuring the minimal radius in the deformed configuration, the bending stresses calculated with formula (20_B) match those given by the nonlinear Finite Element simulation.

B 2.4.4 Torsion of Beams

Torsion in a beam results from a torsional moment acting around the central axis of the beam, or a load whose resultant does not pass through the shear centre axis. If a beam is subjected to tor-

sion, the assumption of planar cross sections is only correct for solid circular sections and hollow circular sections with a constant thickness. Other sections will warp when exposed to torsion. In those cases, the effect of torsional loading can be further split into a part causing twisting and a secondary part causing warping. If a beam is supported by being fixed around its central axis (fork support) and the cross-section can warp freely, torque is only resisted by torsional shear stresses, referred to as St. Venant's torsional shear stress. If the entire cross-section of the beam is fully fixed, it cannot warp freely and the applied torque is additionally resisted by warping torsion, referred to as non-uniform torsion [Francke and Friemann 2005]. Hence, two types of torsion are differentiated:

- pure Saint-Venant torsion (uniform)
- Saint-Venant plus warping torsion (non-uniform)

Non-uniform torsion

If warping deformation is constrained, a beam undergoes non-uniform torsion, which causes normal stress in the cross-section, next to secondary shear stresses. Additionally, elongation occurs when axial displacements are prevented in a torquing beam with a non-warping free cross-section. Warping is commonly considered for I-beams, whereas flat sections exposed to modest degrees of torsion may be considered as warping free [Francke and Friemann 2005: 179]. In connection with the investigations of bending-active structures where deformations are large and tensile normal stresses are advantageous (compare geometric stiffness above), warping of a flat section should also be considered. Secondary shear stresses are still generally negligibly small and will not be discussed in further detail. The following example of a flat section exposed to large degrees of torsion illustrates the effects of nonuniform torsion.

Torsion beam

In some investigated examples in chapter F, bending of flat sectioned beams and shell elements will be overlaid with torsion; therefore, a simple single span beam exposed to large degrees of torsion is introduced here. For the single span beam in Figure B.23, a constant torsional moment is imposed and the resulting forces and shear stresses are analysed. The beam is firmly

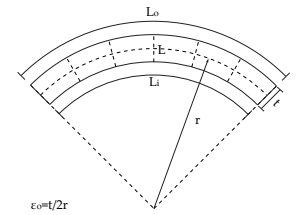


Fig. B.21

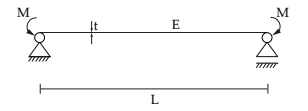


Fig. B.22

Fig B.20 Geometric relations in a largely deflected beam.

Fig B.21 Strain relations in a largely deflected beam segment.

Fig B.22 Analytical and Finite Element simulation results for a largely deflected beam.

clamped to both supports. A rotation of $\varphi_x = \pi/2$ is induced on both ends, leading to a constant torsional moment M_T shown in Figure B.23 a. The primary shear stresses are distributed constant over the length of the component (Figure B.24 b. and c.). The shown membrane forces in Figure B.24 d. are due to elongation of the outer fibres and are considerably larger than those resulting from warping stress. The effect of tensile stress throughout the section due to twisting can additionally be seen in Figure B.25 where the plane principal stresses I are plotted in the middle of the cross-section. The influence of this tensile stress on stiffness will be discussed in detail in chapter F 1.3.4.

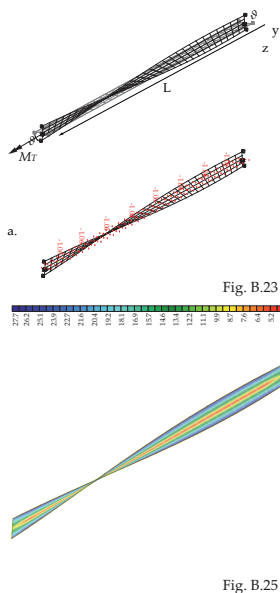


Fig. B.23
 Fig. B.23a. Twisting moment kNm/m
 Fig. B.24b. and c. Principal shear stress at the top and bottom [N/mm]
 Fig. B.24d Principal membrane forces [kN/m]
 Fig. B.25 Plane Principal stress I in the middle of the element [N/mm²]

B3 Precedence of Elastic Materials for Bending-active Structures

The existence of materials of high breaking strain is a precondition for the work with bending-active structures whose form and performance is entirely based on material behaviour. The work in this dissertation draws on existing knowledge in terms of short and long term material behaviour; actual material research is not part of the investigations.

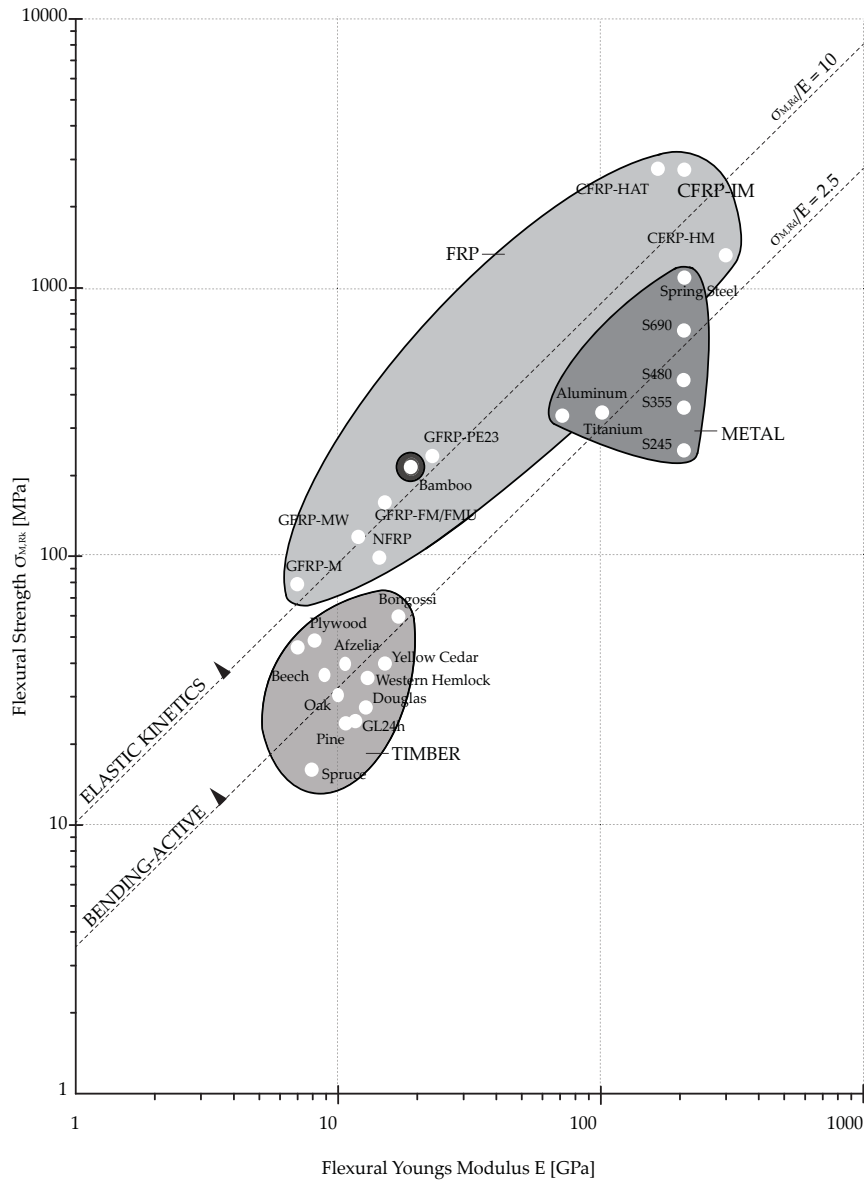
Some traditional building materials such as timber already offer a suitable elastic range. Owing to their low density and high strength combined with low bending stiffness, Fibre Reinforced Polymers (FRP) embody the potential for exploring further lightweight bending-active structures. Continuous developments in the field of FRPs suggest that there will be even more adequate materials to choose from and design with in the future.

B 3.1 Material Overview

From the materials we can consider working with in building and construction, there is a wide range of strength stiffness and densities available. Steel is stiff; rubber is compliant; still, steel may be more adequate for bending active structures since it also offers high strength. Consequentially, the combinations of properties are more important than a singular aspect of mechanical behaviour for finding appropriate materials. From equation (20B) we know that the minimal bending radius is proportional to the ratio of stiffness divided by strength. For bending-active structures, the most important variables to set into relation are Young's Modulus E and permissible bending stress $\sigma_{M,Rd}$.

An effective way of depicting adequate materials for a certain design task was developed by Ashby. In his diagrams he maps out fields in the property-spaces by material classes, and sub-fields by individual materials. He introduces design guidelines in his diagrams to define 'search regions' which identify the design spaces for certain applications [Ashby 2005].

In Figure B.26 a choice of common building materials is listed and plotted on a graph with the ratio of flexural strength against

Fig. B.26 Common building materials with ratio of strength $\sigma_{M,RI}$ [MPa] to stiffness E [GPa]

Metals:			
Type	Flexural Strength [MPa]	Flexural Youngs Modulus [GPa]	Ratio
S245	245	210	1.17
S355	355	210	1.69
S450	450	210	2.14
S690	690	210	3.29
Spring Steel	1100	210	5.24
Titanium	340	102	3.33
Aluminum	330	70	4.71
Timber:			
Type	Flexural Strength [MPa]	Flexural Youngs Modulus [GPa]	Ratio
Spruce	16	8	2
Pine	24	11	2.18
Douglas	30	12	2.5
Western Hemlock	35	13	2.69
Yellow Cedar	40	15	2.67
Oak	30	10	3
Beech	35	10	3.5
Afzelia	40	11	3.64
Bongossi	60	17	3.53
GL24h	24	11.6	2.07
GL28h	28	12.6	2.22
GL32h	32	13.7	2.34
GL36h	36	14.7	2.45
Birch Plywood (6.4 mm)	50.9	12.737	4
Brich Plywood (18 mm)	40.2	10.048	4
Combi-Plywood (6.4 mm)	50.8	12.69	4
Combi-Plywood (18 mm)	35.8	8.95	4
Softwood Plywood (6.4 mm)	29.1	9.462	3.08
Softwood Plywood (18 mm)	23	7.464	3.08
Bamboo	213	19.129	11.13
FRP:			
Type	Flexural Strength [MPa]	Flexural Youngs Modulus [GPa]	Ratio
CRFP-HAT	2800	165	16.97
CRFP-IM	2800	210	13.33
CRFP-HM	1350	300	4.5
P E 23	300	23	13.04
GRFP-M	80	7	11.43
GRFP-MW	120	12	10
GRFP-FM/FMU	160	15	10.67
NRFP	101	14.38	7.02

stiffness on a logarithmic scale, based on the 'Ashby diagrams'. The range of the axis is chosen to include the material classes investigated. Staying in context with building structures, the values are taken from the Eurocodes DIN EN 1993-1995 and 1999, DIN 1052:2004-08, and DIN 17221, as well as from Knippers et al (2011: 77) and Gas et al. (1985).

Based on the experience of the case study structures introduced in this dissertation, adequate materials for bending-active structures offer a ratio of $\sigma_{M,Rk}/E > 2.5$ (with $\sigma_{M,Rk}$ [MPa] and E [GPa]). For elastic kinetic systems, the additional requirements for fatigue control further limit the permissible permanent elastic stress; therefore, ratios of $\sigma_{M,Rk}/E > 10$ are needed. Indicated by the design guideline with the slope $\sigma_{M,Rd}/E$, the listed materials are therefore separated into different groups.

The design spaces clearly indicate FRPs and certain types of timber as adequate materials for bending-active structures. Whereas the basic requirements set for elastic kinetics are only fulfilled by FRPs and interestingly, bamboo. Additionally, long term behaviour must be taken into consideration:

- In static bending-active structures, creep deformation and consequential loss of pre-stress may be of little consequence to the system's integrity. If the pre-stress is not playing a decisive role in the systems stiffness, materials such as timber may be chosen.
- Adaptive and kinetic structures rely, next to a high materials yield strength and low bending stiffness, also on advantageous long term behaviour, allowing for cyclic exposure to large elastic deformation. Furthermore, the resetting effect can only be utilised if no long term permanent creep deformation occurs. Here, FRPs may provide the required material behaviour.

B 3.2 Design Codes and Guidelines for FRP

While building structures that include FRPs in their load bearing elements still need individual technical approval in Germany (ZiE), there is an emerging development in the standardisation

of FRPs as building products. Next to the German guidelines, e.g. BÜV-recommendation [BÜV 2010], the Danish based company Fiberline Composites has been granted national technical approval (abZ approval) for their pultruded Glass Fibre Reinforced Polymers (GFRP) products in German building projects [Dibt 2012].

The following design codes are available for GFRP in Building and Construction for Germany and Europe:

- DIN 18820: glass fibre reinforced laminates
- DIN EN 13121: GRP tanks and vessels for use above ground
- BÜV „Tragende Kunststoffbauteile im Bauwesen [TKB]“ [BÜV 2010]
- The recently national published technical approval (abZ approval) for use Fiberline GFRP profiles in German building projects [Dibt 2012]
- Eurocode on FRP (in work)

All of these codes consider the influence of loading duration and environmental conditions by means of safety factors. Generally, three strength and stiffness influencing factors are recognized:

- Load duration
- Ambient media class
- Member temperature

The safety concept of BÜV and abZ is based on a general material safety factor and a set of influence coefficients, resulting in different overall safety factors for various loading scenarios. The permissible stress is generally therefore given by (27_B):

$$\sigma_{Rd} = f_{k0.05} / [\gamma_M (A_1 \cdot A_2 \cdot A_3)] \quad (27_B)$$

With $f_{k0.05}$: 5 % quantile of strength
 γ_M = partial safety factor: 1.2 (machined)
1.5 (hand laminated) [BÜV]
 A_i : influence coefficients.

Within abZ, the influence factor A_i is directly applied on the action, while all other factors are applied on the resistance side.

In general praxis, the design of bending-active structures should consider three main scenarios:

- Dead load + residual-stress: long load duration, high max pos. temperature: $\gamma_{\text{tot}} \approx 4^*$
- Wind load + residual -stress: very short load duration, mean temperature: $\gamma_{\text{tot}} \approx 1.9^*$
- Snow load + residual -stress: short load duration (<1000m), low temperature: $\gamma_{\text{tot}} \approx 1.6^*$

*Typical values from BÜV and abZ; exact values must be determined specific to each project, a sample calculation from BÜV is given in Appendix C.

Note that the dead load plus pre-stress scenario limits bending stress to 25 % of the limit stress in the from-finding of the curved geometry.

In terms of the material stiffness, it must be noted that, especially for polyester resins, a loss of modulus has to be considered for ambient temperatures above 30°C, with a considerable influence for temperatures higher than 50°C. Here, the aforementioned guidelines introduce a secondary safety concept in which material stiffness is reduced, based on equation (27_B) with stiffness specific influencing factors.

Breaking strength and material stiffness

The breaking strength of FRPs is based on a number of failure criteria described by Puck (1996). Based on the theory of laminates, strength and stiffness of hand laminated, as well as industrially produced elements, GFRPs can be analytically evaluated. For technical approval, however, material tests are necessary to determine the 5 % quantile of ultimate strength.

For industrially produced profiles, mechanical properties are usually given based on standardised material tests. For practical reasons, the same values are given for all structural profiles with a typical longitudinal bending strength of 240 MPa [EN 13706] (see table B.27). L-shaped profiles usually exhibit the lowest strength in the cross-sections of pultruded profiles with very

small 5 % quantil values due to production inaccuracies. Pipes and flat sections, on the other hand, offer the highest strength and reach bending strengths, above 350 MPa in all tests known to the author. In some cases, such as GFRP reinforcement bars, ultimate strength can even exceed 1000 MPa [Weber 2008]. Since the profile shapes used in bending-active structures are predominantly round and flat sections, in a project it may be profitable not to rely on the standard values suggested by companies, but instead perform own material tests. This, however, necessitates technical one-time approval.

The elastic modulus, too, is usually given as a uniform value for all profile shapes which represents the lower limit of the various actual moduli. However, it was found that flat sections, as they are often used in bending-active structures, may have a lower modulus than other larger sections. This is due to the fact that all profiles must have at least two outer layers of fibre mats which have a much larger influence on the sectional properties for thin flat sections than for other cross-section types.

Characteristic stiffness values	
Elasticity modulus E0° [Gpa]	17/23/28*
Elasticity modulus E90° [Gpa]	8.5
Shear modulus G [Mpa]	3.0
Poisson's ratio V0°,90°	0.23
Poisson's ratio V90°,V0°	0.09
Characteristic strength values [Mpa]	
Bending strength, fb,0o	240.
Bending strength, fb,90o	100
Tensile strength, ft,0o	240
Tensile strength, ft,90o	50
Compressive strength, fc,0o	240
Compressive strength, fc,90o	70
Shear strength ft	25

Table B.27

Table B.27 Characteristic stiffness and strength values of pultruded GFRP profiles according to Fiberline product specifications from [Dibit 2012]

* The Young's Modulus varies from 17-28 GPa depending on geometry and reinforcement.

Limits of stress and strain for FRP

The limitations of minimal bending radii given by material strength and stiffness have to be additionally compared to the permissible strain of a material. This is due to the fact that the general stress strain relationship does not consider micro failure

on the surface. This is particularly true for fibre composites where the matrix may be showing micro cracks long before the permissible stress is reached. In the building norms, such limitations of strain are usually considered in connection with chemical harm (DIN EN 13121 8.2.4 maximum strain for polyester resin: 0.23 %). The abZ approval for Fiberline GFRP profiles offers limit strain values deliberately for the approved products:

Maximum axial strain and compression: 0.4 %
 Maximum transversal strain: 0.15 %
 Maximum transversal compression: 0.4 %

A practical example shows the extent of such limitations:
 Consider a flat section with 10 mm thickness made of GFRP with a Young's Modulus of 24,000 MPa. The permissible bending stress depending on the environmental conditions is set to typical values:

- 60 N/mm² long term (permanent bending shape)
- 130 N/mm² short term (wind load)
- The strain limitation for polyester resin is given with 0.4 %

The permissible bending radius for a profile with 10 mm thickness and Elastic-modulus 24000 N/mm² according to equation (20B) is:

$$\text{Long term: } r_{min} = \frac{24000 \cdot 10}{2 \cdot 60} = 2000 \text{ mm} \quad - \quad \varepsilon_{(r=2000)} = \frac{2000 - 5}{2000} = 0.25\% < 0.4\% \text{ OK}$$

$$\text{Short term: } r_{min} = \frac{24000 \cdot 10}{2 \cdot 130} = 923 \text{ mm} \quad - \quad \varepsilon_{(r=923)} = \frac{923 - 5}{923} = 0.54\% > 0.4\% \times$$

While the limitation for axial strain is apparently set high enough not to be violated for long term loading, attention must be paid to additional deformations due to short term loading. Here, careful study of the actually occurring strains in the Finite Element Analysis is needed. However, in most cases it will be found that the additional stresses due to external loads are not pure bending stresses and therefore do not automatically lead to high strains.

Creep and relaxation

Little research has been dedicated to long term behaviour of FRPs (GFRPs in particular) under large bending deformation. The researchers at Université Paris-Est have recently published

first results of long-term bending tests which suggest a temperature and resin dependent long term behaviour. From long term 3-point bending tests with pultruded GFRP pipes, they conclude that GFRPs under permanent loading remains linear-visco elastic if the stress lays under 30 % of the ultimate stress [Douthe 2009]. Considering the safety factor for long term loading of $\gamma_{tot} \approx 4$, derived above, this limitation is automatically fulfilled when following the current design guidelines for GFRP. The creep strains are found to be approximately 8 % of the total strains, independent of the loading level. In this linear elastic range, creep and relaxation can be deduced from each other.

Fatigue

Fatigue in composite materials is dependent on numerous factors including material choice for fibre and resin, fibre lay-up, element dimensions and environmental conditions. While considerable research has gone into the fatigue due to long term dynamic loading with small deflections for aircrafts and windmills, there is little experience with large permanent deformations.

For elastic kinetic systems an additional reduction factor must be introduced to cover fatigue effects caused by cyclic long-term loading. Based on the PhD [Meyer 1992], a reduction factor for laminated GFRP can be determined as follows:

Frequency: transformation time 100sec – frequency = 0.01 Hz
 Number of cycles: 20 year life span with an average of two cycles per day: $\sim 1.5 \times 10^4$.

With the above set of conditions and Figure B.28 we can derive a stress limit of approx. 60 % which corresponds to a safety factor of 1.66.

A similar conclusion is made by Philippidis (1999), showing that a given stress distribution resulting from cycling loads may not lead to fatigue problems if the maximum stress is lower than 60 % of the permissible stresses.

New material developments

The safety factor derived above is based on hand laminated GFRPs with the production standards from 30 years ago. Industrial

DOUTHE, C., BAVEREL, O. and CARON, J.-F. (2006) *Form-finding of a grid shell in composite materials*.

MEYER, J. (1992) *Zur Bemessung von GFK-Bauteilen unter Zuhilfenahme der Linear-Elastischen Bruchmechanik und probabilistischer Versagenskriterien*.

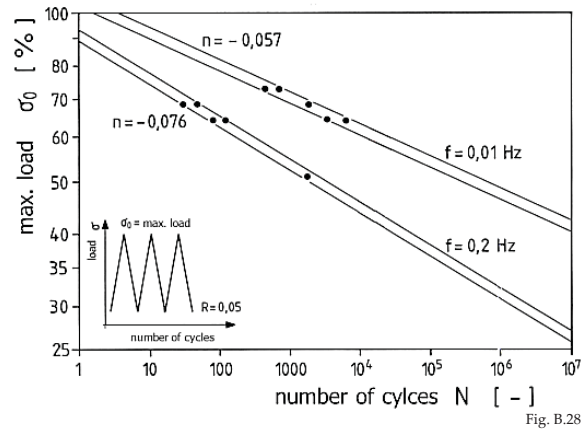


Fig. B.28

production such as pultrusion and continuous improvement of fibre-matrix adhesion suggest that today, GFRP products would reach higher fatigue resistance. However, to the knowledge of the author, there is no new data available that would combine frequency in the range of 0.01 HZ with large elastic deformations and thereby be applicable for the elastic kinetic systems investigated in this dissertation.

On the other hand, material research in FRPs is constantly bringing out new fibre coatings and additives that improve long term behaviour. For example, the fatigue life of GFRP composite with 9 % rubber microparticle in a modified epoxy matrix is about three times higher than that of GFRPs with neat matrix. The suppressed matrix cracking and reduced crack growth rate due to rubber cavitation and plastic deformation mechanisms appears to contribute to the observed enhancement of the fatigue life in GFRPs with modified matrix [Manjunatha et al 2009].

Fig. B.28 Fatigue effects caused by cyclic long-term loading [Meyer 1992].

PHILIPPIDIS, T.P. and VASSILOPOULOS, A.P. (1999) *Fatigue Strength Prediction under Multiaxial Stress*.

MANJUNATHA, C.M., TAYLOR, A.C. and KINLOCH, A.J. (2009) *The effect of rubber micro-particles and silica nano-particles on the tensile fatigue behavior of a glass fibre epoxy composite*.



C Active Bending in Building Structures

C1	Material-driven Form	46
C2	Categorisation	49
C3	Review of Active Bending in Building Structures	52
C 3.1	Behaviour-based Approach	52
C 3.2	Geometry-based Approach	54
C 3.3	Integral Approach	58

C Active Bending in Building Structures¹

Various empiric construction methods known from vernacular architecture are known to have used the elastic behaviour of local building materials in their constructions. In 20th century architecture the use of elastic deformation was mainly utilised as an economic construction method for double curved shell structures. Recent developments in simulation techniques have formed the basis for new exploration in bending-active structures that include new types of surface- and gridshells, membranes with elastically bent battens, bent structural components with membranes as restraining system and various types of adaptive and elastic kinetic structures. This section will review the development of bending active structures. By bringing together important material developments and various historical as well as recently built samples of such structures, the aim is to show coherency in their design approach.

C1 Material-driven Form

In order to guarantee sufficient load bearing capacity of a structure that includes considerable self-equilibrating bending stress, materials of high breaking strain must be chosen. The traditional building materials of soft wood, bamboo and reed offer such characteristics, leading to an extensive use of active bending in the constructions of vernacular architecture across cultures and continents.

In the encyclopaedia of vernacular architecture, it is stated that: *...the use of flexible branches may even have pre-dated the real invention of weaving (...). In fact, in the earliest dwellings the construction principle of weaving seems closely connected to the static mechanism of dome-shaped shelters (...), structural solidity is guaranteed by the presence of the crossed warp that elastically joins together all the tension arches in a single resistant system* [Oliver 2007a: 653] (Figure C.1).

An indication for their lightweight potential and economical material use becomes apparent when considering the fact that such

¹Based on a pre-published article: Lienhard et. al.(2013): *Active Bending, a Review on structures where bending is used as a self formation process*

OLIVER, P. (2007a) *Encyclopedia of Vernacular Architecture of the World*, Vol. 1 Theories and Principles

OLIVER, P. (2007b) *Encyclopedia of Vernacular Architecture of the World*, Vol. 3 Cultures and Habitats

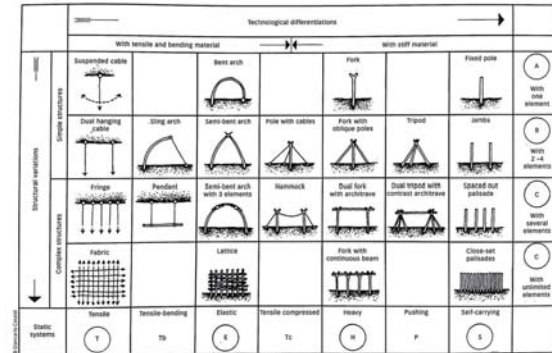


Fig. C.1

structures were predominantly found in areas where wood was rare, where mainly softwood was available or in cultures that had not yet developed the skills to process larger timber pieces [Oliver 2007b: 652].

The industrial revolution advanced iron as a building material. In the on-going developments, steel and reinforced concrete became the dominant materials of 20th century architecture. Along with these materials came a split from a master-builder to a planning architect, a structural engineer using simplified static theories and a constructor. Building what was designed by others systematically limits the highly integrated concept of active bending in building structures. A set of well-defined geometrical and structural typologies is the practical basis for most styles of 19th and 20th century architecture which enabled controlled technological complexity, yet limited geometrical and structural variety. Form-finding strategies based on material and force have been developed, not surprisingly then, by only a few but widely recognized individuals. To mention a few milestones:

- The first tensile roof made with steel strips at the Rotunda in Nizhny Novgorod by Vladimir Shukhov (1895). (Figure C.2)
- Stone Church of Colònia Güell by Antoni Gaudí (1898) using hanging model form-finding. (Figure C.3)
- Zarzuela Hippodrome in Madrid by Eduardo Torroja (1935) considering isostatic lines in the reinforcement of ultra-thin concrete shells. (Figure C.4)

Fig. C.1 Overview of wooden structures from the encyclopaedia of vernacular architecture [Oliver 2007a: 653].

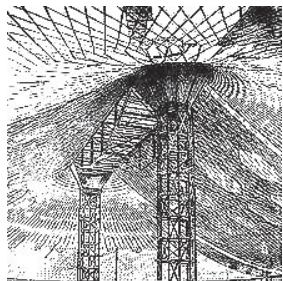


Fig. C.2



Fig. C.3



Fig. C.4

Their work led to a new interest in alternative, lightweight construction principles around the 1950's, with people like Buckminster Fuller, Félix Candela, Heinz Isler, and Frei Otto. Their interdisciplinary teams of architects and engineers contributed to the development of force and material informed structural concepts and the therefore necessary form-finding techniques. This re-introduced the use of active bending principles (see geometry based approach below) which gave traditional construction materials like softwood and bamboo [Gas et al. 1985] a new meaning in construction. However, the enormous time and effort needed for the form-finding, engineering and planning of visionary projects like the Multihalle Mannheim from 1974 [Happold and Liddell 1975] reserved such construction principles to a few seminal projects. Until recently, the lack of engineering techniques for form-finding and structural analysis of bending-active structures inhibited a broader consideration of this approach.

Parallel to the development of lightweight structures, Fibre Reinforced Polymers (FRP) were introduced broadly around the 1950's, offering a unique ratio of high strength to low bending stiffness. The sports industry quickly recognized the potential of FRPs for their elasticity in products like tennis rackets, golf shafts, pole vaults and the camping tent. On the contrary, architects were using these materials to generate primarily free-form geometries and aid in the prospect of industrially manufactured modular structures. Other more industrially oriented building applications use FRPs for reasons of chemical durability and low electrical conductivity. The first architectural constructions made of GFRPs were the "House of the Future" by the Monsanto Chemical Company in 1954 (Figure C.5) and the "Futuro" by Suuronen in 1968 (Figure C.6). Both examples suggest high-tech technology in their formal appearance, yet rely on labour intensive manual lamination techniques for the production of their curved surfaces. With Buckminster Fuller's "Fly's Eye Domes" in 1975, GFRPs reached an intermediate peak in architectural application, with a subsequent sudden drop in implementation related to the oil crisis [Knippers et al 2010a: 13-14].

GAS, S., DRUESDAU, H. and HENNIKE, J. (1985) IL 31 Bambus – Bamboo.

HAPPOLD, E. and LIDDELL, W.I. (1975) Timber lattice roof for the Mannheim Bundesgartenschau.

LIENHARD, J. et al. (2010) Form-finding of Nature Inspired Kinematics for Pliable Structures.

CRAWFORD, R.F. (1971) Strength and Efficiency of Deployable Booms for Space Applications.

GERTSMA, L. W. et al. (1965) Evaluation of one type of foldable tube.

TAN, L.T. and PELLEGRINO, S. (2004) Ultra thin deployable reflector antennas.

In the space industry, where planning and material costs play a comparatively minor role, the use of new materials and their development are closely associated. Here, Carbon Fibre Reinforced Polymers (CFRP) were used to develop elastic deployable structures starting with early investigations on linear deployable booms [Crawford 1971] and tubes [Gertsma et al. 1965] in the 1960's, reaching high complexity in flexible shells such as the "Ultrathin deployable reflector antennas" (Figure C.31) [Tan and Pellegrino 2004: 2]. Next to the significance of material research, these developments also relied on the theoretical analysis of non-linear structural behaviour. New analytical approaches from engineers like Timoshenko in the 1950's [Timoshenko and Goodier 1951] leading to the development and general availability of non-linear Finite Element Methods created the basis of modern engineering mechanics, now offering a complete framework for the form-finding and analysis of bending-active structures.

Today, industrial manufacturing processes for semi-finished FRP products like pultrusion make them more economical and guarantee consistence in mechanical behaviour. Since 2012, the first GFRP products were granted national technical approval (abZ approval) for use in German building projects [Dibt 2012] (see Chapter B3.2). This is a long awaited and important achievement to enable the step from research labs to the building industry for bending-active structures made of GFRPs. One of the first projects to have taken this step is the adaptive façade shading system for the 'Softhouse' at IBA Hamburg 2013 (see chapter D4).



Fig. C.5



Fig. C.6

C2 Categorisation

As described in Chapter B1.1, bending-active structures are understood to be an approach rather than a distinct structural typology. Based on the material selection presented above, a large variety and combination of structural systems can be generated by means of elastic deformation. Taking the potential of a certain material behaviour as a starting point, bending-active structures become an approach rather than a distinct structural typology. Their common denominator is not a circumscribed load bearing behaviour or geometrical definition, but a formation process

Fig. C.2 Rotunda in Nizhny Novgorod by Vladimir Shukhov (1895).

Fig. C.3 hanging model for the stone Church of Colonia Güell by Antoni Gaudí (1898).

Fig. C.4 Zarzuela Hippodrome in Madrid by Eduardo Torroja (1935).

Fig. C.5 House of the Future by the Monsanto Chemical Company (1954).

Fig. C.6 Futuro by Suuronen in (1968).

TIOMOSHENKO, S. and GOODIER, J. (1951) *Theory of elasticity*.

DIBT. Allgemeine bauaufsichtliche Zulassung Z-10.9-299, Pultrudierte Profile aus glasfaserverstärkten Kunststoffen

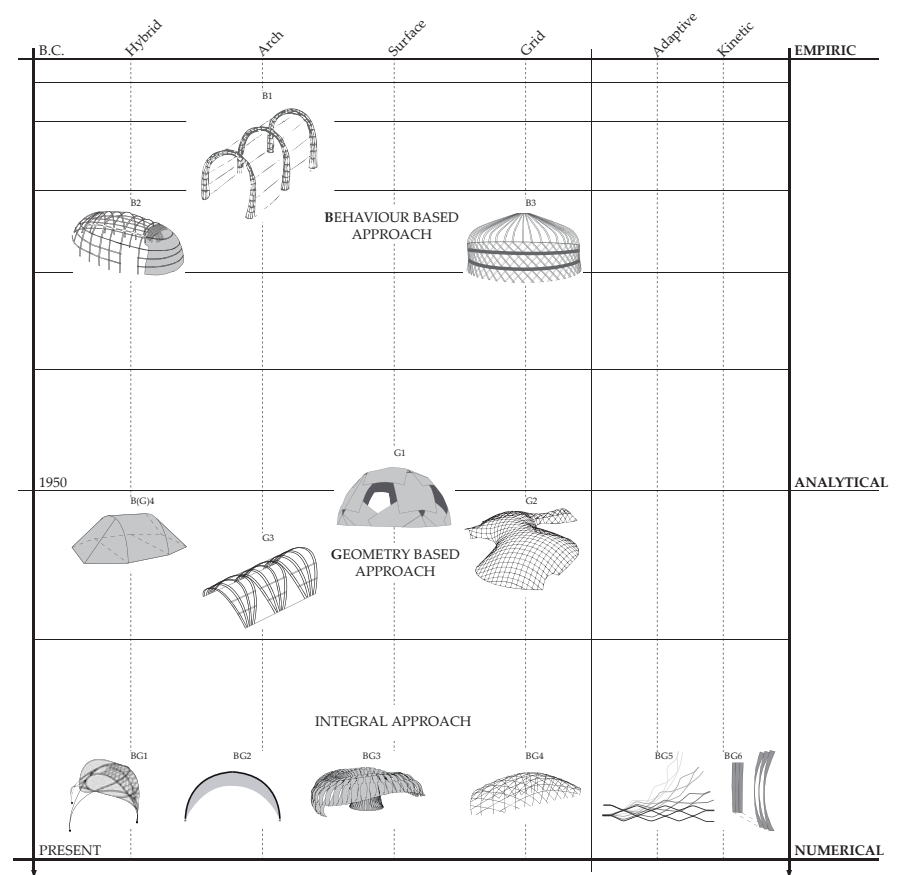
LIENHARD, J. et al. (2013) *Multifunctional adaptive Façade at IBA 2013; design studies for an integral energy harvesting façade shading system*.

during which they are elastically bent. Consequentially, a further differentiation of bending-active structures is suggested based on their design approaches. In a summarising graph (Figure C.7), three such approaches are shown: the behaviour based approach, the geometry based approach and current research that seeks to integrate the two.

- In a *behaviour based approach* bending is initially used intuitively; the system's geometry and structural behaviour is studied empirically. Material limitations are tested physically.
- In a *geometry based approach* the system's geometry is predefined based on analytical geometry or experimental form-finding methods, both of which are used as a controlled means to approximate the actual bending geometry. Material limitations are considered analytically based on moment curvature relation.
- In an *integral approach* the elastic bending deformation is analysed through numerical form-finding, which enables full control of material behaviour based geometry. Material characteristics and limitations are included in the numerical analysis model.

Looking at the historical development, starting with the behaviour based approach, it becomes apparent that this approach leads to the most realised projects and is a recognised construction type still used today. It took until the 20th century for an analytical, geometry based approach to appear. The research on lightweight structures, which became very active in the middle of the last century, led to this approach where elastic deformation is used as an economic way to construct double curved shell structures whose geometry is, however, not directly based on the bending shape itself but various other analytical and experimental form-finding approaches. Enabled by the powerful simulation methods we are equipped with today, the two approaches may be combined by simulating the large bending deformations of the erection or shape adaptation themselves and thereby fully tap the potential of active bending.

The vertical axis in Figure C.7 indicates a historical order of the presented examples and also groups the design approaches ac-



cording to the analysis tools available, reaching from empiric to analytical and finally, modern numerical analysis. The aforementioned interest in alternative, lightweight construction principles around the 1950's becomes visible in the centre of this graph with an accumulation of projects based on a geometric approach.

The horizontal axis offers a loosely formulated categorisation of various expressions of bending active structures into known structural types. Most of the recent examples are deliberately placed off of the exact axis as they begin to explore new in-be-

Fig. C.7 Development of bending-active structures.

tween fields and hybrid forms of the known structural types. The project samples are discussed further in the following chapters and referred to by the given codes. The nature of these approaches is discussed based on some important project samples.

C3 Review of Active Bending in Building Structures

C 3.1 Behaviour-based Approach

Various construction methods known from vernacular architecture make use of the elastic behaviour of their building materials, leading to a recognised construction type which prevails in some cultures and certain applications. In the encyclopaedia of vernacular architecture, these structures are referred to as tension arc systems (see Figure C.1) [Oliver 2007b: 652]. The review on bamboo structures [Gas et al. 1985] differentiates more precisely between curved compression rods and curved tension rods. Putting bending itself in the centre of attention, a more differentiated view is suggested as shown in Figure C.7. There are samples of elastically formed arc and shell structures found in various cultures on every continent. The empiric development of construction methods based on the elasticity of their building materials predominately resulted in similar structures. Among these, the Mudhif cane huts in Ma'dan (South Iraq) are a well-documented example [Gas et al. 1985] (sample B1 in Figure C.7 and Figure C.8). They are permanent structures using reed bundles that are first vertically fixed into bucket foundations and later connected at the top to form elastically bent arcs.

Another very common application is a bending-active construction system for temporary or mobile shelters. The tents of the nomadic tribes in the Middle East are typical examples mobile constructions using active bending for advantageous packaging. These tents are constructed with a skeleton of partially bent wooden ribs in combination with a surface made of black, goat-hair, felt or vegetable fibres. The Iranian Kutuk or Kantuk, for example, use date-palm ribs as frames (arcs), traversed by cane stringers, and covered with a thatch of canes (sample B2 in Figure C.7). Similarly the Yamut [Amirkhani 2010] of the north Iranian Turkmen or the Mongolian Yurt [Oliver 2007: 840] uses a

Project: Mudhif houses
Place: Southern Iraq swamps
Year: since over 5,000, still built today
Material: reed, straw
Form-finding: empiric prototyping
Size: up to 10 m long reed bundles
Architect: Madan people (Marsh Arabs)
Engineer: Madan people (Marsh Arabs)



Fig. C.8

Project: Dorze Tribe House
Place: Ethiopia
Year: still built today
Material: hard wood poles, woven bamboo
Form-finding: empiric prototyping
Size: height: up to 12 m
Architect: people of the Dorze Tribe
Engineer: people of the Dorze Tribe



Fig. C.9

Project: Oca
Place: Amazonian Basin, Brazil
Year: first documented in 1887
Material: wood, sapé, thatch
Form-finding: empiric prototyping
Size: vary according to the number of people
Architect: Yawalapiti people
Engineer: Yawalapiti people



Fig. C.10

Project: Yamut
Place: Iran
Year: __, still built today
Material: wood
Form-finding: empiric prototyping
Size: approx. 3 m high
Architect: Nomadic Turkmen
Engineer: Nomadic Turkmen



Fig. C.11

bent pantographic grid for the skeleton of the walls. In this case also the roof construction is elastically bent (sample B3 in Figure C.7 and Figure C.11).

Still today there are various examples of bending-active structures that are predicated on the behaviour based approach. Next to various arc and gridshell structures built out of green wood or living willow stems [Ludwig et al. 2009], Vo Trong Nghia's considerably large bamboo structures are, for example, built in this manner (Figure C.12) [ARM 2007]. New high strength materials combined with low bending stiffness such as GFRPs and high strength aluminium became popular as of the 1970's. This enabled the first mountaineering and expedition tents with elastically bent supporting arcs, for example. The tent poles could easily be bent by hand into a dome (gridshell) or tunnel (series of arches) configuration (sample B4 in Figure C.7). These high tech tents were developed based on experimental tests of full scale prototypes. In-depth empirical analysis of the products allowed for a secure industrial production. As the analytical understanding and numerical simulation of these tent structures is starting to be considered, they are clearly a significant stepping stone towards the integrated behaviour and geometry based approach described below.

Today, there is an increasing interest by designers and architects to use the advantages from polymers for active bending in various kinds of experimentally conceptualised installations and small pavilion structures. Projects like 'The Loop' [Hoeweler and Yoon 2013] and the 'elastic habitat' [Santini and Taddei 2006], both from 2006, underline a keen interest in the freedom of creating complexly curved shapes *in situ* (Figure C.13 and Figure C.14).

C 3.2 Geometry-based Approach

The intense research on lightweight structures that commenced in the middle of the last century led to an intensified interest in double curved surface- and gridshells. However, the simulation techniques which are starting to be developed are not yet able

LUDWIG, F. et. al. (2009) *Plant stems as building material for living plant constructions*.

Bamboo Bar. The Architectural Review Magazine

HOEWELER and Yoon (2013) www.mystudio.us/projects/12

SANTINI and TADDEI. (2006) www.architettura.it/architetture/20070319/index.htm

Project: Water and Wind Café, Bamboo Bar
Place: Binh Duong, Vietnam
Year: 2008
Material: bamboo
Form-finding: physical models
Size: 250 m², diameter: 15 m, height: 10 m
Architect: Võ Trọng Nghĩa
Engineer: Võ Trọng Nghĩa



Fig. C.12

Project: LOOP
Place: New York, NY
Year: 2006
Material: GFRP
Form-finding: physical models
Size: approx. 2 m x 2 m x 2 m
Architect: Hoeweler and Yoon Architecture
Engineer: Hoeweler and Yoon Architecture



Fig. C.13

Project: Elastic Habitat
Place: Biennale Internationale Design 2006
Saint-Etienne
Year: 2005-2006
Material: flexible plastic tubes
Form-finding: physical models
Size: 40 m³
Architect: Avatar architettura + Peter Lang
Engineer: Nicola Santini, Pier Paolo Taddei



Fig. C.14

Project: Plywood Dome – Church in Korea
Place: Naju, Korea
Year: 1958
Material: plywood
Form-finding: physical models, analytical
Size: diameter: 11.9 m
Architect: Buckminster Fuller
Engineer: Buckminster Fuller



Fig. C.15

to simulate large elastic deformations. The most common form-finding method of the time was the hanging model, which could be handled both experimentally and analytically. Some experimental tests additionally proved the similarity of the hanging chain and the Elastica-Curve (Gas et al. 1985) (See also Figure E.13). In the 1960's, Frei Otto started intensive research on gridshells [Hennicke, 1975]. After a few prototype structures, the Multihalle Mannheim built in 1974 was the first large span gridshell [Happold and Liddell, 1975] (sample G2 in Figure C.7 and Figure C.16). The geometry of the grid was form-found based on experimental hanging models. The timber lathes of the initially flat grid were pushed into the desired form given by the hanging model. The computational simulation methods at the time were not able to simulate the large deformations of the grid that would have been necessary to find the natural bending shape. Only a few more gridshells have been built to further develop this approach. The Hooke Park Workshop (1990) [Hennicke, 1975] (sample G3 in Figure C.7 and Figure C.18) was not a gridshell as such; using a set of elastically bent timber arcs, whose form is based on studies of the hanging model, makes the approach similar to that used for Mannheim. Both structures were engineered by Buro Happold, where an outstanding knowledge in gridshell structures has developed [Harris, 2011]. This led to more recent examples such as the Downland Gridshell (2002) (Figure C.19) [Harris et al. 2003] and the Savill Garden Gridshell (De Groot, 2007) [Harris 2008].

Additional examples of gridshells that use the elasticity of timber to bend the grid into a given analytical geometry include the Polydôme [Natterer and Macintyre 1993] which uses multi-layered timber to shape the geometry of a sphere (Figure C.17, the Japanese Pavilion at Expo 2000 in Hannover [Jodidio and Ban, 2010] that uses cardboard tubes, and the Helsinki Zoo tower [Salokangas, 2003] that lets the grid follow geodesic lines on a free-form surface. The advantage of an easy erection procedure where the geometry is automatically set in position was however partially lost in the above mentioned projects due to the necessity of controlling the final geometry in the erection process.

GAS, S., DRUESDAU, H. and HENNIKE, J. (1985) IL 31 *Bambus – Bamboo*.

HENNICKE, J. (1975) IL 10 *Gitterschalen – Grid Shells*.

HAPPOLD, E. and LIDDELL, W.I. (1975) *Timber lattice roof for the Mannheim Bundesgartenschau*.

HARRIS, R. (2011) *Design of timber gridded shell structures*.

HARRIS, R. et. al. (2003) *Design and construction of the Downland Gridshell*.

HARRIS, R. et. al. (2008) *The Savill Garden gridshell: design and construction*.

Project: Multihalle
Place: Mannheimer Herzogenriedpark
Year: 1973 - 1975
Material: wooden slats, Polyester-PVC Membrane
Form-finding: physical models, force density
Size: 10.500 m³, L: 160 m, W: 115 m, H: 20 m
Architect: Frei Otto, Ewald Bubner, Carlfried Mutschler, Joachim and Winfried Langner
Engineer: M. Dickson, T. Easley, E. Happold, I. Liddell

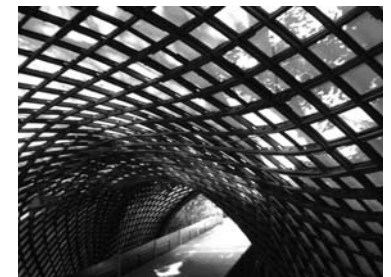


Fig. C.16

Project: Polydôme
Place: Switzerland
Year: 1991
Material: timber, Swiss spruce boards
Form-finding: analytical
Size: span: 25 m, height: 7 m
Architect: Dan Badic & Associés. Morges
Engineer: Bois Consult Natterer. Etoy

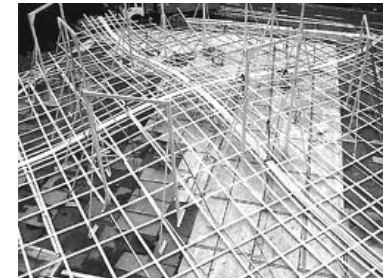


Fig. C.17

Project: Hooke Park Forest School
Place: Dorset, England
Year: 1989
Material: wood poles, PVC-coated polyester fabric
Form-finding: physical models
Size: 18 m wide and 60 m long
Architect: R. Burton (ABK Architects) and F. Otto
Engineer: Buro Happold



Fig. C.18

Project: The Weald and Downland Gridshell
Place: Weald & Downland Museum, Sussex, England
Year: 1996 - 2002
Material: oak sourced from Normandy
Form-finding: physical models, FEM
Size: 50 m long, 24 m wide and 7-11 m high
Architect: Edward Cullinan Architects
Engineer: Buro Happold



Fig. C.19

NATTERER, J. and MACINTYRE, J. (1993) *Polydôme: A Timber Shell, Switzerland*.
 JODIDIO, P. and BAN, S. (2010) *Shigeru Ban: Complete Works, 1985 – 2010*.
 SALOKANGAS, L. (2003) *Wooden Observation Tower, Helsinki, Finland*.

A unique approach for making surface shells was introduced by Buckminster Fuller. As part of his studies on geodesic domes, Buckminster Fuller developed the Plydome Structures in 1957 [Gorman, 2005] (sample G1 in Figure C.7 and Figure C.15). The global shape is defined by a sphere; he uses plywood panels that are predominantly bent around one axis and interconnected on the topological points of the geodesic dome.

C 3.3 Integral Approach

Recent developments in simulation techniques now allow form-finding and analysis of structures that derive their complex curved geometry solely through the erection process in which they are elastically deformed. This has provided the basis for various probes that include new types of surface- and gridshells, membranes with elastically bent battens, bent structural components with membranes as restraining systems and various types of adaptive and elastic kinetic structures.

The integration of elastic beams (sail battens) in a form-active surface for extremely light and integrated primary structures in mechanically pre-stressed membranes has been a challenge for numerical form-finding methods. Such hybrid structures have recently been investigated in the work on 'Spline Stressed Membranes' [Adriaenssens 2008]. This work was motivated by a membrane structure for the Expo Seville 1992 with integrated curved tensegrity beams [Barnes et al 1996]. Some prototypical work has also been done on the so-called Bat Sail [Off 2010] (Figure C.23). As the stiffness of a hybrid system is much higher than the stiffness of the bent element itself, very small cross-sections are feasible. These characteristics make the combination of active bending particularly applicable for temporary and mobile constructions [Burford and Gengnagel 2004] [Gengnagel 2005]. The Lightweight Structure Unit - a group of Architects and Engineers from the University of Dundee and the Technical University of Munich developed small and medium span prototypes for rapid deployable shelters based of this conceptual idea between 1999 and 2004. Ongoing research explores the possibilities combining elastically bent elements with restraining membranes on the level of building components as membrane

Project: Composite Gridshell

Place: France

Year: 2005

Material: composite materials such as carbon and glass fibers

Size: height: 5.8 m, width: 13 m, length: 13.5 m

Form-finding: physical models, Dynamic relaxation

Architect: LAMI-ENPC and Laboratoire NAVIER

Engineer: LAMI-ENPC and Laboratoire NAVIER



Fig. C.20

Project: Membrane restrained arc

Place: University of Dundee

Year: ca. 1999

Material: GFRP rods, Polyester-PVC Membrane

Form-finding: physical models, FEM

Size: width: 6 m, height: 3 m

Architect: N.K. Burford and F.W. Smith

Engineer: N.K. Burford and F.W. Smith



Fig. C.21

Project: Strut and cable braced cantilever

Place: UK, Munich

Year: 2002

Material: GFRPs and Aluminium rods, Polyester-PVC Membrane

Form-finding: physical models, FEM

Size: cantilevered free span: 13 m, width: 6 m

Architect: Lightweight Structures Unit (Dundee)

Engineer: Universität München, C. Gengnagel



Fig. C.22

Project: Bat-Wing-Sail Research Project

Place: Dessau, Germany

Year: 2006-2007

Material: GFRP rods, Polyester-PVC Membrane

Form-finding: physical models, FEM

Size: approx. 10 m x 6 m

Architect: IMS – Institute for Membrane and Shell Technologies, R. Off

Engineer: TUM



Fig. C.23

restrained arcs [Alpermann et al 2012] (sample BG2 in Figure C.7 and Figure C.21) or membrane restrained columns and girders [Alpermann and Gengnagel 2013]. The shape of the bent elements can be controlled by the patterning of the membrane and the pre-stress in the membrane restraining system. The membrane stabilises the slender beam elements against buckling and reduces deformation. Current projects explore the new formal and functional possibilities in *textile hybrid* systems (see Fig. C.25 [Ahlquist and Menges 2013] and the M1 Project in Chapter D3).

On the level of bending-active building components, the prototypical pedestrian bridge which is pre-stressed through bending from the researchers at Université Paris-Est UR Navier [Baverel et al 2010] (Figure C.26) and the timber arch component based on textile weaving patterns by the IBOIS from EPFL Lausanne must also be mentioned [Weinand, Y. 2009].

Recent research studies have analysed methodologies to generate developable grid structures by simulating their resulting geometry based on the erection process from an initially planar configuration. The final geometry of highly elastic gridshells results from a shaping process where the grid members are progressively elastically bent. In order to obtain the resulting gridshell geometry, several research studies have developed form-finding methods reproducing this erection process. [Douthe 2006] [Li and Knippers 2011] (sample BG4 in Figure C.7 and Figure C.20) Current studies analyse these structural effects for a variety of surface geometries and grid configurations.

Providing the right material properties and a reversible deformation process, active bending may also be used for adaptive structures. A visionary project was constructed in 2002 at the Architectural Association school (AA) in London. The so called Hybird [Menges 2004] (sample BG5 in Figure C.7 and Figure C.30) is an adaptive grid shell with three locally curved layers

- ALPERMANN, H., GENGNAGEL, C. and LAFUENTE HERNÁNDEZ, E. (2012) *Case-studies of arched structures using actively-bent elements*.
 ALPERMANN, H. and GENGNAGEL, C. (2013) *Membrane restrained girder*.
 AHLQUIST, S. and MENGES, A. (2013) *Frameworks for Computational Design of Textile Micro-Architectures and Material Behavior in Forming Complex Force-Active Structures*.
 BAVEREL, O. et. al. (2010) *Concept of a beam prestressed by bending: Application to a footbridge in composite materials*.
 WEINAND, Y. (2009) *Innovative Timber Constructions*.
 DOUTHE, C., BAVEREL, O. and CARON, J.-F. (2006) *Form-finding of a grid shell in composites materials*.
 LI, J. and KNIPPERS, J. (2011) *Form-finding of grid shells with continuous elastic rods*

Project: GFRP and membrane pavilion
 Place: Stuttgart
 Year: 2004
 Material: GFRP flat sections, lycra
 Form-finding: physical models, Force-density for membrane
 Size: 3 x 3 x 3 m
 Architect and Enigneer: Don-U Park, Alexander Hub, ITKE- University of Stuttgart (Prof. Jan Knippers)



Fig. C.24

Project: Material Equilibria Installation
 Place: Copenhagen, gggallery
 Year: 2012
 Material: knitted fabric and GFRP
 Form-finding: physical models and spring based computational model
 Size: 3 x 4 x 3 m
 Architect and Engineer: Sean Ahlquist, ICD - University of Stuttgart (Prof. Achim Menges)



Fig. C.25

Project: Beam pre-stressed by bending
 Place: France
 Year: ca. 2009
 Material: GFRP
 Form-finding: FEM, Dynamic relaxation
 Size: span: 10 m
 Architect: Université Paris-Est, UR Navier
 Engineer: Université Paris-Est, UR Navier



Fig. C.26

Project: Muscle ReConfigured
 Place: TU Delft, Netherlands
 Year: 2004
 Material: HYLITE panels, Festo Muscle
 Form-finding: physical models and approx. parametric computational models
 Size: height approx. 3 m, length: 9 m
 Architect: TU Delft prof. ir. K. Oosterhuis and Hyperbody Research Group
 Engineer: Hyperbody Research Group



Fig. C.27

- MENGES, A. (2004) *Emergence: Morphogenetic Design Strategies*.
 HYPERBODY RESEARCH GRP. (2005) *Muscle reconfigured - Programmable Architecture*.



Fig. C.28

of GFRP lathes. The global curvature of the shell can be adapted by changing the coupling length between the locally curved elements. Similar studies of spatial adaptations were undertaken in 2004 by the 'Hyperbody Research Group' [Hyperbody 2005] (Figure C.31).

Some research projects and prototype constructions have investigated the use of active bending for kinetic structures. While this approach has already been taken quite far in disciplines like aerodynamics (Figure C.30), only a few projects have been realised in a large scale architectural context, such as the Thematic Pavilion at EXPO 2012 in Korea Yeosu [Lienhard and Knippers 2012] (sample BG6 in Figure C.7 and Figure C.28 and C.29). The kinematic media façade promotes 108 individual GFRP lamellas that are deformed by controlled buckling. The facade can therefore adapt to light and physical building conditions and allows the artistic staging of special lighting effects. It has a total length of 140m and a height between 3 and 14m.

Project: Bionic kinetic facade - Thematic pavilion - Expo 2012

Place: Yeosu, South Korea

Year: 2012

Material: GFRP lamellas (108)

Form-finding: FEM

Size: length: 100 m, height: 14 m

Architect: SOMA architects from Vienna, Austria

Engineer: Knippers Helbig

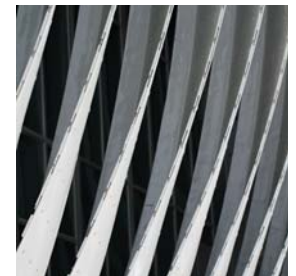


Fig. C.29

Project: Hyagrid adaptable architecture

Place: London

Year: 2002-03

Material: fiber-composites, elastic members

Form-finding: physical models and prototypes, FEM

Size: -

Architect: AA EmTech and Design, S. Felipe, J. Truco

Engineer: Sylvia Felipe and Jordi Truco, EmTech



Fig. C.30

Project: Ultra Thin Deployable Reflector Antennas

Place: London, UK

Year: 2004

Material: carbon-fibre-reinforced-plastic

Form-finding: computational/analytical

Size: diameter: 4.6 m

Architect: Lin Tze Tan, Sergio Pellegrino

Engineer: Lin Tze Tan, Sergio Pellegrino



Fig. C.31



D Introduction of Case Studies

D1 Temporary Static Structure: ICD/ITKE Research Pavilion 2010	66
D 1.1 Project Specifications	67
D 1.2 Form-finding	67
D 1.3 Structural Behaviour	68
D 1.4 Gained Insights	70
D 1.5 Acknowledgements to the Project Team	71
D2 Permanent Textile Hybrid Structure: Umbrella for Marrakech	72
D 2.1 Project Specifications	72
D 2.2 Form-finding	73
D 2.3 Structural System and Behaviour	73
D 2.4 Gained Insights	76
D 2.5 Acknowledgements to the Project Team	77
D3 Temporary Textile Hybrid Structure: M1	78
D 3.1 Project Specifications	78
D 3.2 Form-finding	79
D 3.3 Structural System and Behaviour	80
D 3.4 Gained Insights	80
D 3.5 Acknowledgements to the Project Team	83
D4 Permanent Adaptive Structure: Softhouse	84
D 4.1 Project Specifications	84
D 4.2 Form-finding	85
D 4.3 Structural System and Behaviour	86
D 4.4 Gained Insights	88
D 4.5 Acknowledgements to the Project Team	89
D5 Elastic Kinetic Research Demonstrator: Flectofin®	90
D 5.1 Specifications	90
D 5.2 Form-finding	90
D 5.3 Structural Behaviour	94
D 5.4 Gained Insights	95
D 5.5 Acknowledgements to the Project Team	97
D6 Reflection on the Role of FEM in the Design Processes	98
D7 Reflection on Structural Typologies Presented by the Case Study Structures	101

D Introduction of Case Studies

In accordance to the definition of bending-active structures being understood as an approach rather than a distinct structural type, this dissertation is not based on a framework set by clearly distinguished structural categories which is studied and classically reflected upon with a case study at the end. Here it is chosen to present the many case studies in the beginning, highlighting the variegation in applying active bending to integral structural concepts. The projects will be introduced with general information in this chapter, generating new findings in a creative and practical exploration of the subject. Important and individual findings from each case study are summarised here. In the subsequent chapters on form-finding and structural behaviour these findings will be continuously analysed in more detail on abstracted models and eventually, in more detail through the case studies themselves.

Each project was built in collaboration with a team of architects and other engineers and at times, even biologists. The authors personal involvement is clarified at the end of each the following chapters. In general, the personal contribution was always in the context of form-finding and structural analysis.

D1 Temporary Static Structure: ICD/ITKE Research Pavilion 2010

At the end of July 2010 the Institute of Computational Design (ICD) and the Institute of Building Structures and Structural Design (ITKE) at the University of Stuttgart realised a temporary research pavilion made of plywood. The design of the pavilion was the result of a student workshop which focused on the integration of physical experiments and computational design tools to develop bending-active structures.

The project was published and discussed in several conference papers and architectural journals. The descriptions below are based on Lienhard et. al (2011a), in Fleischmann et al. (2011) the design framework is discussed in a broader picture.

LIENHARD, J., SCHLEICHER, S. and KNIPPERS, J. (2011) *Bending-active Structures – Research Pavilion ICD/ITKE*.

FLEISCHMANN, M. et. al. (2011) *Material Behaviour: Embedding Physical Properties in Computational Design Processes*.



Fig. D.1



Fig. D.2

D 1.1 Project Specifications

The research pavilion demonstrates an alternative approach to computational design where the generation of form is directly influenced by the characteristics of the material. The structure is entirely based on the elastic bending behaviour of 6.5 mm thick birch plywood strips. The strips were robotically manufactured as planar elements, and subsequently connected to coupled arch systems with approx. 4 m span (see Figure D.3). A radial arrangement and interconnection of the self-equilibrating arch system led to the final torus shaped design of the pavilion. Due to the reduced structural height, the connection points locally weaken the coupled arch system. In order to prevent these local points from reducing the structural capacity of the entire pavilion, the locations of the connection points between the strips need to change along the structure, resulting in 80 different strip patterns constructed from more than 500 geometrically unique parts.

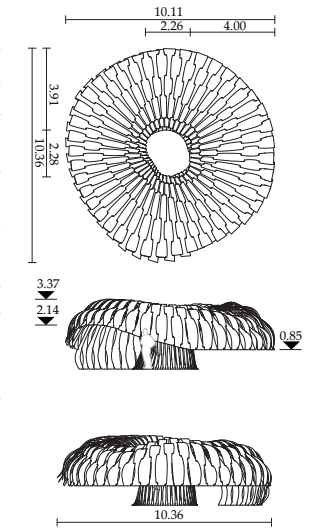


Fig. D.3

D 1.2 Form-finding

The shifting of the connection points and adaptation of the boundary conditions to a given site was made possible by a parametric design model that includes all relevant material and geometric constraints given by the coupled arch system. This computational design model became one of the essential interfaces which helped to coordinate and mediate various design and fabrication factors. While this purely geometric model was an abstraction of the actual equilibrium shape, which also neglects additional deformation due to dead load, it already gave feedback about the range of design possibilities made available by this process. More importantly, it also defined the unrolled geometry of the strips, including all connection points. This information was di-

Fig. D.1 Outside view of the ICD/ITKE Research Pavilion 2010.

Fig. D.2 Inside view of the ICD/ITKE Research Pavilion 2010.

Fig. D.3 Plan and side views of the view of the ICD/ITKE Research Pavilion 2010. Dimensions in meter.



Fig. D.4



Fig. D.5

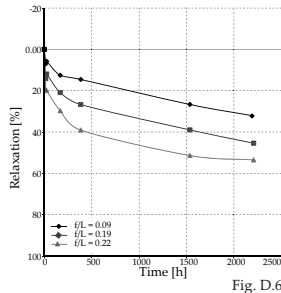


Fig. D.6

rectly transferred into the input geometry of the Finite Element model and the cutting patterns, also automatically created for the robotic manufacturing. Given the unrolled geometry and connection points of the coupled arches, it was possible to form-find the pavilion structure by using elastic form-finding cables which work with a temporary reduction of elastic stiffness that enables large deformations under constant pre-stress (Figure D.8). This newly developed form-finding method can be applied to many different types of bending active structures and will be discussed in more detail in chapter E3.

D 1.3 Structural Behaviour

It was found that the pavilion developed additional geometrical stiffness due to the fact that the arc segments induce a tension force into the straight segments. Here, the deflection under dead load was reduced by 15 % due to the residual stresses. This effect will be studied in more detail in chapter F1. In the case of the research pavilion, this so-called stress stiffening effect was reduced over time due to relaxation. Therefore, creep and relaxation tests were started parallel to the erection of the pavilion (Figure D.5). In Figure D.6 the results from these tests can be seen, where depending on the amount of bending curvature, a maximum of 50 % relaxation was reached. It was therefore possible to calibrate the residual stress in the Finite Element model to the actual situation of the pavilion structure. Deformation tests with local loading could therefore also evaluate the correlation of the Finite Element Modelling with the physical structure before and after partial relaxation of the residual stresses. The relaxation of the material could also be observed by the remaining curvature in the plywood strips after dismantling the pavilion (see Figure D.9)

Static load test

A static loading test was performed with five 0.18 kN weights hanging in two rows from the apex of the inner arcs. The deformation was measured along two lines, using intersections, with a theodolite (see Figure D.10). These measurements were compared to Finite Element calculations with 0 % and 40 % relaxation as well as fully hinged and stiff connections between the arcs (see Figure D.11). Here, the stress stiffening effect can be seen clearly when comparing deformation at 0 % and 40 % relaxation. Also,

the influence of the connection stiffness plays an important role, showing that neither fully stiff nor fully hinged connections seem to represent the actual structural behaviour. The closest correlation between the FE model and actual measurement is found with 40 % relaxation and stiff connections showing an average of 15 % offset between the two load deflection lines. The stiff connections, however, overestimate the stiffness in load transfer to neighbouring non-loaded arch segments; this phenomenon was also found with the dead load deflection on the entrance area.



Fig. D.7



Fig. D.4 FEM model of the basic coupled arch.

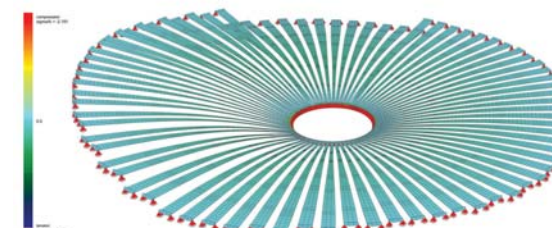


Fig. D.5 Long-term relaxation and creep tests of the birch plywood used in the pavilion.

Fig. D.6 Results from the relaxation tests of plywood bent to various rise to span ratios over the period of 3 months.

Fig. D.7 Paper model of the pavilion structure made from planar laser cut strips.

Fig. D.8 FEM form-finding of the pavilion structure starting with planar strips.

Fig. D.8



Fig. D.9

Structural behaviour

In the initial calculations the stiffness of the multiple connection points between the arches was overestimated. The connection points were strengthened by two wooden wedges feeding in between the plywood strips; this was estimated to be a stiff connection. On site, it was noticed especially that the splitting of the wooden wedges drastically reduced stiffness which led to unexpectedly high dead load deformations. With as many as five connection points per pair of arches and over 200 in total, small slippage in each individual node accumulates to significant deflection of the overall structure. Additional struts were added to the entrance arch to compensate for this.

Material

Initial material tests to evaluate the elastic bending capacity of the plywood strips were made during a humid weather period while the actual construction of the structure fell into a time of extreme drought and heat. This difference in humidity of the plywood led to some cracking at the highly bent components which could be improved only marginally by irrigation since the wood was already sealed. Even though the plywood strips showed significant creep deformation after disassembly of the pavilion (see Fig D.9), it was found that the structure preserved its springback capacity under critical external load. This was proven when a section of the structure was loaded to the point of snap-through buckling and sprung back to its original shape after unloading with only minor damage at the connection points.

Design and construction

Fig. D.9 Remaining curvature in the plywood strips after dismantling the pavilion.
Fig. D.10 Deformation measurements along two lines, using intersections, with a theodolite.
Fig. D.11 Comparing measurements to Finite Element calculations with 0 % (p1) and 40 % (p06) relaxation as well as fully hinged (kp) and stiff (kf) connections between the arches.

The ICD/ITKE Research Pavilion's new structural ideas could be combined advantageously with modern computer based design and calculation methods. As bending-active structures may reach extremely complex geometries based on the nonlinear deformation of post buckling shapes, it is in connection with modern computational design and analysis methods that we may carry this design approach to go beyond the complexity of single layered gridshells, still using the advantage of generating complex curved geometries from linear or planar construction components. In terms of an iterative design methodology, only



Fig. D.10

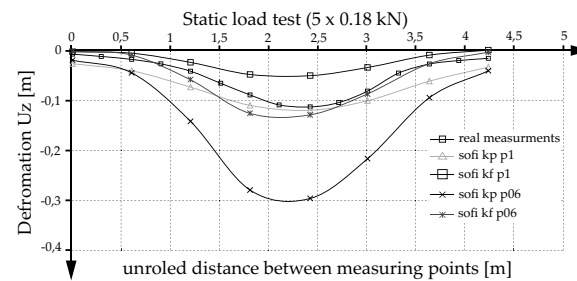


Fig. D.11

one iteration between the computational design model and the Finite Element simulation model was possible, since both were developed newly during the design period. For future projects a closer link and iteration between these models is desirable.

D 1.5 Acknowledgements to the Project Team

The student team included Andreas Eisenhardt, Manuel Vollrath, Kristine Wächter & Thomas Irowetz, Oliver David Krieg, Ádmir Mahmutovic, Peter Meschendorfer, Leopold Möhler, Michael Pelzer and Konrad Zerbe. Responsible for the scientific development were Moritz Fleischmann (project management), Simon Schleicher (project management), Christopher Robeller (detailing / construction management), Julian Lienhard (structural design), Diana D'Souza (structural design), Karola Dierichs (documentation).

The author's personal involvement included conceptualisation of the design studio, FEM form-finding and FEM Simulation, and loading tests.

D2 Permanent Textile Hybrid Structure: Umbrella for Marrakech

In 2011 a new type of membrane structure was developed at the Institute of Building Structures and Structural Design and realised in collaboration with HFT Stuttgart. The project was based on a student workshop that developed shading solutions for an outdoor plaza space at an architecture school in Marrakech, Morocco. The design proposal of a funnel-shaped membrane roof was further developed by the author with the aim of minimizing anchoring forces to the surrounding buildings. The introduction of a bending-active supporting structure for the free edges of the membrane proved to be a very efficient solution. After the successful test setup in Stuttgart, which took place in June 2011, the structure was mounted by students from Stuttgart and Morocco in March 2012.

The project was published and discussed in several conference papers and textile membrane journals. The descriptions below are based on Lienhard and Knippers (2012a).

D 2.1 Project Specifications

The structure features six elastically bent glass fibre rods with a length of approx. 7.5 m. The rods push out three additional corner points on both free edges of the structure. The funnel-shaped membrane has a span of approx. 11 m x 11 m and an eaves height of 5.5 m resulting in a membrane surface of approx. 110 m² (Figure D.15).

The mounting procedure and functioning of the structure was checked through installing the structure on the University campus in Stuttgart. Here, the supports at the sidewalls of the courtyard were replaced by masts and guying cables where the low point was directly anchored to the ground. This setup also allowed for some simple deformation tests with point loads applied to the free corners to evaluate the precision of the Finite Element simulation.

Pre-stress was induced with a special pulling device that could be attached to the arm end. In order to reduce friction in the mem-

Fig. D.12 Temporarily braced umbrella structure during test setup in Stuttgart, Germany.

Fig. D.13 Final installation of the umbrella structure in Marrakech Morocco

Fig. D.14 Detail view of the eccentrically attached GFRP rods.

Fig. D.15 Plan and elevations of the umbrella in its final setting in Marrakech, Morocco. Dimensions in meter.

LIENHARD, J. and KNIPPERS, J. (2012) *Permanent and convertible membrane structures with intricate bending-active support systems*.



Fig. D.12

Fig. D.13



Fig. D.14

brane sleeve, which holds the GFRP rod, during the pre-stressing process and to ensure even stress distribution, the sleeve and rod were treated with silicon spray. In most membrane structures the approximate shape is already reached long before the entire pre-stress is induced. Since the curvature of the beam is largely dependent on the pre-stress of the membrane, it was observed that large wrinkles disappeared abruptly during the final stage of pre-stressing. This may be another indication for the tight interdependence between the bending- and form-active part of the structure.

D 2.2 Form-finding

The form-finding of membrane structures with bending-active support system necessitates a combined form-finding of the form- and bending-active elements (Figure D.16). There are multiple approaches that can be followed to achieve such a combined equilibrium system. The relatively simple geometry of the umbrella allowed the form-finding of the bent beam elements and pre-stressed membrane elements to be calculated in one combined calculation run (see chapter E3.3). In this approach, controlling the stability of the beam during form-finding is difficult, since the stabilising effects, the membrane has on the beam, are only activated in the post-form-finding configurations. This necessitates a re-calibration of the beam stiffness during the form-finding.

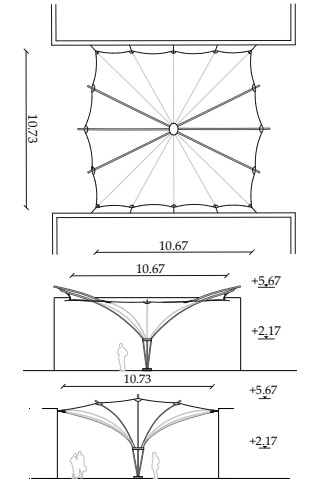


Fig. D.15

D 2.3 Structural System and Behaviour

Positioned in the plane of the membrane, elastic beams are only stabilised in the plane of the membrane and may, due to their

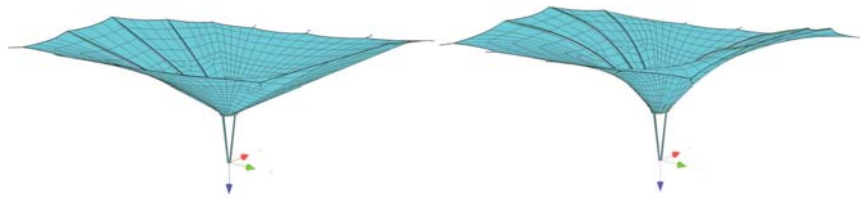


Fig. D.16

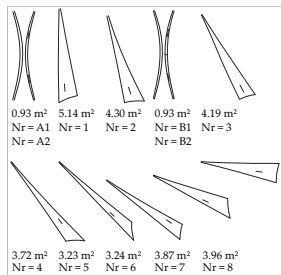


Fig. D.17

elasticity, still fail when snap-through buckling (curvature inversion) is provoked under external loads. Controlling this by adding stiffness to the beam itself is not an option if the beam is to be bent into a significantly curved geometry with sufficient remaining load bearing reserves. A practical solution has been used for several years in the design of camping tents; by attaching the beam eccentric to the surface, a significant rise in stiffness can be observed. The effectiveness of such minimal changes to the overall system was quantified by an FEM comparison of the umbrella with in-plane beams and eccentrically attached beams.

It was found that an eccentric attachment of the beam elements to the membrane could significantly increase the stiffness and prevent failure due to snap-through buckling. The eccentricity was set to be maximal in the middle of the beam and gradually reduced to zero at either end (Figure D.14). A rise of only 1/60 of the span proved to be sufficient to gain significant stiffness in comparison to a system where beam and membrane lay in the same plane (see chapter F.1.4).

Comparison of alternative systems

A critical feature in the development of the funnel-shaped design was the minimization of anchoring forces to the surrounding buildings at its site in Marrakech. In the original design, the free spans across the courtyard between buildings were generated with guying cables, resulting in exceedingly high tension loads at the cables' anchoring points (Figure D.22). The alternative system with actively bent beams within the membrane surface was introduced, replacing the external guying cables and therefore creating an internal shortcut system which cantilevers freely. In Fig D.18 these two systems are compared to a classical umbrella

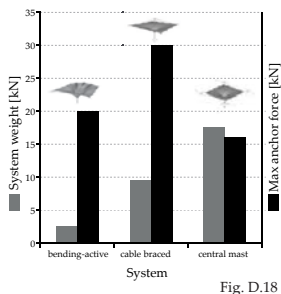


Fig. D.18

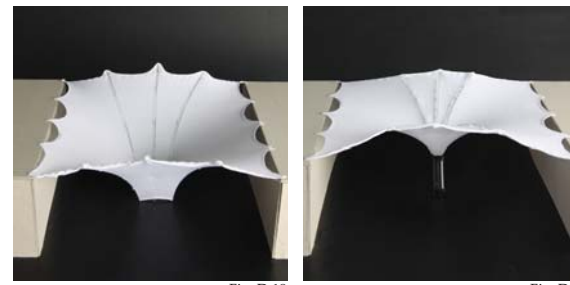


Fig. D.19

Fig. D.20

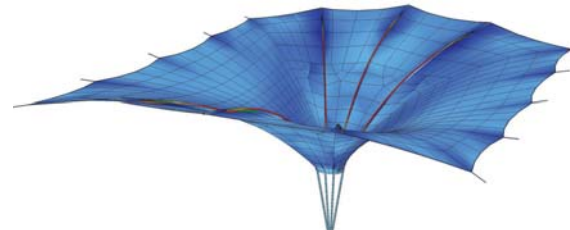


Fig. D.21



Fig. D.22

Fig. D.23

construction. All three systems were simulated with the various loading conditions given for the site in Marrakech and sized accordingly. When comparing the mass and maximum tension anchoring forces of the three systems, the true lightweight potential of Textile Hybrids becomes apparent.

Static load test

The deformation tests with point loads applied to the free corners show very good coherence with the FE model. With a point single load 0.14 kN on the middle arm, a vertical deformation of

Fig. D.16 Combined form-finding of form- and bending-active elements using transient stiffness method.

Fig. D.17 Cutting pattern of a symmetrical quarter of the membrane funnel.

Fig. D.18 Comparison of system weight and maximum anchoring forces of the bending-active umbrella to two alternative reference systems.

Fig. D.19-D.20 Form studies with physical models.

Fig. D.21 Form-found FE model with bending active GFRP rods.

Fig. D.22 Reference system 1 with cable bracings.

Fig. D.23 Reference system 2 with central mast and steel levers.

272 mm was measured (Figure D.25), compared to 288 mm in the FEM analysis (Figure D.24). The maximum deflection difference of less than 4 % is a very satisfying result.

D 2.4 Gained Insights

Structural behaviour

With the cantilevering conditions of the bending-active beams, the system shows very high deflections, especially for wind pressure load cases. While these deflections cause no problems for the ultimate limit strength, they may be of concern for the serviceability of the structure. In the case of the umbrella, no surrounding neighbouring elements could be damaged by the deflecting arms; even for the heavy design winds it was therefore approved to be safe. As a fact, these large deflections even offer additional safety to the structure, since the elasticity leads to a dissipation of forces acting on the structure. It may therefore be concluded that the expectantly high deflections in a Textile Hybrid structure must be studied carefully, yet should be allowed as long as no damage can occur and the system can always spring back into its original state.

The stiffening of the structure with an eccentric attachment of the elastic beams was an interesting finding which will be discussed in more detail in Chapter F.1.4.

Material

The chosen materials are standard marked products with polyester PVC for the membrane and pultruded GFRP pipes for the elastic beams. All metal parts are made of stainless steel, which enables a gluing of the solid milled connection details into the ends of the GFRP pipes using SIKA Bond AT-14 (Polyurethane-Hybrid) glue. A year after construction in Marrakech and after having been exposed to several storms and extreme heat no damage, fatigue or relaxation of the system is reported.

Design and construction

The overall design was already set when the idea of introducing bending-active beams to the project was suggested. The potential for expanding on the formal possibilities of tensile membrane

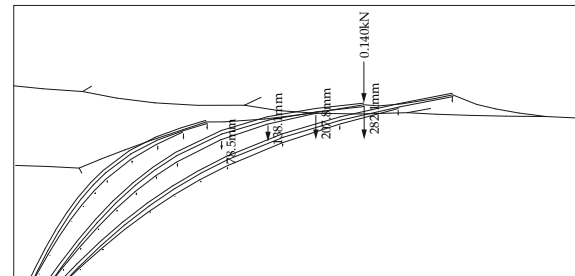


Fig. D.24



Fig. D.25

structures with integrated elastic beams could therefore undergo no further exploration. However, important knowledge was gathered which could feed into the later project of M1 discussed in the following chapter.

D 2.5 Acknowledgements to the Project Team

The work on the Umbrella structure for Marrakech was part of a cooperative student Project with the HFT Stuttgart.

Supervision: Prof. Fritz-Ulrich Buchmann (HFT)

Student team: Selim Alemdar, Christine Anja Göritz, Raphael Klein, Alexandra Siblid (HFT)

Structural design: Julian Lienhard, Antonis Galanis (ITKE Universität Stuttgart)

Construction, detail Design and Manufacturing: Albert Stöcker, Selim Alemdar, Julian Lorenz (HFT)

The author's personal involvement included structural design, FEM form-finding and patterning and FEM simulation, detail design, and construction supervision for test setup.

Fig. D.24 FEM deformation test with 0.14 kN point load on the free edge.

Fig. D.25 Physical deformation test with 14kg point load on the free edge.

D3 Temporary Textile Hybrid Structure: M1

The Textile Hybrid M1 at La Tour de l'Architecte showcases the research on hybrid form- and bending-active structure systems by the Institute of Computational Design (ICD) and Institute of Building Structures and Structural Design (ITKE) with students of the University of Stuttgart and ABK Stuttgart. The scientific goal of the project was the exploration of formal and functional possibilities in highly integrated equilibrium systems of bending-active elements and multi-dimensional form-active membranes (termed "Deep Surfaces"). The resulting multi-layered membrane surfaces allow not only structural integration, but also serve as a functional integration by differentiating the geometry and orientation of the membrane surfaces. The site selected for the design is a historical and structurally sensitive tower in Monthoiron, France. The tower is based on a design by Leonardo Da Vinci from the 16th century, which brought the owners to the idea of making the tower usable for exhibitions. On the basis of a spatial program, a Textile Hybrid system was developed where short-cutting of forces produced a minimization of the loading on the tower. In the context of this project, the M1 was developed as a representative pavilion.

The project was published and discussed in several conference papers and architectural journals. The descriptions here are based on Lienhard et. al. (2013a).

D 3.1 Project Specifications

The Textile Hybrid system was constructed with GFRP rods of diameters ranging from 3 to 24 mm in combination with textile membranes as continuous surfaces and open-weave meshes. The elastic rods gain their stiffness from active bending into curved leaf-shaped modules which are networked into a global structural system. Stress stiffening effects are activated by further deformation of the system through the integration of a pre-stressed membrane surface, and therefore create a fully Textile Hybrid system. The M1 structure is comprised of 110 m of GFRP rods, 45 m² of membrane material covering an area of approx. 20 m², and anchored to the ground with three foundations resting against the existing stone structures which neighbour the tower.

LIENHARD, J. et. al. (2013) *Extending the Functional and Formal vocabulary of tensile membrane structures through the interaction with bending-active elements*.



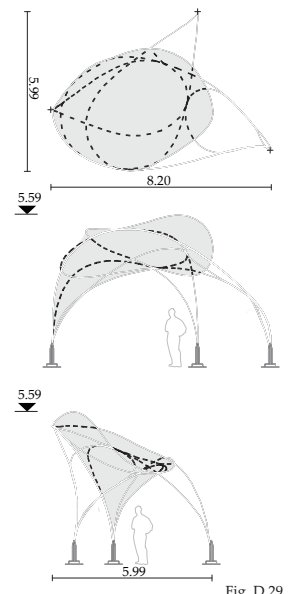
Fig. D.26



Fig. D.27



Fig. D.28



In total, the Textile Hybrid structure weighs approximately 60 kg (excluding foundations), with clear spans ranging from 6 m to 8 m (Figure D.29). The global form orients the structure towards an existing arched wall which once defined a large domed space and also overlaps an area that holds the foundation of one of the tower's buttresses below ground. The longest span of the structure is designed to run across this part of the courtyard, preventing any of the structure from invading the area where the tower foundations sit below.

D 3.2 Form-finding

For generative studies, a spring-based modelling environment developed by Sean Ahlquist was utilised alongside exhaustive physical form-finding experiments. The computational modelling allowed for complex topologies to be developed and altered, quickly registering feedback from the prototypical physical studies (Figure D.30). For the form-finding and analysis of the structure, FEM was utilised. Here, the parameters of the complex equilibrium system were explored to determine the exact geometry and evaluate the structural viability. Based on the previously developed elastic cable approach (see C1.3 and E4.3), the beams were initially straight elements and gradually deformed into interconnected curved geometries, finally being reshaped by the inclusion of pre-stressed membrane surfaces. The geometric data therein was determined initially by the physical form-finding models in defining the lengths and association points on the rods for the topology of FE beam elements (Figure D.32). Given the unrolled geometry and connection points of the rods, it was possible to simulate the erection process and therefore the residual stress in a Finite Element based form-finding process. By means

Fig. D.26 The Textile Hybrid M1: Internal view of multilayer membrane system with integrated cells.

Fig. D.27 External view in the context of the tower ruin.

Fig. D.28 Top view.

Fig. D.29 Plan and side view with basic dimensions and elevations in meter.

of automatic mesh generation, the membrane surfaces were added and a final form-finding of the fully coupled Textile Hybrid was undertaken (see Figure D.34). This form-found structural analysis model allowed verification of the geometrical shape, including its residual stress, as well as analysis of the deformations and stress levels under external wind loads. Furthermore, the form-found membrane surfaces could be processed directly by the textile module of the software for patterning (Figure D.33). Thus, all three design models, the physical and both generative and specific simulation techniques, informed each other in this iterative design process.

D 3.3 Structural System and Behaviour

The structure system of the M1 successfully leaves behind any kind of circumscribed typology and is developed rather from the set boundary conditions into a system that continuously passes from cantilevering to arc and finally, to grid-like conditions. At the macro-scale of the structure, the leaf-like geometries of the rods are interwoven with various lashing and lacing techniques to lock the topology into a rigid frame. These textile-based detailing methods are continued at the base of the structure where the rods are tied into bundles and laced to the GFRP foundation posts. Because of the wind-protected position inside the courtyard and very low snow loads in Western France, this temporary structure could be designed with extremely small cross sectional profiles, which were a necessity given by the design intentions from working with elastically bent closed loops. For the maximal wind pressure and snow load cases, deflections were high enough for the leaves to start touching the existing walls near the foundation points. Such nonlinear support conditions were modelled with compression only springs in the Finite Element model. Structural stability could only therefore be approved.

Fig. D.30 Physical models of the M1: Design study, final design and geometry model for rod topology.

Fig. D.31 Form-found FE model with bending-active rods and pre-stressed membrane.

Fig. D.32 Unrolled geometry of rods A-F with connection points between rods marked in red.

Fig. D.33 Cutting pattern for upper and lower membrane generated in the FE model.

D 3.4 Gained Insights

Structural behaviour

Working with the locally tight bending radii given by the basic leaf topology, would, in cases of higher loading, necessitate a discontinuous cross-sectional sizing. This would be achieved



Fig. D.30

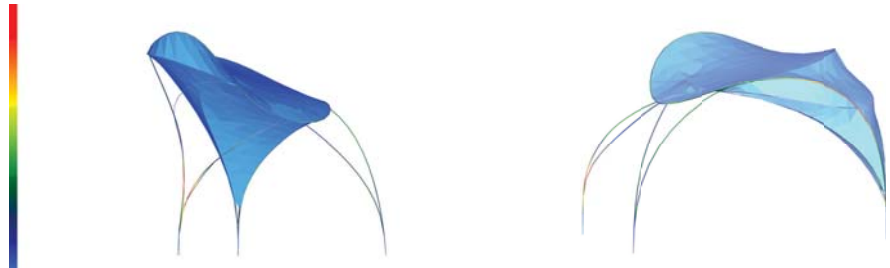


Fig. D.31

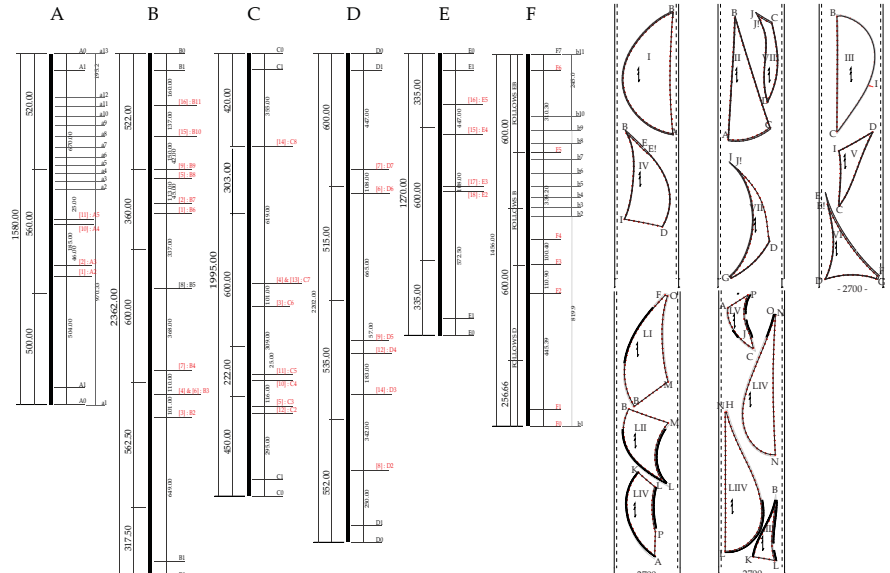


Fig. D.32

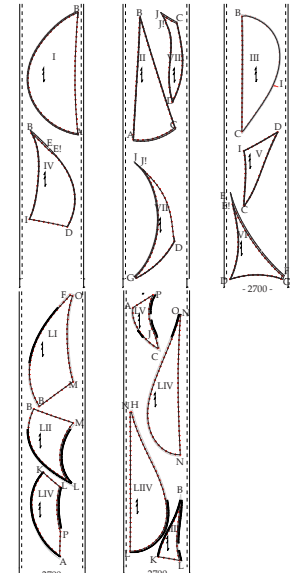


Fig. D.33

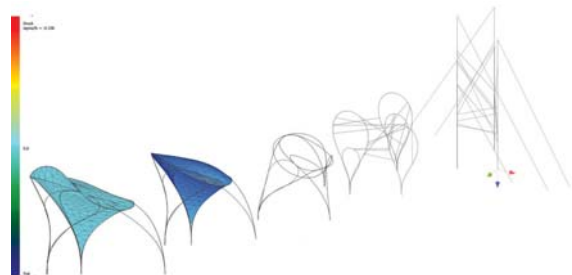


Fig. D.34

by choosing larger and stiffer sections in the regions of smaller bending curvature. Such differentiation in sizing of a continuous element would unfold further potential in the design of bending-active structures and could have greatly contributed to the M1 project. Here, additional stiffness was solely generated by bundling rods wherever they ran parallel. During the construction it became very clear that such bundling can only develop real additional stiffness, if sufficient shear stiffness between the individual elements is established. The simple lacing connections (Figure D.35-36) could not transfer such forces; therefore, carbon fibre belts were laminated around the bundled rods in places of high shear strain such as the large arch in the back of the structure (Figure D.37).

It was found that the equilibrium shape derived from the FEM simulation could, in some places, easily revert into multiple other equilibrium states. This was found in the cantilevering edge of the upper membrane which unveils a true bi-stability. A more critical situation was found in one of the partially horizontal inner rods. Such potential weak points of the structure could have been detected in the FEM simulation by applying various small size asymmetric loads between the form-finding steps to analyse the rigidity of the equilibrium state. On site, some amendments with additional bracings of small bending leaf modules were introduced to stabilise the system. Unfortunately, due to a very tight schedule and delays in the construction phase, no additional loading tests could be performed.

Details

The lacing connections at the crossing points proved to be an excellent and very lightweight connection principle for this type

of construction (Figure D.36). Already, the loading tests in the lab had proven the structural capacity of this joint where failure occurred from constriction of the GFRP pipes and no tearing or slipping of the strings was found (Figure D.35). For the parallel connections however, it is difficult to control the slipping of the connections; here, shrinking tubes were used to maximise friction. For the basic leaf elements, which reach individual lengths beyond 30 m, it was a particular challenge to connect the individual 6 m pieces into a long and continuously elastic rod. Here, a permanent connection principle was developed that consisted of an inner rod glued with flexible two component Sikaflex-553 2K glue. The connection was additionally reinforced by laminating a glass fibre belt around the outside of the connection. This connection proved to work very efficiently for pure bending but had some weaknesses for combined bending and torsion loading, which occurred in one place of the structure that consequently needed additional reinforcement.

Design and construction

The project M1 demonstrates how new types of lightweight structures can be developed when established structural types are overcome for the exploration of fundamental material behaviours in their capacity for balancing minimal material use with multi-functionality. By freely exploring the interdependency of form and force in a hybrid form- and bending-active system, a structure could be developed that overcame restrictions from geometrical grids and distinct structural types.

D 3.5 Acknowledgements to the Project Team

Student Team: Markus Bernhard, David Cappo, Celeste Clayton, Oliver Kaertkemeyer, Hannah Kramer, Andreas Schoenrunner

Scientific development: Sean Ahlquist, Julian Lienhard

Funding: DVA Stiftung, The Serge Ferrari Group, Esmery Caron Structures, "Studiengeld zurück" University of Stuttgart

The author's personal involvement included tutoring, FE-Simulation, FE form-finding and patterning, detail design, and construction supervision.

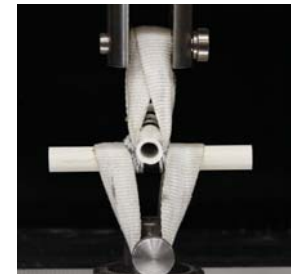


Fig. D.35



Fig. D.36



Fig. D.37

Fig. D.34 FEM form-finding of the Textile Hybrid based on the rod topology given by the physical model.

Fig. D.35 and D.36 standard lacing detail applied at the cross nodes; in a lab test and on site before membrane installation.

Fig. D.37 Bundled rods with carbon fibre belt reinforcement to assure sufficient shear stiffness between the rods

D4 Permanent Adaptive Structure: Softhouse

As part of the international exhibition 'Bauausstellung' IBA 2013 in Hamburg, Germany, architects from KVA MATx team and engineers from Knippers Helbig Advanced Engineering have developed an integral energy-harvesting façade shading system for their 'Softhouse' project. Its overall energy concept includes an energy-harvesting hybrid textile roof featuring flexible photovoltaics, which contribute to the creation of a micro-climate for the building as a shading roof for the terrace and glass façade. This responsive façade is based on a textile-based hybrid system, using textile membranes and GFRP in an intricate form- and bending-active structure. The system undergoes two modes of shape adaptation, tracing the sun horizontally in a daily rhythm and vertically in a yearly rhythm. The form-finding and simulation of the initial system, as well as its shape adaptations and the performance of all positions under wind and combined snow loads, set a particular challenge to the engineering of the project. Multiple design studies were undertaken to develop a system that satisfies the at times diametrically opposed demands from architecture, building physics, structural engineering and technical approval.

The Softhouse project was published and discussed in conference papers and several architectural journals. The descriptions here are based on Lienhard et al (2013b).

D 4.1 Project Specifications

The adaptive façade shading system consists of a parallel arrangement of 32 individual strips which are combined in sets of 8 per housing unit. Each strip is a Textile Hybrid system with a 4 m open mesh membrane attached to a cantilevered 6 m pultruded GFRP board 500 x 10 mm (Figure D.40). Flexible photovoltaic cells are attached to the upper third of the membrane, continuing to the apex of the shape-adaptive GFRP board. In a yearly cycle, the GFRP boards on the roof top change their bending curvature and therefore adjust the PV cells to the vertical angle of the sun, while the daily east-west sun tracking and daylight harvesting is achieved by a twisting of the vertical membrane strips in front of the façade in a range of $\pm 90^\circ$. The membrane strips are at-



Fig. D.38

Fig. D.39

tached to cantilevering GFRP boards which work as compound springs compensating the change in length of the membrane strip through twisting.

D 4.2 Form-finding

The two modes of shape adaption described above can be achieved by various mechanisms. In all cases, a system had to be developed that is able to compensate the nonlinear change in length of the membrane strip due to twisting (Figure D.41 and D.42). An intricate system was developed in which a cantilevering GFRP board works as a compound spring to the attached membrane strips and therefore freely compensates the nonlinear change in strip length during twisting. On top of the roof, the cantilevering board continuously evolves into a bending-active arc system which offers a change in rise and curvature due to the kinematics of the underlying steel structure.

For reasons of enabling a twisting range beyond 180° , a directly actuated system with a turning drive was chosen as shown in Figure D.39.

The form-finding of the continuously shape-adaptive system was divided into several sub routines, starting with a straight GFRP board which is pulled onto its given supports using the elastic cable approach (see chapter E4.3). Simultaneously, uniform pre-stress is assigned to the membrane strips which are coupled to the bent GFRP boards in a last form-finding step where equilibrium and stress distributions are harmonised by an equalisation routine that reiterates the equilibrium of the system

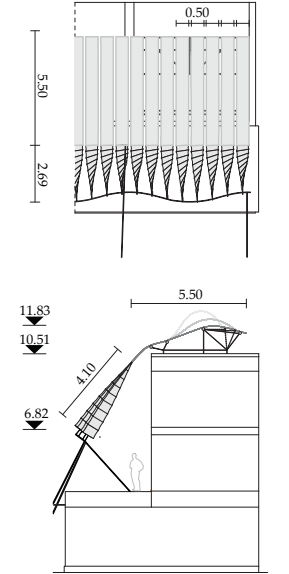
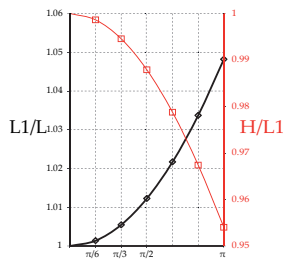


Fig. D.40

Fig. D.38 - D.39 'Softhouse' building at IBA Hamburg May 2013.

Fig. D.40 Plan and side view of the Softhouse facade with basic dimensions in meter.



without additionally applied loads. For the shading system of the 'Softhouse', only the support at the eaves was pre-defined in the geometry. For the other supports only the heights were defined. By attaching the cables to horizontally sliding supports, the form-finding guarantees minimal constraining forces.

For the twisting membrane strips it was important to control symmetry and equidistance of the cross bars. This is difficult to maintain in a simultaneous form-finding with the cantilevering GFRP boards. Therefore, the membrane strips were form-found separately (Figure D.44 b). In a second step the membrane is coupled to an already elastically deformed GFRP board (Figure D.44 c). The subsequent equalising calculation leads only to minimal change in the equilibrium position since the position of the cantilevering beam was already known from previous simultaneous form-finding investigations. In order to include the winter position of the GFRP boards with maximally bent arcs in the FEM model, the kinematics of the steel structure were included to simulate the shape adaptation (Figure D.44 d).

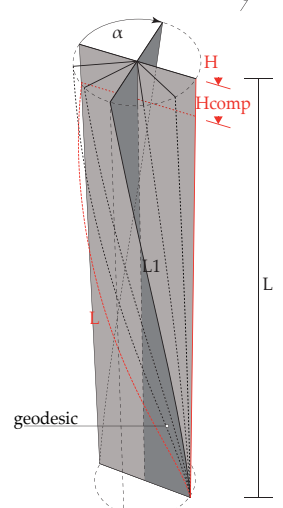


Fig. D.42

D 4.3 Structural System and Behaviour

The varying structural system and shape lead to a highly differentiated load simulation, adapting snow loads according to the varying degree of incline and cp pressure values for the various wind directions to the different twisting positions of the membrane, as well as the inclination of the GFRP boards on the roof. For the safety of the structure, a storm position was defined where the membrane strips are twisted 90° and therefore offer maximum stiffness due to double curvature. In the twisted position, the membrane strips are less susceptible to flagging due to continuously changing cp values along the strip. On the roof top, the winter position of fully bent GFRP boards may only be adopted at wind speeds below 12 m/s.

Overall, the system is characterised by highly nonlinear behaviour which excludes superposition of loads and therefore leads to a very involved and time consuming structural analysis.

Wind tunnel tests were performed to define minimal pre-stress and maximal wind speed in the untwisted position in order to



Fig. D.43

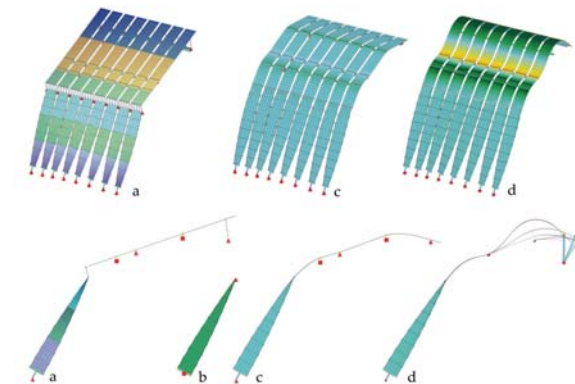


Fig. D.44



Fig. D.45

Fig. D.41 Nonlinear change in length of the membrane strip due to twisting.

Fig. D.42 Geometric relations in a twisting strip.

Fig. D.43 Basic tests of twisting textile membrane strips with physical models.

Fig. D.44 Form-finding sequence of the continuously adaptive shading system.

Fig. D.45 Testing various modes of shape adaptation on the finished structure.

control flagging of the membrane strips (Figure D.46). It was found that 0.3 kN/m pre-stress provides sufficient aerodynamic stability to the twisted membrane strip. No critical flagging is observed in the untwisted configuration for wind speeds up to 10 m/s.

D 4.4 Gained Insights

Structural behaviour

The deflection of the cantilevering boards and the harmoniously pre-stressed membranes show that the form-found geometry and predicted behaviour match the FEM analysis. The commercial context of the project unfortunately did not allow static loading tests for further verification.

Material

Several types of GFRP boards were investigated in the design and pricing phase. Even though hand lamination could be a valid alternative in terms of costs and mechanical properties on paper, comparative 3-point bending tests quickly revealed that stiffness and strength reserves of industrially pultruded GFRP boards are significantly higher than those of the hand lamination. Still, companies will only guarantee permissible stress values that lie in the range 50 % - 70 % of the measured breaking stress. Together with the load and environmental condition dependent safety factors that are additionally applied according to the documents of technical approval, the material safety factors are in a range of 5 to 7 (see also Chapter B3.2).

In the process of approval it was decided to choose a Fiberline product which offers the first GFRP products granted national technical approval (abZ approval) for use in German building projects [Dibt 2012] since 2012. This greatly facilitated the process of individual case approval needed for the membrane system, which would have otherwise included extensive material tests for the GFRP boards.

Design and construction

While the adaptive basic system of twisting membrane strips and bending-active GFRP board displays a high degree of struc-



Fig. D.46

tural and functional integration, its connection to the building structure could not be resolved in a continuously logical manner. Continuing changes to the function and design of the adaptive shading system could not be fully iterated with the already set design of the housing units. This is a common challenge in a typical design process, which becomes very apparent in this project and highlights the necessity for simulation techniques that can be included more quickly and easily in the design process. Overall, the project was able to prove that GFRPs in the unconventional context of a hybrid bending-active system can be realised within the strict rules of German building codes and individual case approval.

D 4.5 Acknowledgements to the Project Team

Architect: Kennedy & Violich Architecture, Ltd

Structural Engineer: Knippers Helbig Advanced Engineering

The Soft House design team also includes G2 Landschaft (Hamburg), Buro Happold MEP (Berlin) and the Soft House manufacturing consortium is Textilbau GmbH (Hamburg), Holzbau Merkle (Bissingen)

The author's personal involvement as freelance engineer for Knippers Helbig Advanced Engineering included conceptual and structural design of the adaptive façade system, FE Simulation, and FE form-finding and patterning.

Fig. D.46 Wind tunnel tests of twisted and planar membrane strips (Wacker Ingenieure - Wind Engineering).



Fig. D.47

D5 Elastic Kinetic Research Demonstrator: Flectofin®

The focus of the Flectofin® project is the optimisation of deployable systems in architecture using bio-inspired solutions. The development of a basic functional mechanism necessitates a process of creativity and/or inspiration. In the last decade, the use of nature as an inspirational source to solve technical problems has become increasingly recognised, leading to the field of biomimetics having become a recognized science. The Flectofin® uses these principles and is based on the sophisticated pollination mechanism of *Strelitzia reginae*, a South African plant which is evolutionarily adapted to bird pollination, also known as the 'Bird of Paradise' flower (Figure D.47).

The Flectofin® project was published and discussed in many conference papers and several scientific journals, augmented by a large number of articles in print and online journals. The descriptions here are based on Lienhard et. al (2010a) and Lienhard et. al (2011b).

D 5.1 Specifications

The Flectofin® principle suits a wide range of applications, from small-scale microsystems to large-scale architectural building components. Exemplary, it is used for the conceptualisation of an adaptive façade shading system (Figure D.48 and D.49). The bending of the fin can be induced by eccentric displacement of a support (Figure D.50), while on-going research is developing a bending actuator that works on the basis of temperature deformation or alternatively an integration of shape memory nithinol wires in the laminate. The fins allow for opening angles ranging from -90° to +90°. Basic dimensions of the system are given in Figure D.50.

D 5.2 Form-finding

Form Inspiration

The compliant mechanism of the Flectofin® is based on the *Strelitzia reginae*, a South African plant which is evolutionarily optimised for weight transfer of birds [Rowan 1974]. The flow-

LIENHARD, J. et al. (2010) *Form-finding of Nature Inspired Kinematics for Pliable Structures*.

LIENHARD, J. et. al. (2011) *Flectofin: a nature based hinge-less flapping mechanism*.



Fig. D.48



Fig. D.49

er-bird-interaction comprises a reversible deformation which enables a so-called valvular pollination mechanism. The flower features a protruding perch of two adnate, blue petals which act as a landing platform (Figure D.51 (a)-(c)). When the bird lands on this structure to reach the nectar at the base of the flower, its weight causes the perch to bend downwards (Figure E.51 (b),(c)). This bending triggers a sideways flapping of the petal laminae, and the previously enclosed anthers (male sexual flower parts) are exposed so the pollen can be attached to the birds feet and chest (Figure E.51 (c),(f)). When the bird flies away, the open perch resets to the protective closed state again due to its elastic properties. A section through the perch was prepared by biologist and research partner Simon Poppinga which reveals a monosymmetric build-up (Figure E.51 (d),(f)). There are three reinforcing lateral ribs on each side, which are loosely connected by thin petal laminae. The lower ribs are joined on a cellular level, thus forming a composite rib. The uppermost ribs carry the thick wings which cover the sheath cavity when it is closed. The ribs consist mainly of fibrous tissue with vascular bundles, hence relative rigidity, and serve mainly to carry the bird's weight [Endress 1994]. A constricted zone seen in a microscopic section between the upper ribs and wings shows no fibrous tissue, which indicates higher flexibility in comparison to the surrounding zones, enabling the elastic sideways bending of the wings (F in Figure E.51 (e)). This kinematical system was verified by rebuilding it as a physical model that demonstrates similar adaptive behaviour (Figure E.52.)

The mechanism in *Strelitzia reginae* seems to exploit the potential of an unsymmetrical bending motion as an integrative part within a reversible deformable structure with multiple deflected

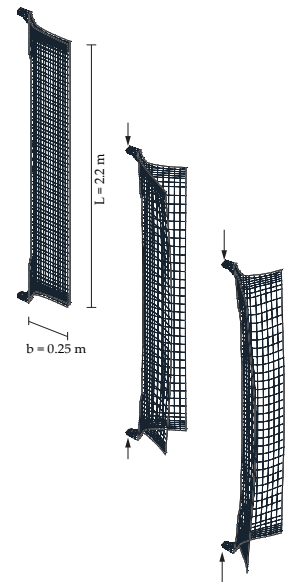


Fig. D.50

Fig. D.47 South African Male Southern Masked-Weaver pollinating *Strelitzia reginae* (Photo Ruslou Corts).

Fig. D.48 Façade Mock-up with three Flectofin lamellas with various degrees of opening.

Fig. D.49 Close-up view of the fully actuated Flectofin lamellas.

Fig. D.50 Basic actuation principle and dimensions of the Flectofin lamella.

ENDRESS, P.K. (1994) *Diversity and evolutionary biology of tropical flowers*

equilibrium positions. The Flectofin® principle is thus an instrumentalisation of this failure mode. This highlights how nature and engineering differ in problem solving and shows that the structures and principles identified in biological concept generators can provide impulses and innovative means to achieve elastic kinetics in technical structures in a previously unknown manner. In the second level of abstraction, the Flectofin® principle is converted into several possible structural configurations, one of which are shown in Figure D.50. The beam element, for example, can be supported as a cantilever or single span beam as well as any other structural system in which continuous bending can be induced. In the wing of the Flectofin®, the stiffness near the backbone is increased. This is a major difference to the *Strelitzia reginae* which shows a distinct localised area of high flexibility near the rib. By stiffening the region near the backbone, the entire wing is forced into a more uniform bending deformation. Therefore, the bending radius is largely increased which reduces bending stress and stabilises the wing in all positions against wind induced deflections.

From an engineering perspective, the flapping mechanism in *Strelitzia reginae* can be described as a hinge-less movement, in which an external mechanical force (the weight of the bird) initiates a complex deformation of multiple structural members (ribs, laminae and wings). They are linked in such a way that the kinetically stored elastic energy can reset the system so that this mechanism is not only reversible but also repetitive. The actual mechanism behind this movement is known to engineering as lateral torsional buckling, a failure mode that is attempted to avoid by sizing structural members to adequate stiffness or introducing eccentricities as shown in the physical models in. The models of a suspended bridge in Figure D.53. show lateral buckling for the upper system where all hinges are in a line. For the lower system eccentricity leads to stability and thereby avoidance of sideways tilting of the cable bracings when the main beam is starting to flex. What is known as a failure in engineering is thus instrumentalised by the plant for a highly effective compliant mechanism.

Form Optimisation

An important question in the development of the Flectofin® was the reduction of stress peaks at the transition of a semi-elastic

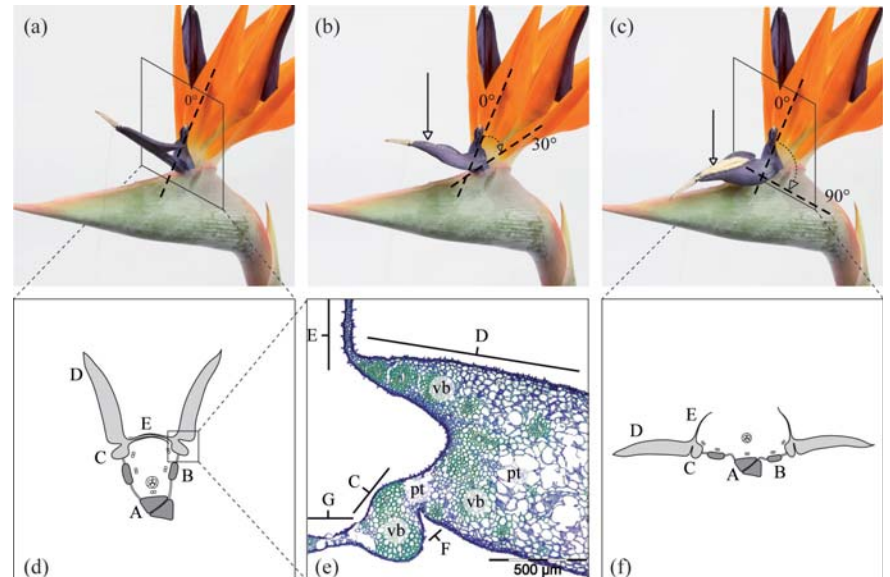


Fig. D.51

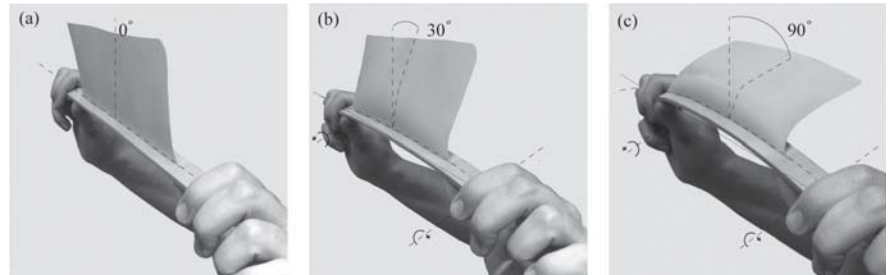


Fig. D.52

Fig.D.51 The elastic deformation in the *Strelitzia reginae* flower.(a)–(c) the investigated flower. When mechanical force is applied (as indicated by an arrow in (b) and (c)) the sheath-like perch opens; (a), (d): closed state, (c),(f): open state. (d),(f): schematic drawings of sections through the perch; A: composed lower ribs, B: middle ribs, C: uppermost ribs, D: wing, E: Flange.(e): section through uppermost rib (C) and lower wing (D); vb: vascular bundles, pt: parenchymatous tissue, F: constricted zone between uppermost rib and wing G: lamina.

Fig. D.52 Abstraction of the deformation principle in the flower of *Strelitzia reginae*, realised with a simple physical model. Bending the backbone (here by hand) causes the attached lamina to deflect up to 90° sideways, initiated by lateral-torsional buckling (b) to continue as unsymmetrical bending (c).

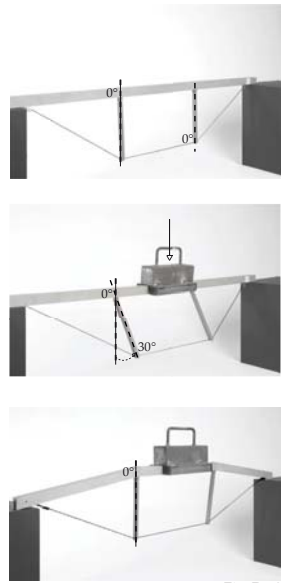


Fig. D.53

D.53 Models of a suspended bridge showing lateral buckling for the upper system where all hinges are in a line. For the lower system eccentricity leads to stability and thereby avoidance of sideways tilting of the cable bracings when the main beam is starting to flex.

shell element to a beam element. ‘Biological solutions’ to this particular problem are found in many plant species. Being exposed to wind or other forces, plant leaves have developed several strategies to avoid notch stresses in the transition areas from leaf lamina to petiole. The most common solutions are based on gradual transitions achieved through changes in fibre orientation, variable thicknesses and optimised contour lines. In the Flectofin®, the change of thickness and fibre orientation within the shell element enables a stress harmonisation throughout the entire surface (Figure D.54 a and c). This was made possible by increasing the stiffness in the shell element at the transition to the beam element. Hereby, the bending is forced further into the surface, leading to larger bending radii and, consequently, smaller stresses. Remaining notch stresses on either ends of the shell element were reduced by optimising the contour line. Figure D.54 b shows how the contour geometry of *Eucalyptus spec.* leaves were applied to the shell geometry. The stress peaks were considerably reduced by this application of tension triangles [Mattheck and Burkhardt, 1990)]. These geometrical optimisations reduce the maximum notch stress to approximately 60 % of the permissible stresses for standard GFRP.

A further development to stabilise the inactive position is shown in Figure D.55 A-E, with a configuration of two wings that theoretically interpenetrate in pos. A. Therefore, they rest in pos. B where they push against each other and share a large contact area which highly increases their stability. Due to their concave curvature in the inactive state, the wings will bend outwards when the backbone is actuated as shown in pos. B-E. As a positive side effect of the symmetrical deformation, the eccentric forces in the backbone are induced by the bending of the wings counteracting each other. This limits the torsion in the backbone and results in a more filigree profile. This double Flectofin® is a further development of the initially proposed façade component, which has an increased shading efficiency and higher wind stability.

D 5.3 Structural Behaviour

The compliant mechanism of the Flectofin® is described as systematised failure and deformation. More specifically, uniaxial bending of the beam causes an unsymmetrical bending motion of

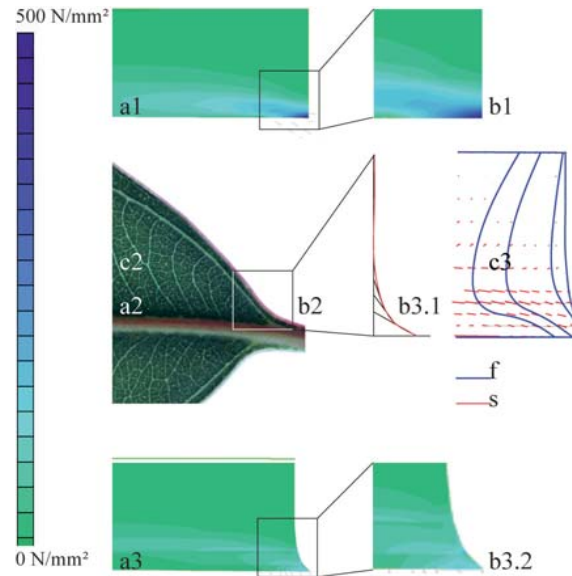


Fig. D.54

the shell element which is triggered by torsional buckling. Such instability is observed in beams with slender profiles exposed to in-plane bending. When the bending reaches a critical point, the beam undergoes a combined deformation involving both out-of-plane bending and torsion [Simitses and Hodges 2006]. While lateral-torsional buckling is usually initiated on the compression side of a beam, in the case of the observed system, the compression side is reinforced by the backbone and held by the supports; consequently, it is the tension side that is deviating into out-of-plane bending due to its low lateral stiffness. This coupled deformation of torsion and flexion is also referred to as warping.

D 5.4 Gained Insights

Structural behaviour

While the FE simulation with perfectly symmetrical geometries and consistent mechanical properties suggests the existence of a robust mechanism for both the single as well as the double Flectofin®, the usual discontinuities from manufacturing caused some unpredicted behaviour in the elastic kinetics of the sys-

Fig. D.54 Reduction of stress concentrations using the contour geometry of a *Eucalyptus spec.* leaf. a1: high stress at the transition to the backbone, a2: thickening of the leaf at the transition to the rachis a3: stress reduction due to additional material in this zone. b1: high notch stress, b2: contour line of *Eucalyptus spec.* leaf, b3.1: abstraction of contour line using tension triangles, b3.2: reduction of notch stress up to 90 %. c2: leaf venation of *Eucalyptus spec.* c3: placement of reinforcement fibres (f) according to principle tensile stress lines (s) and leaf venation.

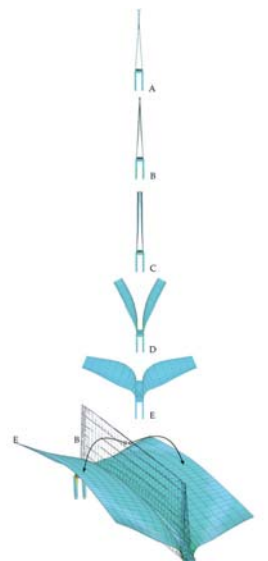


Fig. D.55

Fig. D.55 Simulation of a double Flectofin®, A: theoretical position of the planar wings, B: real position of the wings pushing against each other, C-F: opening of the wings due to bending of the backbone.

tem. A long period of optimising the manufacturing technique and adopting the geometry for a more robust mechanism was needed to guarantee a functioning of the compliant mechanism. Specifically, the curved attachment of the thin-shell wings to the backbone stabilise the mechanism into a set unfolding direction. In the case of the Flectofin®, this logic of curved line folding was discovered accidentally from manufacturing tolerances but is understood as a key to the function of the mechanism because of parallel investigations of other plant movements such as the Aldrovanda discussed by Schleicher et. al. (2011).

Material

The system's inherent material requirements for high strength and low bending stiffness are most adequately fulfilled by FRPs. After a comparison of different high modulus fibres, glass fibres were selected because they are much cheaper than carbon fibres, more translucent, and have a better weather resistance than aramide fibres, for example. Many different glass fibre woven fabrics and non crimp fabrics that differ in their fibre lay-up and area weight were tested for stiffness, resistance against wind induced vibration, and the 90° bending properties near the base of the backbone. So far, the desired high strength and low stiffness properties were achieved by arranging 4-8 very thin plain woven fabrics with an area weight of 80 g/m² in a set of layers (Figure d. 56 and B-D in Figure D.57). In order to further reduce tension forces at the edges of the fin, in particular at the meeting point of the wing and the backbone, glass rovings were spread out along the direction of forces (F in Figure 57). For the matrix, an ultra-flexible epoxy resin was chosen that was additionally treated with several dyestuffs to satisfy diverse optical demands. In order to achieve the essential high quality in the laminate, the Flectofin® was fabricated by a manufacturing method called the vacuum bagging process (VAP). A special layer of air-permeable foil is used to eliminate trapped air in the laminate, thus, enhancing the material's largely dynamic properties. This manufacturing technique was one of the keys to a successful production of immaculate and mechanically consistent elements.

Design and construction

One of the main advantages of the Flectofin® is the diversity of structurally stable positions which the structure can attain be-

tween fully opened and closed. The system is thus adaptable to different boundary conditions which could optimise efficiency in shading systems. A significant expansion of possible future applications is given by the fact that the system functions without a straight turning axis; it can therefore be adapted to facades with curved geometries. (These aspects of the Flectofin® and other biologically inspired compliant mechanisms are studied elaborately in the Doctoral thesis of my colleague S. Schleicher "Bio-inspired Compliant Mechanisms for Architectural Design")

As a proof of this concept, it inspired the façade of the Thematic Pavilion at the EXPO 2012 trade-fair in Yeosu, Korea, by Soma Architects and Knippers Helbig Advanced Engineering (see Figure C.28. Knippers Helbig Advanced Engineering was then commissioned with the planning and constructional design of this kinetic facade. In a first investigation, it was determined whether the Flectofin® principle could be magnified to the large scale of 108 lamellas with varying heights between 3 m and 14 m. It was proven that up-scaling of the basic principle is possible, yet could not entirely fulfil the architectural intentions of the facade. Inspired by the Flectofin®, an alternative elastic mechanism was developed, based similarly on structural failure (buckling). These further developments show the potential for such basic discoveries, in this case, the instrumentalisation of failure and deformation.

D 5.5 Acknowledgements to the Project Team

The work on the Flectofin Project is supported by the funding directive BIONA by the German Federal Ministry of Education and Research. The research team included Simon Schleicher (ITKE), Simon Poppinga (PBG) Tom Masselter (PBG), Lena Müller (ITV), Julian Sartori (ITV) and the company clauss markisen.

The author's personal involvement included management of the research project, abstraction of the biological role model, Finite Element simulation and optimisation, planning and supervising of the prototype productions.



Fig. D.56

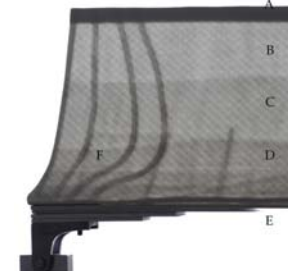


Fig. D.57

Fig. D.56 Fabrication with multiple layers of woven glass fibre and lamination with vacuum bagging process (VAP).

Fig. D.57 Thin walled laminate for a Flectofin®. A: edge reinforcement. B-D: stepped laminate with 4 to 8 layers. E: backbone made of a GFRP pultrusion profile. F: enclosed force distributing glass rovings.

D6 Reflection on the Role of FEM in the Design Processes

The case study structures exhibit various degrees of integration of Finite Element Methods in the design process. While FEM is used for form-finding and structural analysis in all cases, its integration in an iterative design methodology varies.

In Figure D.58 the design methodology of each case study project is illustrated on the basis of a process diagram which includes design phases and modelling environments. The general layout of these diagrams as well as the inclusion of search regions in the early design phases is based on the iterative design process diagrams by Rittel (1982). Rittel talks about the creative act that lies between the collection and analysis of information and the synthesis, leading into the execution and communication of the result. When analysing the process diagrams in Figure D.58 two moments of creativity become visible in the design of a bending-active structure. The first is situated in the beginning of the process and mostly uses physical modelling as a quick but materially informed method of funnel management to create the basis of a physically feasible system from an infinite room of possibilities. The second moment lies between the form-finding and the structural design phase, where adaptations and specifications in the design are made to enable the construction phase. Here, Finite Element Analysis processes information between the form-finding and structural design phase and thereby becomes part of the actual design phase rather than a mirroring instrument to parallel check feasibility of a decision taken in other modelling environments. This integration of FEM in the creative process of a design methodology requires a setup of bidirectional information flow to enable fast iterations in the creative design phases.

The research pavilion 2010 marks the beginning of this study and therefore tools were not developed far enough to adequately integrate FEM in the general design process. FEM then remained in a somewhat classical parallel path, securing structural analysis, material definitions and sizing of elements.

In Textile Hybrid projects like the Marrakech umbrella, the M1 and the Softhouse the continuous mechanical description of the form-finding and analysis model is of particular importance,

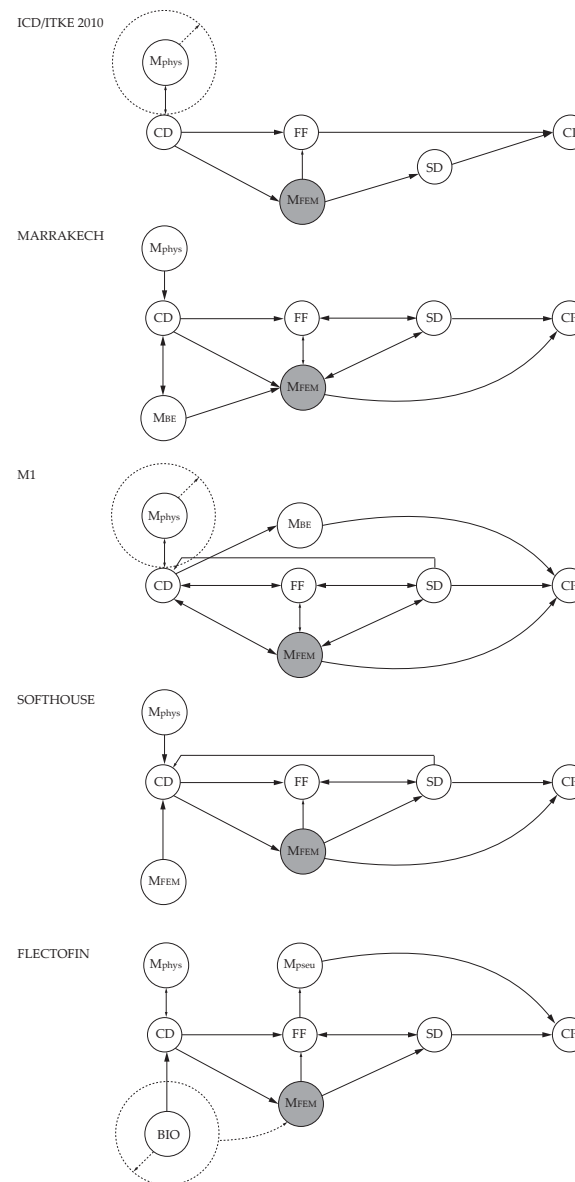


Fig. D.58 Design methodologies applied to the case study structures with focus on the role FEM took in the process.

Design Phases:
CD: Conceptual Design
FF: Form-finding
SD: Structural Design
CP: Construction Plan

Modelling environments:
Mphys: Physical model
MFEM: Finite Element Modelling
MBE: Behaviour based computational modelling
Mpseu: Pseudo rigid body model
BIO: Biology

Fig. D.58

since it enables the generation of the cutting patterns of the membrane and the exact length of the bending-active elements directly from the FE model. This aspect is indicated in Figure D.58 by showing the direct flow of data from the FEM model to the construction plans. The importance of directly linking form-finding to subsequent structural analysis will be discussed in further detail in chapter E. The largest degree of integration is achieved in the M1 project where the FE model becomes a central part of a fully iterating process.

The search space for the Flectofin® is in biology. Building physical models is therefore part of an abstraction process of a principle already found, rather than the creative process in itself. FEM is then used to fathom the understanding of the mechanism by offering a look inside the mechanical behaviour. On the basis of pseudo rigid body models a parallel modelling environment could be set up, allowing to explore the geometric boundary conditions of the Flectofin® principle more freely. This geometric definition was based on the behaviour found from FEM and may be used to generate the starting geometry of various parametric conditions for a precise FEM form-finding and analysis (See also E3.3).

The design methodologies were developed further through each case study project, intending to find ways of integrating the Finite Element Analysis more interactively in all phases of the design. The individuality of each project however also requires adaptations of the design methodology beyond what is already developed. Therefore, no generally ideal process can be defined, but rather an ideal degree of interaction between the modelling environments, which themselves are chosen specific to the project.

D7 Reflection on Structural Typologies Presented by the Case Study Structures

If the attempt is made to summarise and describe the structures presented in this chapter on the level of structural typologies the descriptions could be phrased as follows:

- The research pavilion ICD/ITKE is composed of 5-hinged arcs.
- The Umbrella Marrakech is a hybrid, featuring post-buckled compression rods.
- The M1 Project is a hybrid, composed of rigidly fixed arcs-, cantilever- and gridshell typologies in one continuous system.
- The adaptive shading system of Softhouse continuously evolves from a one hinged and one sided rigidly fixed arc into a cantilever and furthermore a form-active membrane strip.
- The Flectofin®, upon actuation, deveates sideways due to lateral torsional buckling and thereby gradually changes from a beam type element to a beam supported warping shell.

Such attempts to describe the case study structures with the concept of structural typologies are, if anything, restrictive, and in some cases, like a 5-hinged arc, a post-buckled compression rod and lateral torsional buckling, suggests the imminent failure of the system. While this supports the definition of bending-active structures made in B1.2, it also raises the question on which level they belong to a common family at all. What is their common denominator? For now it can be summarised that they raise the same questions. How is a system designed and form-found that relies on the physical behaviour of elastic deformation, and how does the resultant residual stress state influence its structural capacity and behaviour? The two following core chapters of this dissertation are dedicated to these questions and will analyse them with both abstract structural models as well as the case study structures themselves.



E Form-finding and Simulation

E1	Variables of the Form-finding Process	104
E2	Form Development	106
E 2.1	Physical Models	106
E 2.2	Developments Beyond Types	109
E 2.3	Scaling of Material Behaviour	110
E 2.4	Generating Data for Subsequent Form-finding Steps	110
E 2.5	Form Inspiration for Elastic Kinetics	111
E3	Analytical Approximation	113
E 3.1	Similarities	113
E 3.2	Mechanical and Geometric Equivalent Systems	115
E 3.3	Geometric Equivalence	116
E4	Computational Form-finding	118
E 4.1	Advantages of Finite Element Method	118
E 4.2	Incremental Load Steps	120
E 4.3	The Elastic Cable Approach	125
E 4.4	Form-finding of Textile Hybrids	127
E5	Validation of FE Simulation	130

E Form-finding and Simulation

Form-finding is generally understood as the process of developing the geometric form of a structure based on mechanical behaviour. In contrast to a common design process, form-finding is a deterministic process in which the setting of the physical boundary conditions leads to a single solution. From a strictly mechanical point of view, form-finding can be defined as an optimisation process, in which a target stress field is given and the corresponding geometrical form is searched for. Therefore in structural engineering, the term form-finding is mostly linked to tensile membrane structures, as well as catenary arches and shells, in which form-finding automatically includes form-optimisation based on structural behaviour. The geometry of bending-active structures has to be form-found similarly based on mechanical behaviour; however, stresses belong to the solution and therefore 'form-finding' does not automatically include the aspect of structural optimisation. Beyond the definition of boundary constraints, the 'form-finding' of bending-active structures involves the adjusting of more variables which include setting the length and mechanical properties of the bending-active elements and introducing various couplings and inner constraints. It may therefore be more precise to speak of a 'form-developing' process. However, despite having more variables of physical boundary conditions, it is still a deterministic process, objectively based on mechanical behaviour, and shall therefore generally be referred to as 'form-finding'.

This section will introduce various approaches to the form-finding of bending-active structures and the necessity of their interaction.

E1 Variables of the Form-finding Process

The design process of bending-active structures can be summed up as an aligning of mechanical and geometrical variables to generate a structurally and architecturally functioning result from a physically informed deterministic form-finding process. Similar to membrane structures, the built geometry is a result of the erection process, where the structure is tied to its boundary points.

The self-defining shape of the structure is previously discretised by a cutting-pattern in the case of a membrane and the unrolled geometry in the case of a bending-active structure. In contrast to membrane structures, the form-finding result does not automatically define a structurally sound system which may be linked to the fact that bending-active structures offer far more variables which influence the form-finding result. The list below shows the governing design variables in comparison to form-active structures:

	Bending-active	Form-active
Geometric		
Boundary points and edges	input	input
Length and surface dimension	input	output
Sectional dimensions	input	not considered
Surface/element curvature	output	output
Mechanic		
Material stiffness	input	not considered
Stress	output	input
Sum of input variables	4	2
Sum of output variables	2	2

The fundamental differences in the form-finding of form- and bending-active structures lie in the definition of length and surface dimension, the simulation of material behaviour and the consideration of residual stress:

- In form-active structures, the surface dimensions are the minimal result defined by the stress state and boundary conditions which are independent of their input dimensions. In terms of material behaviour we simply consider the fact that a membrane serves only to carry tension forces by simulating a surface under pure tension. The actual mechanical material properties of the membrane, however, are not considered since the form-finding is purely based on the equilibrium of tension forces and only geometrical stiffness is considered. Residual stress is a target input.
- In contrast to this, the form-finding of bending-active structures



Fig. E.1



Fig. E.2



Fig. E.3



Fig. E.4

is largely influenced by the length of a beam or dimension of a surface that is bent as a result of the constraining boundary conditions as well as the mechanical behaviour of the beam or shell elements. While the geometry of a single and homogeneous elastica curve is independent of size and material, the structurally necessary coupling of several bending-active components results in a material dependent geometry. Residual stress is part of the solution.

Having doubled the amount of input variables in the form-finding process of bending-active structures, as opposed to form-active structures, opens room for exerting architectural influences and thereby noticeably complexifies the general design process. Putting these input variables into a functioning relation, which satisfies both mechanical behaviour and architectural specifications, becomes the challenge and potential of this form-finding and the general design process. Because of this unique combination of freedom and complexity, it is found that a computational simulation technique alone does not offer necessary tools for developing bending-active structures. The combination and integration of various modelling techniques into a design process are necessary to successfully develop complex bending-active structures. These include physical, behaviour based, computational and Finite Element based modelling, which will be discussed in the following chapters.

Especially when considering elastic kinetics, the question of a starting idea for a compliant mechanism is possibly the most critical point of the design process. Here it was found that the abundance of biological organisms offers a great source of inspiration. This potential was used in particular for the Flectofin®, introduced in Chapter D5.

E2 Form Development

E 2.1 Physical Models

A physical structural model as a means for structural analysis has lost its significance since the invention of analytical structural engineering and computational mechanics. With today's pow-



Fig. E.5



Fig. E.6

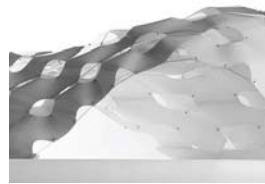


Fig. E.9



Fig. E.8



Fig. E.7



Fig. E.10

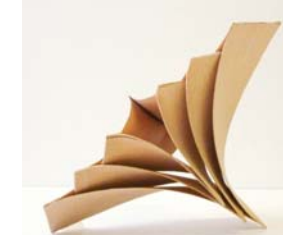


Fig. E.11



Fig. E.12

Fig. E.1 - E.12 Physical model studies made by students at the University of Stuttgart in various workshops and classes taught by the author.

Fig. E.1 - E.4 Basic bending-active components. (Diploma Thesis D. Sommer)

Fig. E.5 - E.8 Basic Textile Hybrid components. (Students from the M1 Project)

Fig. E.9 Bending-(Re)active plates shell (studio A. Schönbrunner, N. Haberbosch)

Fig. E.10 - E. 11 Arrays of bending-active components. (Students from the design class 'bend it')

Fig. E.12 Elastic kinetic component based on the Finray® effect. (Diploma Thesis M. Vollrath and A. Eisenhard)

erful computational means, the necessity for structural physical models has been reduced to some dynamic problems, e.g. wind tunnel testing [Harris and Sabnis 1999].

Physical form-finding models were of great importance to the development of lightweight shell and membrane structures that emerged around the 1950's. The form-finding methods at the time were purely experimental. Photogrammetry or other analogue measurement methods were used to transfer the form-found geometries to the planning process. Bending-active grid-shells which were developed around the same time were often form-found based on hanging models (see C2.2).

While computational form-finding methods have rendered possible a fully digital planning process, physical form-finding is still used in the conceptual design phase of tensile membrane structures. Only a few years ago, membrane engineers would still recommend a working method that starts with physical models and uses computational form-finding once the general definitions are made. In today's praxis however, the advanced graphical interfaces and interactive simulation possibilities have made physical models rare in the design and development of membrane structures. The computational means for simulating bending-active structures, however, have not been developed as far. Here, physical structural models have preserved their importance as a form-finding tool in the early design stages. Output from such experimentations serves to provide topological data where more precise geometric and mechanical behaviour can be explored computationally. The great potential of developing elastic kinetics via physical model studies was shown in the dissertation of former ITKE colleague Dr. Reza Matini (2007).

E 2.1.1 Interaction and Short-Cutting

The instant feedback of mechanical behaviour is possible with the construction of a physical model and is indispensable in finding ways for short-cutting forces in an intricate equilibrium system. Holding an elastically bent element in your hands directly shows the spring back tendency of the system and therefore holds information for the position and direction of necessary constraints.

HARRIS, H.G. and SABNIS, G.M. (1999) *Structural modelling and experimental techniques*.

MATINI, M.R. (2007) *Biegsame Konstruktionen in der Architektur auf der Basis bionischer Prinzipien*.

Allowing for slippage in the interlocking points of a computational analysis model with discrete nodes is very difficult; in physical models, interlocking points may easily be moved or built, allowing slippage. Therefore complex but harmoniously stressed equilibrium systems may be found.

As an initial effort in design exploration of Textile Hybrids, physical form-finding enables the development of geometries for the interaction of pre-stressed membranes and configurations of bending-active elements. Output from such experimentations serves to provide topological data for further computational simulation.

E 2.2 Developments Beyond Types

In chapter B1.1 the concept of bending-active structures as an approach rather than a distinct structural type was introduced. If, consequentially, we may not draw from a set of predefined solutions, such freedom leads to the question of an adequate methodology for a structurally informed design process. In the projects presented in section D, the work with physical models plays a key role in the conceptual design phase. In the case of the research pavilion ICD/ITKE, and even more so the M1 project, physical models became the basis for extended design explorations.

Working with physical models allows for an instantaneous and intuitive change of the input variables to an immediate form-finding result. This synchronicity offers indetermination in the design process with physical form-finding models yet stays within mechanical feasibility. In the creative process of building physical models, basic principles for short-cutting forces and coupling smaller units into larger structural systems are easily unveiled because of the instant mechanical feedback from the model. The process, often unintuitive due to the complexity of form-force relationships, therefore enables exploration of diversity in form not restricted by a delimiting catalogue of types. Once a principal system is developed, the variation of length and surface dimension allows the fine tuning of geometry and structural interaction. No other modelling environment, other than physical model building, allows working with this variable so easily.

Figures E.1-12 show a set of design models which all feature fully shortcut bending-active systems. The studies offer prototypical solutions of topological arrangements for the interconnection within networks of bending-active elements in combination with form-active textiles.

E 2.3 Scaling of Material Behaviour

Substantial for the exploration of bending-active structures is the fact that the geometry of uniform singular elements is independent of material behaviour and scale (see Elastica B2.4). Comparative physical form-finding experiments may therefore initially be carried out at various scales. However, stiffness is often largely overestimated by small scale models when materials of higher strength such as spring steel are used or section sizes are not chosen according to the permissible permanent bending stress (see B3.2). This may result in improper simulations of beam deformations and interaction. Such scale-dependent conditions must be studied carefully by computational means, augmenting the physical form-finding (see chapter F2). The stiffness-dependent interaction of membrane pre-stress and elastic beams can similarly be approximated only by physical form-finding experiments.

E 2.4 Generating Data for Subsequent Form-finding Steps

While dynamic relaxation allows the simulation of elastic bending based on already approximated curved elements, the input geometry for a finite element analysis is actually required to be straight or planar if shape and residual bending stresses are to be simulated correctly (see chapter E4). Whether or not the input data for these computational simulations is approximated or planar, in both cases, it has to be based on a physically feasible system. Similar to the cutting pattern of a membrane, the unrolled geometry of a bending-active structure, together with the constraining boundary conditions, defines both the topology and the geometry of the system. Unrolling the geometry of a physical model makes it very easy to digitalise the geometry and topological arrangement of the flat or planar elements. Therefore, input data may be generated for computationally simulating the erection process to precisely form-find the bending-active structure.

E 2.5 Form Inspiration for Elastic Kinetics

The question of form-finding in elastic kinetics is first of all a question of form and functional inspiration, since the development of a compliant mechanism cannot be achieved by a definition of boundary conditions and objective optimisation criterion only.

In the previous chapters, the importance of physical models as a part of the design process for bending-active structures was discussed. Physical models help define initial force- and material-informed systems. When adding the variable motion, defining the relationship of structure and function in a principal compliant mechanism of a now kinetic system becomes all the more complex. Similar to static bending-active structures, the final geometry is a result of form-finding; in this case, with multiple target positions.

When applying the logics of pseudo rigid-body-models (see E.3.2), such systems may be developed with the rules of kinematics by placing discrete hinges in the elastic zones. This approach, however, will, per its own definition, limit the developer to the logics of rigid body models where systems are composed from types. In this dissertation two methods were used to develop elastic kinetic systems entirely borne out of a typology free elastic thinking. Biomimicry was used as a source of inspiration for basic principles (see Chapter D.5.2 and Schleicher et al 2013) and Eigenmode analysis for the assessment of kinetic degrees of freedom in a predefined system.

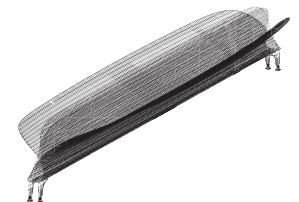


Fig. E.13

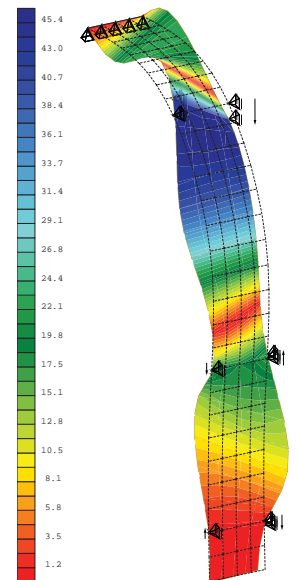


Fig. E.14

E 2.5.1 Form Inspiration from Buckling Modes

As explained in chapter B.2.3 the first Eigenmode is related to the first Euler buckling mode and therefore describes a relatively low energy state of large deformation. The Buckling Mode deformation of a structure can therefore be assumed to have a maximised output deformation versus ratio input energy. This is because the Buckling Mode will tend to have minimal resistance for the input energy of a given frequency. Through mimicry of the Buckling Modes, by enforcing displacements with slipping supports shown in a Buckling Mode analysis, very efficient compliant mechanisms may be found. Particularly interesting are those

Fig. E.13 First Buckling mode of the Flectofin with slipping support, showing the opening mechanism.

Fig. E.14 Buckling mode of a facade cladding element as form-inspiration for a compliant mechanism. Showing amplified deformation and stress on local x direction [N/mm²].

Buckling Modes which lead to large displacements in slipping supports and thereby facilitate a largely amplified mimicry of the deformed shape associated to the particular Mode. Through this approach mechanisms can be developed that are completely independent of typology-based thinking and grid-based geometric considerations. This enables a design process of compliant mechanisms through bottom-up informing of design ideas rather than top-down resolving design intentions. The argument of an Eigenmode analysis leading to valuable inspirations for elastic kinetic systems is supported by the Eigenfrequency analysis of the Flectofin® shown in Figure 13. Here, the first Buckling Mode of the system, with slipping support on one side, shows the exact opening mode of the lamellas resulting from pushing the support inwards.

This approach is only mentioned in connection with the argument of an inspirational source for mechanically informed ideas to develop compliant mechanisms. This is explained through the following example.

Example of designing a compliant GFRP façade cladding

In Figure 14 a typical section of a façade is given which architecturally may want to be cladded with a shading system similar to the Softhouse (Chapter D.4). As claddings play an important role in the visual appearance of a façade, the design process may be initiated by design intentions concerning geometry and topological arrangement which are not yet mechanically informed by the aspect of elastic kinetics. The façade section was modelled with the standard mechanical properties of GFRP and is supported statically defined to offer maximum deformability in the Buckling Mode analysis. The slipping supports indicate direction and magnitude of actuators which can mimic a particular Mode shape. In this study Eigenmode 7 shows the largest open to closed ratio and may be therefore chosen for rebuilding the same element as a compliant shading system with actuators that work in the direction indicated by the slipping supports of the Buckling Mode analysis.

Fig. E.15 Parametric study of elastica and catenary based on FEM form-finding results to quantify the similarity of the two curves.

Fig. E.16 repeating the study from E.15 with a physical models, built with a CFRP rod and a bicycle chain.

E3 Analytical Approximation

The complexity and limitations of analytically describing even simple bending geometries such as the elastica curve is discussed in chapter B2.4. While analytical methods were used extensively before computational analysis of large bending deformations become easily feasible, they only play a role in the computation of splines and validation of computational analysis today. Analytical approximations of bending geometries play an important role in the development of compliant mechanisms and may also be relevant for parametric design models where the accuracy only needs to meet the needs of clarifying and design intentions.

E 3.1 Similarities

There are numerous well known geometric and structural definitions of curves which offer simple analytical descriptions and may therefore be easier to integrate in a design process than the elastica curve. Comparing other curves to the elastica, both geometrically as well as structurally, may unveil curve definitions that can serve as an approximation of the elastica. At the same time, such a comparison enables the structural performance of the elastica to be measured in comparison to other curves.

E 3.1.1 Comparison of elastica to catenary and circular arch

In order to quantify the similarity of elastica, catenary and circular arc, a parametric study of the three arcs is undertaken. They are modelled according to the specifications in Appendix D. All arcs have a span $L = 3000$ mm with varying rise f and covering ratios $f/L = 0.05$ to $f/L = 0.8$. Each of the catenary and elastica arcs were computationally form-found with increasing beam length. The beam length was equally increased in 13 steps for all three arc types, leading to varying rise to span ratios. The arcs are loaded with an external constant linear load $P_z = 0.8$ kN/m. The graph in Figure E.17 shows the resulting maximum vertical deflections U_z at the apex for the three types of arches across the investigated f/L ratios. For comparability reasons, the load on all three arches is a projected load in global Z direction. Still the catenary is form-found according to a cable under dead load.

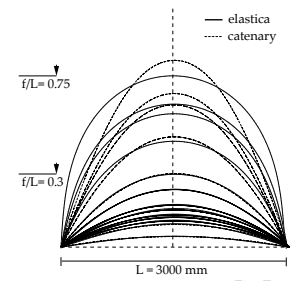


Fig. E.15

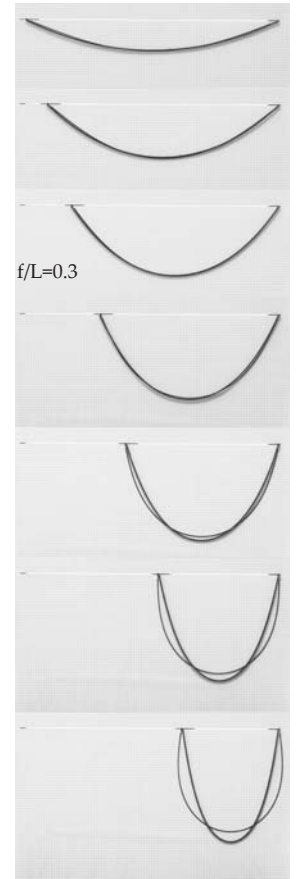
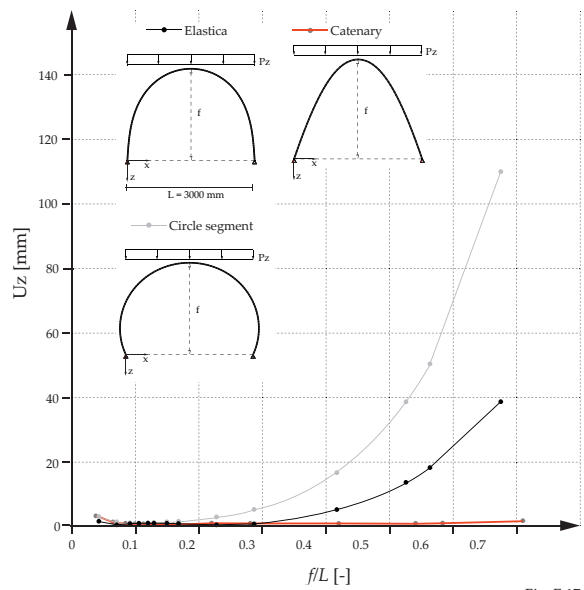


Fig. E.16



In Figure E.15 and E.16 the arc lines are compared geometrically on the basis for the CAD geometry exported from the FE analysis as well as through physical models, built with a CFRP rod and a bicycle chain. For reasons of better readability, only the elastica and catenary arc are shown in this graph. It can be observed that the curves match up to a ratio of $f/L=0.3$ very closely. A similar comparison was carried out by Hennicke (1975: 35) showing the same results. A comparison of a circular, catenary and parabolic arc was carried out by Allen and Zalewski (2009: 67), also showing that the curves match very closely for the smaller rise to span ratios.

Catenary: The analysis of the maximum vertical deformations U_z in Figure E.17 impressively confirms the catenary as being an ideal geometry for a rigid arc exposed to vertical loads. Even with a very large f/L -ratio, the resulting deformations are comparatively small. The main reason for the small deformations is per definition, the axial load transfer of the catenary.

HENNICKE, J. (1975) IL 10 Gitterschalen – Grid Shells.

ALLEN, E. and ZALEWSKI (2009) *Form and Forces. Designing Efficient, Expressive Structures*.

Elastica: Up to an f/L -ratio of approx. 0.3, the deformations of a bending-active arc are very close to the deflections of the catenary. With a larger f/L -ratio, the resulting deformations rise exponentially and substantially surpass the deformations of the catenary. As of the ratio $f/L=0.3$, the loads are transferred increasingly by bending moments which rapidly reduce rigidity of the arc.

Circular Arc: Similar to the elastica, the circular arc performs comparable to the catenary at small f/L -ratios. Here, bending moments increase rapidly already at f/L -ratios > 0.2 . Therefore, the deflections increase exponentially and surpass largely those of the elastica.

This comparison clearly shows a restricted performance range of the elastica to serve structural needs only in a limited range of rise to span ratios. On the other hand, it also shows that, when working inside the performance range, the elastica provides a structurally, very rigid arc geometry, for predominantly vertical loading. Recalling the fact that gridshells, like the Multihalle Mannheim, were form-found based on hanging models, (C.2.2) this comparison underlines the validity of the experimental form-finding approach.

E 3.2 Mechanical and Geometric Equivalent Systems

Pseudo-rigid-body models

For the mechanical description of compliant mechanisms (see B1.2) in small scale technical applications, so called ‘pseudo-rigid-body models’ are developed, which interpret compliant mechanisms as rigid-body mechanisms. This approach enables the use of decades of research in mechanical systems and therefore unifies compliant mechanism and rigid-body mechanism theories. Here, the flexible elements of a mechanism are represented in an abstracted form of rigid elements and hinges. By applying torsional springs at the hinges, both geometric, as well as force relations, can be approximated by calculating the virtual work of the system. Such an ‘equivalent’ rigid-body mechanism replaces in-depth nonlinear analysis and therefore offers a closed form analytical description. The analytical descriptions may then

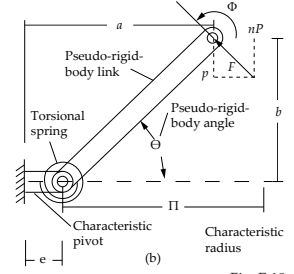
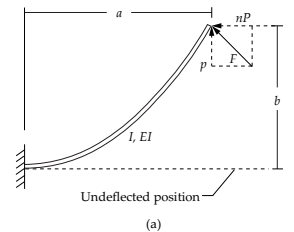


Fig. E.18

Fig. E.17 Load deflection comparison of Elastica, catenary and circular arc for various rise to span ratios. Based on [Howell 2001].

Fig. E.18 Rule for a cantilever beam with a force at the free end, and its abstraction pseudo rigid body model. Based on [Howell 2001].

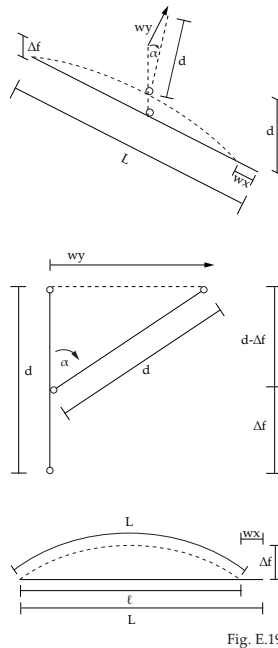


Fig. E.19

be used for fine-tuning and parametric studies of the compliant mechanism.

Figure E.18 shows the well-known rule for a cantilever beam with a force at the free end, and its abstraction as a pseudo rigid body model. Based on the observation that the tip of the beam traces out a nearly circular arc, the flexible cantilever is approximated by a stiff cantilevering beam with a torsional spring stiffened hinge that is located at an offset of $e = l \cdot \gamma \cdot l$. The location of this offset provides the geometric similarity and the spring stiffness K_t structural equivalence. This system is described by Howell (2001) where γ is given based on empiric measurements as a factor of $\gamma_{\text{average}} = 0.85$. Based on the general equation of virtual work (1_E), Howell derives the spring stiffness (2_E) in which the stiffness coefficient is $K\Theta_{\text{average}} = 2.65$.

$$\delta W = F \cdot \delta z + T \cdot \delta \theta \quad (1_E)$$

$$K_t = \gamma \cdot K_\theta \cdot \frac{EI}{L} \quad (2_E)$$

This system shows how the observation of a geometric rule combined with basic principles of analytical structural mechanics can convert a complex nonlinear system into an easy to handle set of linear equations. Such an observation of geometric behaviour and interdependencies was also used in the two projects discussed below. The general relevance of pseudo-rigid-body models, not only for compliant mechanisms in miniature mechanics but also for elastic kinetic systems on an architectural scale, is discussed in more detail in the PhD of S. Schleicher.

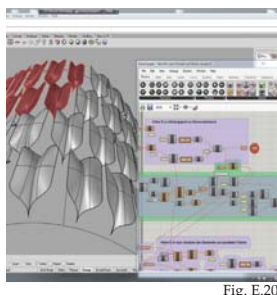


Fig. E.20

HOWELL, L.L. (2001) *Compliant Mechanisms*.

out-of-plane bending. The trigonometric relations, illustrated in Figure E.19, lead to equation (4_E). By equating equation (3_E) and (4_E), the change of angular relations in the wing could be set into relation with the rise of the backbone in (5_E). This equation is put into the parametric modelling environment Grasshopper inside the CAD software Rhino (Figure E.20). The basic function is augmented by nurbs surfaces approximating the curvatures. This rendered possible extensive parametric studies of populating complexly curved surfaces with Flectofin® units.

$$\Delta f = \sqrt{\frac{(L-l_1) \cdot 3 \cdot l_1}{8}} - \sqrt{\frac{(L-l_2) \cdot 3 \cdot l_2}{8}} = 0 \quad (3_E)$$

With $l_i = L - w_{x,i}$

$$w_y = \sqrt{d^2 - (d - \Delta f)^2} \quad (4_E)$$

$$\alpha = \arccos \left(\frac{d - \sqrt{\frac{(L-l_1) \cdot 3 \cdot l_1}{8}} - \sqrt{\frac{(L-l_2) \cdot 3 \cdot l_2}{8}}}{d} \right) \quad (5_E)$$

For the research pavilion ICD/ITKE 2010, a geometric equivalence system is based on observations of geometric rules and approximation with B-splines. Here, students of the design class built a series of 2D test strips which are scanned and analysed for repeating geometric rules. A basic principle is found that showed a constant angle between the arch segments (Figure E.21). By analysing basic elastica curves, the control points of B-splines could be fit by a trend-line function; based on these approximations, a parametric design model was programmed including all relevant material and geometric constraints given by the coupled arch system. This computational design model became one of the essential interfaces which helped to coordinate and mediate various design and fabrication factors. It also defined the unrolled geometry of the strips including all connection points, which were directly transferred into the input geometry of the Finite Element model and the cutting patterns.

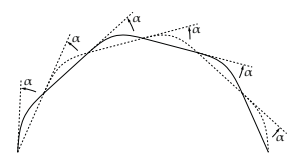


Fig. E.21

Fig. E.19 Geometric equivalence relation of the Flectofin based on the logic of pseudo rigid body models.

Fig. E.20 Rhino Grasshopper definition of a parametric Flectofin lamella based on the geometric definitions made in E.17.

Fig. E.21 Constant angle between the arc segments of the coupled arch.

E4 Computational Form-finding

Using computational mechanics for the form-finding of bending-active structures offers a direct integration of the form-finding result into the subsequent structural analysis and computer-assisted design and fabrication processes. There is an abundance of different methods used in computational analysis of structures and structural dynamics, which are preferred depending on their application in different industries, a good overview is given by Rabindranath et.al. (2011). A typical numerical method for simulating large deformations and nonlinear behaviour in civil engineering is the Finite Element Method (FEM). Among architects Particle Spring Based Methods have become popular in computational design (also referred to as Mass Spring Systems MSS). Particle Spring Based Methods were developed by the computer graphics industry to simulate physical behaviour. These mostly custom programmed software routines offer a high degree of interaction and integration into design processes [KILIAN and OCHSENDORF 2005]. For civil engineering purposes, the FEM software packages offer expedient means for subsequent structural analysis with the use of a large variety predefined subroutines. For the work of this dissertation focus is laid on the FEM technique, which enables in depth analysis of structural behaviour.

This section will introduce practical approaches to solving the form-finding question with the use of FEM. Some practical and custom programmed routines in nonlinear FEM will be introduced in connection with the simulation of large deflections. Here, the commercial FEM software Sofistik® is used, which offers custom programming in the parametric interface Teddy. For validity, some basic bending-active systems are compared to physical models in their form found geometry and furthermore, to results attained with the FEM software Ansys®.

E 4.1 Advantages of Finite Element Method

The necessity for simulation of large elastic deformations in order to form-find bending-active structures poses no problem to modern nonlinear finite element analysis. However, currently available Finite Element programs do not serve well as a de-

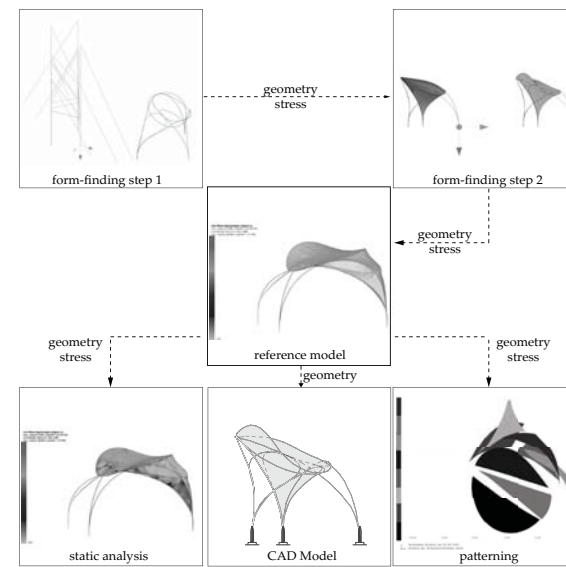


Fig. E.22

sign environment, the input data for the pre-processing of the simulation has to be generated with either physical form-finding or behaviour based computational modelling techniques. The necessity and advantage of FEM in the development of Textile Hybrids in particular lies in the possibility of a complete mechanical description of the system. Provided that form-finding solvers are included in the software, the possibility of freely combining shell, beam, cable, coupling and spring elements enables FEM to simulate the exact physical properties of the system in an uninterrupted mechanical description (Figure E.22). These include: mechanical material properties, asymmetrical and varying cross-sections, eccentricities coupling and interaction of individual components, nonlinear stress-stiffening effects, nonlinear simulation of stresses and deflections under external loads (e.g. wind and snow), patterning and compensation.

It is often said that Particle Spring Based Methods using dynamic relaxation have a computation time advantage over FEM for systems of large deflection; however, this is rapidly diminished with an increasing number of elements per beam and large de-

Fig. E.22 Continuous mechanical description of the structural FEM model from form-finding to patterning on the example of the M1 project.

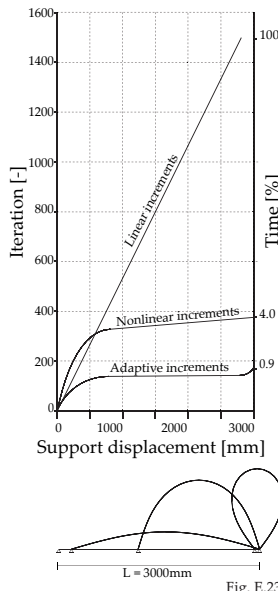


Fig. E.23

flections. Comparative tests by Douthe (2006) show that computation time for the form-finding of an elastic gridshell is faster with FEM when the element length was set sufficiently small. For larger elements, computation time increased significantly or no convergence was reached at all in FEM, while the spring based method converges quicker with increasing element size. The use of step size adaptive incremental deformation additionally drastically reduces the iteration steps and time needed in an FEM simulation (see below).

E 4.2 Incremental Load Steps

For nonlinear Finite Element Analysis with large deformations, such as snap-through and bifurcation buckling problems, the arc length method is developed as an efficient algorithm to trace the equilibrium path with small load increments in the neighbourhood of critical points. This powerful incremental iterative solution procedure in nonlinear FEM is available for software packages like Ansys®, however, not for Sofistik® which only offers line search methods with the option of updated tangential stiffness (Newton Raphson). In addition Sofistik® offers incremental load steps with step size control through limit load iteration. However, this method may only be applied to force and displacement loads and not to temperature or pre-stress. The importance of the latter in form-finding bending-active structures will be explained in chapter 4.3. In order to still be able to profit from Sofistik® as a civil engineering purpose FEM environment, the author developed custom programmed routines which enable incremental-iterative calculation for all external and internal load definitions.

The basic calculation procedure for incremental load steps is based on the option of primary load cases. Here, the deformations and strains of an already solved load case may be referred to through calling it as a primary load case to the calculation of a current load case. Therefore, a pre-stress state may be linked to another load case and calculation time is quicker and easier; convergence, if part of the solution, is already known through the primary load case.

In Figure E.24 the general setup of the calculation routine is

Fig. E.23 Comparison of computational costs using linear, nonlinear and self-adaptive load increments for the form-finding of an elastica curve with 3 m span to its fully closed form.

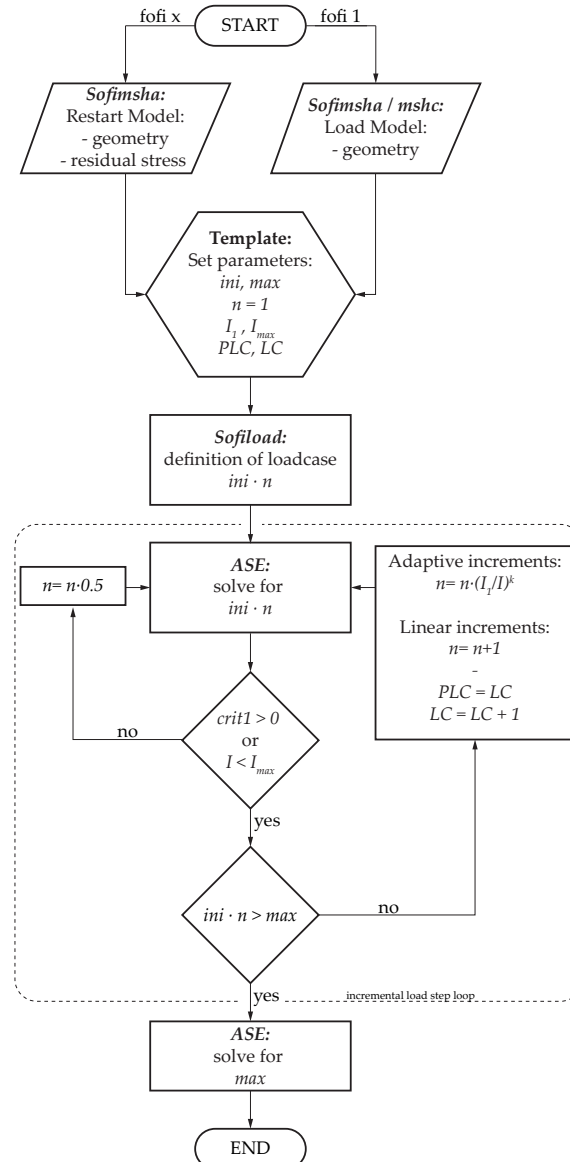


Fig. E.24 Process diagram for incremental load step form-finding of bending-active structures with commercial FEM software Sofistik®:

ini: start increment
max: maximum increment
n: load factor

Iteration:
I: optimum number
Imax: maximum number
k: root ($0.5 < k < 0.8$)

Load case:
PLC: primary load case
LC: Load case

Fig. E.24

shown as a flow chart. Here, several existing programmes from Sofistik® are linked which prepare the model to be solved inside the program 'ASE'. An iteration loop with different options for the load step sizes is programmed around 'ASE'. The functioning of the loop is based on continuously setting the primary load case, one step prior to the current load case. Therefore, the load increments are stacked onto the solution of an increasingly large deformation until the target magnitude of the load is reached.

Several different options for controlling the size and intervals of the load steps were programmed by the author. In the simplest case of linear step size control, an initial load increment is defined which is then linearly increased; this option is slow because the step size is permanently set according to convergence criteria of local nonlinearities. For generating equilibrium path graphs, the linear option is chosen because it offers equidistant load steps. To speed up the calculation, nonlinear load steps may be defined which use small load steps in the beginning and then enlarge the steps once the post-buckling curve is set and only further deformed, in the case of a buckling problem, for example. The custom setting of nonlinear step sizes, however, requires knowledge of the systems behaviour. Therefore a routine for adaptive step sizes is programmed which automatically adapts to the systems nonlinearities (see below). A comparison of the computational costs and iterations required for the form-finding of an elastica curve with the afore mentioned methods of step size control is given in Figure E.23.

This load increment loop may be used for several different types of loads defined inside 'Sofiload' and factored by the variable n . Figure E.24 therefore similarly applies to any type and number of force or displacement loads. For pre-stress loads, as used in the elastic cable approach discussed below, the functioning of the primary load cases slightly changes. Since pre-stress (also temperature) is an inner stress state, it is also saved in the primary load case. Therefore, recalling the same load case with a constant factor $n=1$ already leads to a linear increase of the pre-stress load and consequently to a slightly changed routine shown in Figure E.25.

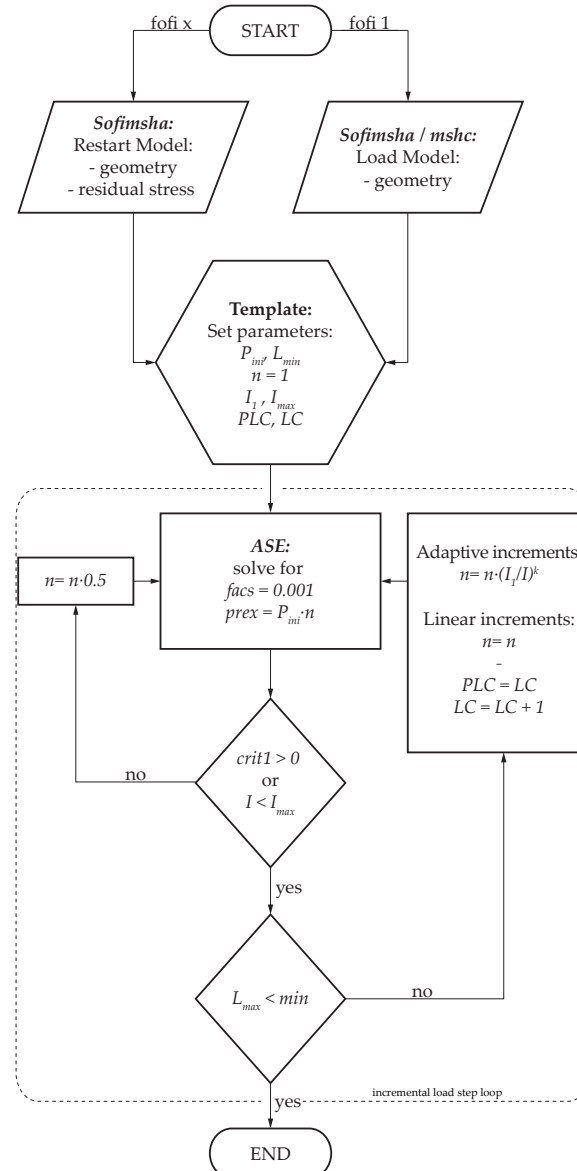


Fig. E.25 Process diagram for incremental load step form-finding of bending-active structures with commercial FEM software Sofistik® for using the elastic cable approach:

P_{int} : start value of pre-stress

I_{max} : maximum increment

fac_s : stiffness factor

pre_x : pre-stress factor

n : load factor

Iteration:

II : optimum number

I_{max} : maximum number

k : root ($0.5 < k < 0.8$)

Load case:

PLC : primary load case

LC : Load case

Fig. E.25

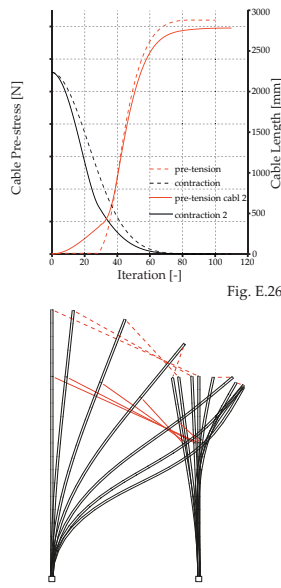


Fig. E.26

Adaptive step size control

Based on the principles of adaptive step size control often used in the arc length method, a similar option is programmed into the load increment loop introduced above. The optimal size of a load step depends on several factors, such as the degree of the nonlinearity of the problem, the path tracking algorithm and the iteration method.

In general, the number of iterations needed to reach convergence in one load step is proportional to its size. Therefore, small load steps also require less iteration than large load steps. On the other hand, the computational cost increases with decreasing increment size and the number of increments because more load steps are required to reach the target load. For an efficient and robust analysis, it can therefore be helpful to adapt the step size during the calculation. Here, the number of required iterations for an increment can be an indicator for the nonlinearity of the system and therefore be used to set the size of the next load step.

Ramm (1981 p. 76) suggests a method for automatic load incrementation where the step size is scaled in relation to the number of iterations of a previous load step I_i to the desired number of iterations I_t . Ramm found that a factor I_i/I_t leads to oscillations in the number of iterations required and therefore suggests using the square root of this factor. Based on this, equation (6e) shows a simple possibility to adaptively control the step size based on the number of iterations needed for the last load increment I_i set in relation to a target iteration number I_t . It was found that a target of 30-50 iterations leads to the fastest total calculation times. With the parameter k , the influence of the iteration control on the change in step size can be controlled. Based on Ramm's suggestion, $k = 0.5$ is used. Practical higher values of $0.5 < k < 0.8$ can achieve faster computing times. In addition, upper and lower limits for the size of the load steps are defined.

$$n = n \cdot \left(\frac{I_i}{I_t}\right)^k \quad (6e)$$

Fig. E.26 Form-finding behaviour of the elastic cable approach for the system in E.25 showing the reciprocal dependency of cable pre-stress and length for two cables in relation to the iterations of the linear incremental loop.

Fig. E.27 Sample system composed of two differently sized masts with fixed supports which are connected at the top and an additional inner point. Using the form-finding routine shown in Figure E.23, both cables of the system are simultaneously pre-stressed incrementally.

RAMM, E. (1981) *Strategies for Tracing the Nonlinear Response Near Limit Points*.

HARTMANN, F. and KATZ, C. (2004) *Structural Analysis with Finite Elements*.

LEWIS, W. J. (2003) *Tension structures*.

The inclusion of the adaptive load increments now renders possible a much faster and more stable form-finding of bending-active structures. The example of form-finding an elastica sequence up to the point of the end nodes touching each other shows the advantage of this approach. The graph in Figure E.23 shows the iteration behaviour comparing adaptive increments to linear increments, showing the drastic differences in computation time. This routine is being developed further and integrated into parametric design environments by my colleague, R. La Magna.

E 4.3 The Elastic Cable Approach

As the geometry of a bending-active structure becomes more complex in a coupled system, so do the equilibrium paths in the deformation process. Here, it is no longer possible to simply deform a structure into its elastically deformed shape by a number of linear support displacements. The restrained stresses either become so big that no convergence can be reached in the simulation process, or the definition of the displacement path for each support has to be defined individually in a very time consuming process. In some cases, where two bending-active elements are constrained by coupling them in space, the position of the displacements are unknown; here, a definition of the bending shape via support displacements is practically not possible. Such an example is given in Figure E.26 and E.27. As a practical approach for form-finding coupled bending-active systems in FEM, the author developed a new strategy using contracting cable elements to pull associated points from an initially planar system into an elastically deformed configuration. These cable elements work with a temporary reduction of elastic stiffness which enables large deformations under constant pre-stress. This method was originally developed for the form-finding of tensile membrane structures using, for example, the transient or modified stiffness method. For further information on this method, see Hartmann and Katz (2004: 507) and Lewis (2003: 41). For the form-finding of coupled bending-active systems, the great advantage is that the cables allow complete freedom of the equilibrium paths that are followed during the deformation process. The pre-stress that is independent of the change in element length also allows the simultaneous use of several cable elements in the different positions of the system (compare Figure E.26). Once the cables are contracted

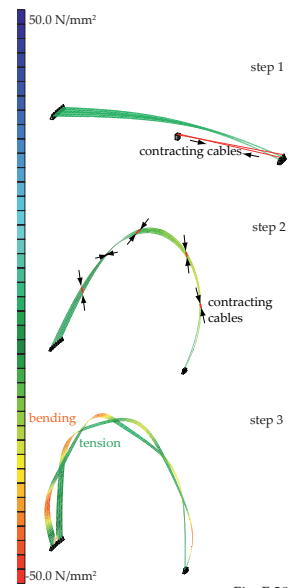


Fig. E.28

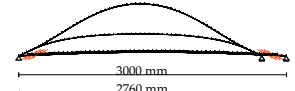
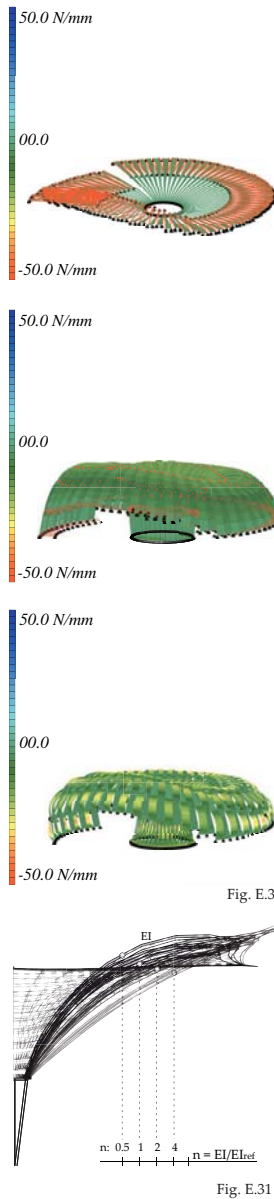


Fig. E.29

Fig. E.28 Form-finding of the coupled arch: Step 1: form-finding of main arches with contracting cable elements between two supports. // Step 2: form-finding of coupled arch system with contracting cable elements between two arch segments

Step 3: fixing the equilibrium with coupling elements at the connection points.

Fig. E.29 Form-finding of the double arch with contracting cables between two beam elements of different length.



to nearly zero length they can be replaced by various types of coupling elements for the following structural analysis. Referring back to the basic equilibrium equation in nonlinear FEM (5_B) we can derive equation (7_E) for the pre-stressing cable used here:

$$\left(\frac{EA}{l} \begin{bmatrix} 1 & -1 \\ -1 & 1 \end{bmatrix} + \frac{P_x}{l} \begin{bmatrix} 1 & -1 \\ -1 & 1 \end{bmatrix} \right) \cdot \begin{bmatrix} u_1 \\ u_2 \end{bmatrix} = \begin{bmatrix} F_1 \\ F_2 \end{bmatrix} \quad (7_E)$$

If Young's modulus E is temporarily set to zero, elastic stiffness would disappear and tangential stiffness would be entirely based on the ratio pre-tension to length. Material stiffness therefore has no influence on the behaviour of the elastic cable which is thereby only constrained by the elements it is attached to. As such, the cable has become a free load defined by the magnitude of pre-tension and the rigidity of the elements in between which it is contracting.

The advantage of form-finding complex coupled equilibrium systems is shown by the example in Figure E.27. This system is composed of two differently sized masts with fixed supports which are connected at the top and an additional inner point. Using the form-finding routine shown in Figure E.25, both cables of the system are simultaneously pre-stressed incrementally. The graph in Figure E.26 shows the reciprocal dependency of cable pre-stress and length for the two cables in relation to the iterations of the linear incremental loop. Even though both cables are assigned with the same pre-stress increments, their actual pre-stress differs depending on the deformation of the system. Also, the moment of total contraction of the cable elements is reached at different iterations and still, the calculation continues after one cable has already contracted to a length close to zero. This astonishingly stable convergence behaviour enables the form-finding of far more complex systems such as the ICD/ITKE research pavilion (Figure E.30) and the M1 project (Figure D.34).

E 4.3.1 Elastic Cable Approach in the Case Study Structures

Research Pavilion ICD/ITKE

Form-finding of the research Pavilion ICD/ITKE was separated into three subsequent steps (Figure E.30). In a first step, 80 contracting cables simultaneously pull the flat plywood strips into



Fig. E.32

the simply curved half torus shape. Thereafter, two sets of 205 contracting cables simultaneously form the coupled arch systems and then couple the arc pairs to a continuous torus shell. The nodal positions of the final equilibrium shape are entirely defined by the inner constraints. Such a system could not have been found numerically without the elastic cable approach. In fact, it was this project that ignited the research and development of this approach, and therefore laid the basis for the later case study structures.

Textile Hybrid - M1

Form-finding of the beam elements in the M1 was separated into four subsequent steps. Starting with the straight beams, the loop modules were all form-found simultaneously by first forming an arc and then droplet shape. Based on the topological connection points given from the physical model, the loop elements were successively joined into a coupled system by contracting a final set of cables between the common nodes of the structure.

Softhouse

For the Softhouse project, the permanently curved storm position of the GFRP boards was also form-found using the elastic cable approach. Here, only the support at the eaves is pre-defined in the geometry. For the other supports, only the heights are defined. By attaching the cables to horizontally sliding supports, the form-finding guaranteed minimal constraining forces (Figure D.41 and F.43).

E 4.4 Form-finding of Textile Hybrids

The form-finding of membrane structures with bending-active

Fig. E.30 Form-finding of the 2010 ICD/ITKE research pavilion using the elastic cable approach in three subsequent form-finding steps.

Fig. E.31 Influence of the beam element stiffness on the form-finding result of the Marrakech umbrella.

Fig. E.32 Form-finding of an elastic hybrid with the simultaneous approach.

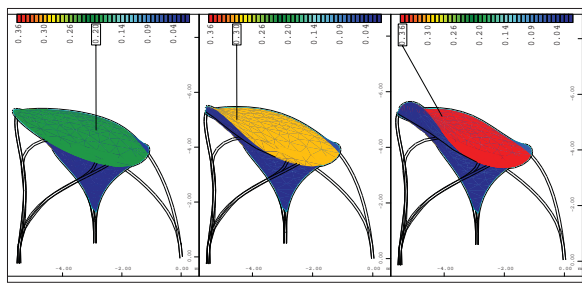


Fig. E.33

support systems (*Textile Hybrid*, see also B1.1) necessitates a combined form-finding of the form- and bending-active elements. There are three principal approaches that can be followed to achieve such a combined equilibrium system:

Additive

The form-finding of the bending-active and form-active structure are separated. The two systems are coupled together once the separate entities are form-found. A subsequent equalising calculation of the coupled system, where stress is referenced but no additional loads are applied, will find the systems final equilibrium shape. This approach is possible for systems where the membrane has a small or predictable influence on the bending-active structure.

Successive

The process is separated into first, the form-finding of an elastically bent beam structure and second, the form-finding of the membrane attached to the beams. Here, the second form-finding step serves to generate an intricate equilibrium system which is based on further deformations in the beam structure.

Simultaneous

Some scenarios also allow the simultaneous form-finding of the bending-active beam elements and pre-stressed membrane elements. For numerical form-finding, the bending of beam elements requires out-of-plane forces on the beam; this may be achieved by eccentricities and/or three-dimensional input of the membrane-mesh (see Figure E.32).

Using FEM software Sofistik® for the form-finding of Textile

Fig. E.33 Form-finding of the M1, showing the influence of various membrane pre-stress ratios on the shape of the bending-active structure.

Hybrids has the advantage that the form-finding and patterning routines for tensile membranes are already included in the software. These routines could easily be combined with any of the above mentioned approaches as well as the load increment loop introduced above. Therefore, any of these approaches may be chosen depending on the individual nature of the form-finding problem. For the case study structures that included tensile membranes, all three of the aforementioned approaches were used.

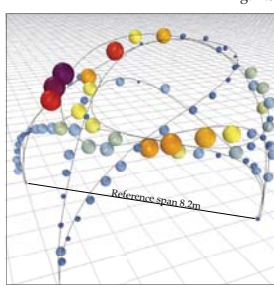
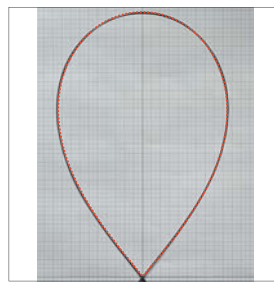
E 4.4.1 Form-finding of Textile Hybrids in the Case Study Structures

Umbrella Marrakech

For the relatively simple geometry of the umbrella, the *simultaneous* form-finding approach is used. Here, controlling the stability of the beam during form-finding is difficult, since the stabilising effect the membrane has on the beam is only activated in the post form-finding configurations. This necessitates a temporary restraining of the beam perpendicular to the bending plane. This was particularly the case because Sofistik® uses the transient stiffness method where the large deformations which occur during the form-finding are enabled by a temporary reduction of the elastic stiffness in the membrane and edge-cable elements. Floating coupling elements are used to control the distance between the mechanically pre-stressed membrane elements and elastically deformed beam elements (See Figure D.16). The influence of the beam element stiffness on the form-finding result is illustrated in Figure E.31.

Textile Hybrid - M1

The complexity of the M1 geometry necessitates a separation of the form finding steps and applying the *successive* approach (See Figure D.34). After the form-finding of the beam elements introduced above, the membrane mesh is generated on the given boundary conditions of the edge beams. Because of the general elasticity of the structure, the membrane pre-stress largely deflects some of the beams and therefore has a significant influence on the overall geometry of the final equilibrium state (Figure E.33).



Softhouse

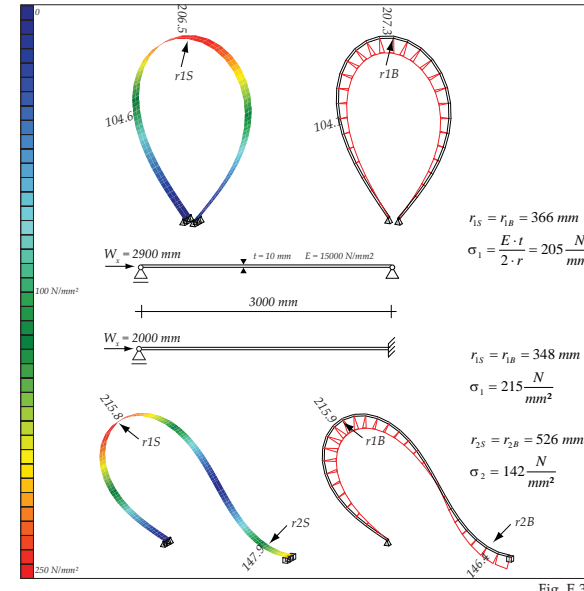
For the twisting membrane strips of the Softhouse it is important to control symmetry and the equidistance of the cross bars. This is difficult to maintain in a simultaneous form-finding with the cantilevering GFRP boards. Therefore, the membrane strips are form-found separately. Applying the *additive* approach, the membrane is coupled to an already elastically deformed GFRP board. The subsequent equalising calculation leads only to minimal change in the equilibrium position since the position of the cantilevering beam is already known from previous simultaneous form-finding attempts (see Figure D.44).

Fig. E.34 Scan of an elastically deformed guitar string compared to the CAD output of the Sofistik® FE form-finding (red dotted line) showing perfect matching of the two curves.

Fig. E.35 - E.36 Comparison of the M1 physical form-finding model to the FE form-finding result with photogrammetric 3D scan. Spheres indicate distance between scan and FE model points, with mean error shown in percentage of reference span.

E5 Validation of FE Simulation

The simulations in this dissertation are all based on nonlinear finite element theory 3rd order using the program 'ASE:3' in the Finite Element software Sofistik®. For validation of these simulations, form-finding results of some basic systems were compared to physical models, analytical stress determination and FEM results from Ansys®.

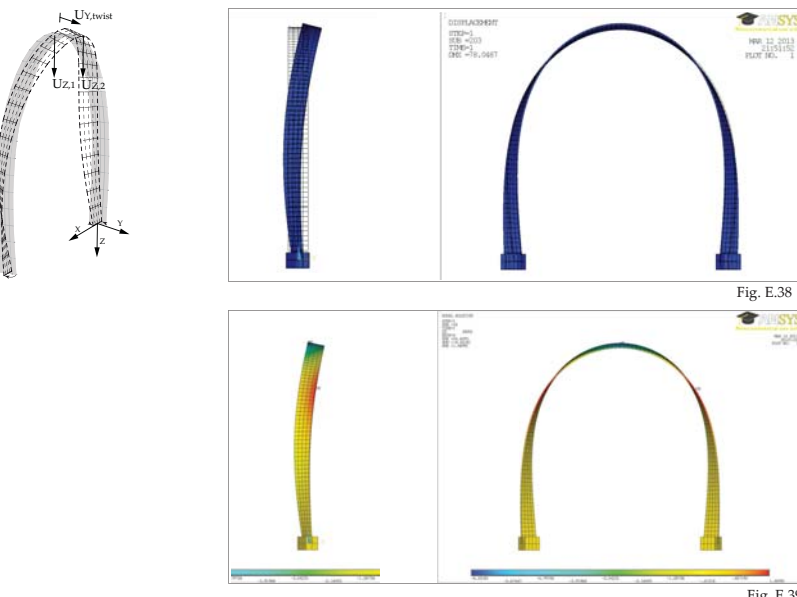


Experimental Testing

Since the geometry of an elastica curve is independent of its mechanical properties, the scale and material of the physical model does not need to be similar to the analysis model. Therefore, an elastica with touching end supports was verified experimentally and compared to the deformation results from a FEM form-finding. For the experimental model, a 1 mm thick spring steel wire is formed into a loop with touching ends. The same system was form-found using the load increment loop introduced above. In Figure E.34, a scan of the wire is compared to the CAD output of the Sofistik® FE form-finding (red dotted line) showing perfect matching of the two curves. This experiment proves that the FEM form-finding used in this dissertation produces geometrically correct results for large in-plane deformations.

For a more complex three dimensional shape the physical form-finding model, which delivered the rod lengths of the M1 (see Chapter D3.2), was compared to the FE form-finding result. Figure E.35 shows the setup for the photogrammetric 3D scan. The spheres in Figure E.36 show the distance between scan and

Fig. E.37 Comparison of stress values for shell (s) and Timoshenko beam elements (b) and the analytical approximation as a validation.



FE model points. The mean error is shown in percentage of reference span. The average error is below 2 % and thereby supports the accuracy of the FEM form-finding methods used in this work. Some of the errors > 2 % result from the different rod diameters used in the FEM form-finding, whereas the physical model is built with the same diameter for all rods. This is particularly visible in the areas of large span, where stiffness in the physical model is largely overestimated.

Analytical comparison

Figure E.37 shows a comparison of normal stress for shell (s) and Timoshenko beam elements (b) and the analytical approximation from equation (20_B) as a validation. Minimal differences are found comparing beam and shell elements. Differences to the analytical estimation of the bending stress are due to the fact that the numerical simulation includes normal forces.

Comparison of different FE Programs and Solvers

Besides the 3D scan of the M1 model, the above made tests are performed on relatively simple 2D geometries, the form-finding

Fig. E.38 and E.39 Form-finding and analysis result of the torsional arc in Ansys using shell element 181.

Tab. E.40 Comparison of Sofistik and Ansys analysis results.

	Sofistik		Ansys	
Deformation [mm]	Beam element	Shell element	Beam element 189	Shell element 181
U _{Z₁} 100 [N] geom nonl	8.53	8.37	8.35	8.2
U _{Z₁} 100 [N] nonl	8.11	8	8.05	7.84
Stiffening ratio [%]	-5.18	-4.62	-3.7	-4.57
U _{Y₁,twist}	40.6	59.4	55.86	75.19
U _{Z₂} 50 [N] geom nonl	2.05	2.9	x	5.63
U _{Z₂} 50 [N] nonl	3.3	3.19	x	6.55
Stiffening ratio [%]	37.88	9.09	x	14.04
U _{Z₂} 500 [N] geom nonl	17	17.2	x	19.18
U _{Z₂} 500 [N] nonl	18.9	18	x	21.73
Stiffening ratio [%]	10.05	4.44	x	11.73
U _{Z₂} 1000 [N] geom nonl	44.2	43.3	x	44.31
U _{Z₂} 1000 [N] nonl	46.3	44.3	x	49.64
Stiffening ratio [%]	4.54	2.26	x	10.74

Tab. E.40

of which did not necessitate a saving and restarting of several form-finding steps. Because the latter bears a risk for numerical errors, a more complex shape is form-found with the two commercial FEM programs Ansys® and Sofistik®.

The comparison is done on an elastica arc with a flat cross section at the position where the tangents at the supports are vertical. In this position, opposite support rotations of 80° around the vertical axis are applied to the arc. This creates a torsion effect which forces the arc into an out-of-plane bending, making the tip bend sideways into the global Y direction. This three dimensional deformation is free of external constraints; therefore, the equilibrium position is highly influenced by the mechanical behaviour of the system. In experimental model tests, it is found that the equilibrium state can even become bi-stable in certain scenarios. This system is chosen for comparison to show the limitations and differences that can occur between different software packages and modelling techniques. The basic mechanical data given in Appendix D, and was set to be the same for all simula-

tions. Similarly, the meshing of beam and shell elements is also set to be the same between all simulation models. And finally, all force and deformation loads are applied in the same direction and magnitude. The comparison includes a modelling of the system with shell and beam elements in Sofistik® and Ansys® (Ansys see Figure E.38 and E.39, Sofistik see Figure F.26). For each system, results of a fully geometric nonlinear analysis including stress-stiffening are compared to the results of a nonlinear analysis in which the form-found geometry only, without consideration of the residual stress state, is analysed. Table E.40 shows the results in comparison where sufficient agreement between all four models is found when the simple elastica is loaded with an external point load. All four simulations similarly show that the compression stress from form-finding the elastica leads to negative geometric stiffness in the structure for geometric nonlinear analysis with a de-stiffening of approx. 5 %.

Even though modelled in exactly the same way, the sideways deformation due to support rotation shows significant differences between the systems. In both software packages the shell elements show larger sideways deformation than the beam elements. This may be due to the fact that the sideways deformation is influenced by torsional warping. Warping is the effect of transverse shear forces leading to out-of-plane bending. Warping is automatically considered when modelling with shell elements but usually neglected in the analysis of beams. In Ansys® for beam analysis, the consideration of warping effects needs to be deliberately switched on; similarly, for Sofistik® beam elements, warping torsion can be considered in nonlinear analysis with up to 7 degrees of freedom per node. It seems, however, that especially on flat sections as modelled here, the different implementations of considering warping between the element types leads to significant differences in the deformation result of this little constraint system. Because of the differences in sideways deflection, it is important to notice that the twisted arcs compared are different in geometry and residual stress state, leading to obvious differences in stiffness. Still, the system behaviour under external load can be compared for the influence of residual stress. Here, all systems show a distinct stress stiffening effect for the torsion arc structure. The explanation for this stress stiffening by torsion is given in chapter F 1.3.

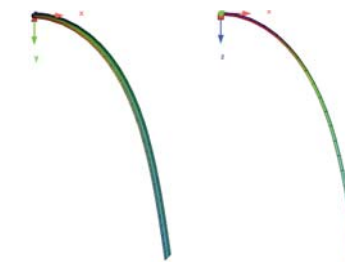


Figure 3: Deformed structure: a) Beam elements b) Quad elements

Fig. E.41

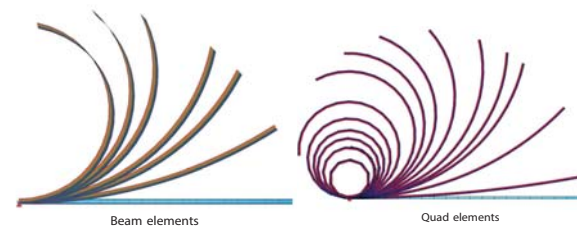


Fig. E.42

For the Ansys® beam element it was not possible to analyse the twisted arc with external loads because a geometry update is necessary before applying external loads. Here, a software error was unveiled in Ansys® which suppresses the information of the cross-section orientation after a geometry update. This problem could not be immediately resolved by the Ansys® support and will apparently be solved in the next update. Having detected a software error in the widely used and highly recognized FE software Ansys® may also underline the fact that numerical form-finding of bending-active structures is uncommon and that great caution must be taken in the interpretation of the results.

In general the results in Table E.38 suggest that the simulation of structural behaviour is reliable, whilst geometry of the equilibrium in largely deflected states may show different results which are dependent on meshing and simulation techniques. This qualification however only applies for extreme examples such as the investigated twisted arch with largely nonlinear effects and a relatively unstable state of equilibrium.

Fig. E.41 Sofistik benchmark Nr. 7 showing the classical problem of a cantilever beam undergoing large deformations under the action of a vertical load at the tip. [Sofistik 2013a]

Fig. E.42 Sofistik benchmark Nr.8 showing the classical problem of a cantilever beam undergoing large deformations under the action of a moment load applied at the tip. [Sofistik 2013b]

E 5.0.1 Potential Simulation errors

The investigations on the structural behaviour of bending-active structures in section F are mostly based on an analysis of stiffness and the influence of residual stresses therein. Therefore it is important to recognize that FE simulations may overestimate stiffness due to a number of so-called 'locking' effects. These particularly appear in nonlinear simulations with large deflections. In general, most locking effects in commercial FE software are considered in the programming of the elements. Fine meshing with harmonious and planar quad geometries helps to avoid locking phenomena. Therefore, great care must still be taken in the modelling of a system.

Shear locking

Shear deformation can lead to wrong results for very thin beams because the internal energy from bending deformation is proportional to the cube of the thickness t^3 , while that from shear deformations is proportional to t . Therefore, the bending strain energy for very small thicknesses disappears. This is incorrect for a beam exposed to combined shear and bending deformations because physically, the bending deformations should always provide the largest part of the energy. This phenomenon is referred to as shear locking.

Membrane locking

Membrane locking is a stiffening effect in beam and shell elements which occurs when pure bending deformations are accompanied by membrane stresses. The effect occurs only in curved elements. Membrane locking may occur when a curved surface is modelled with 4 Node shell elements in such a way that the four nodes are far from lying on a common plane. In this case, the bending vector of one element may act like an in-plane moment or drilling moment on the neighbouring element. For very thin elements, a similar effect to shear locking causes the locking of bending deformations by the unrealistically higher membrane resistance of the neighbouring elements.

In order to detect and avoid such locking phenomena, benchmarking tests are performed comparing load deformation behaviour of typical systems to analytical results and other FE results.

A recognized set of benchmarking tests is given by Macneal and Harderer (1985).

Sofistik® benchmark

Similar to these proposed problems by Macneal and Harderer, some benchmarking tests are available for Sofistik® beam and shell elements under large deformations. Benchmark No. 7 in figure E.41 shows the classical problem of a cantilever beam undergoing large deformations under the action of a vertical load at the tip. The comparison considers beam and shell elements compared to an analytical result. Results are presented in terms of the motion of the tip of the cantilever. Accuracy of the solution is shown in the perfectly matching load deflection curves in [Sofistik 2013a]. In benchmark No. 8 [Sofistik 2013b] the classical problem of deflection of a cantilever beam of linear elastic material is here, extended for the case of a moment applied at the beam tip. The concentrated moment causes the beam to wind around itself, i.e. deflect upwards and bend towards the built-in end. The stress results are compared to formula (20_B). It is found that accuracy of the deformation solution for the shell elements is good, whereas for the beam elements it is insufficient for very large deformations. Here, the benchmarking test does not reach convergence with the beam elements (Fig. E.42). Similar tests with beam elements by the author using the incremental loop introduced above however, also successfully solved this problem using beam elements (see Figure B.22).

Concluding upon the above made validation tests and the benchmarking results by Sofistik®, correctness of the simulation results shown in this dissertation can be assumed. The apparent influence of meshing was considered in all simulation models and where possible, simple analytical checks were undertaken. In addition, the precision of the simulation results in comparison to the built geometry and load deflection behaviour on the case study structures shown in section D supports the correctness of the simulation techniques.



F Structural Behaviour of Bending-active Structures

F1	Stiffness and Stability	141
F 1.1	Measures of Stiffness	142
F 1.2	Pre-analysis of Stress-stiffening in Basic Structural Systems	147
F 1.3	Stiffness Development in Basic Bending-active Systems	149
F 1.4	Stiffening Effects of Case Study Structures	160
F2	Scaling and Stability	166
F 2.1	General Introduction to Scaling	166
F 2.2	Dimensional Analysis of Elastica	167
F 2.3	FEM Analysis of Elastica	171
F 2.4	Scaling of Case Study Structures	172

F Structural Behaviour of Bending-active Structures

The section on structural behaviour investigates the question of stiffness and scaling. The curved geometries of bending-active structures are also referred to as post-buckled curves; a sudden loss in stability is therefore less common than large deflections. The given elasticity, however, can provoke a sudden curvature inversion (snap-through), the investigations on stiffness and scaling therefore include analysis of stability.

Stiffness and stability

In general, the stiffness of bending-active structures can be distinguished on 3 different levels:

- Geometry related: Curvature and load orientation
- Topology related: System (macro scale) and cross-section (micro scale)
- Stress related: Based on residual stress

While the geometry and topology related stiffness of a bending-active structure correspond to the generally known load bearing mechanisms in beam theory, the influence of initial stress unveils some new insights to the load bearing of bending-active structures and will therefore be focused upon in this chapter.

Scaling and Stability

This chapter will analyse the scaling effects in bending-active structures. By means of dimensional analysis it will clarify at which power each influencing factor effects scaling. The analysis of stress-stiffening effects and their influence on stability will be included in the scaling investigations. This will offer the basis for some more general conclusions and thereby derived design rules for the scaling of bending-active structures.

F1 Stiffness and Stability

Using the elastic behaviour of a material to shape a curved geometry will always raise the question of deformation and stability under external loads. Controlling this by increasing the elastic stiffness is not an option if the elements are to be bent into a significantly curved geometry with sufficient remaining load bearing reserves. We may therefore speak of a paradoxon that underlies all bending-active structures which, in order to be solved, needs to be understood to find the gaps in which the relation between form-defining elasticity and structural stiffness allows for a structurally sound system.

The key to this lies in the understanding and activating of both elastic as well as geometric stiffness reserves. In order to do so, some basic bending-active systems are analysed in this chapter. Three approaches are used to visualize the separate stiffness components and analyse the general structural behaviour of each system:

- Analysing the progression of stiffness during the elastic form-finding process by separating stiffness components
- Analysing the general behaviour of the bending-active structure by means of Eigenfrequency analysis
- Analysing a particular load bearing mechanism by comparative load deflection curves.

In these investigations there are always two differentiated cases:

- The geometric nonlinear case, in which stress stiffening effects resulting from the shape defining residual stress (initial stress) are fully considered. In the following indicated by "geometric nonlinear", short: "geo. nonl."
- The reference case that is geometrically identical to the geo. nonl. case, but does not consider residual stress. In the following indicated by "reference geometry", short: "ref. geo."

All basic systems analysed in this chapter have an initial span of 3 m and mechanical properties according to Appendix D.

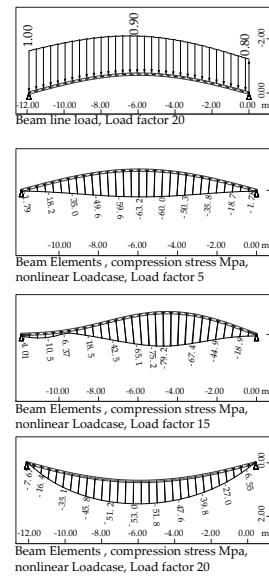


Fig. F.1

Fig. F.1 Asymmetrical line load on the elastica arc showing compression stress and deformation to the point of snap-through buckling.

Fig. F.2 Separated progression of stiffness for several rise to span ratios of the elastica arc with constant elastic stiffness and total beam length.

Fig. F.3 load deformation curve for an asymmetric line load is applied to the elastica arc of rise to span ratio 0.15, comparing the geometric nonlinear case to the reference geometry case.

F.1.1 Measures of Stiffness

Different strategies of measuring stiffness in a structure with various degrees of abstraction are introduced through the example of the elastica arc in this section. These strategies will be used in the following analysis of various bending-active structures.

Progression of stiffness in an elastica arc

In chapter B2.1, Figure B.6 visualises the separation of the three stiffness components that act in a largely deformed structure; elastic stiffness K_e , initial displacement stiffness K_u , and geometric stiffness K_g . In this case, the progression of stiffness components is analysed for each instant of a snap-through problem. Similarly, each deformation step in the form-finding progress of a bending-active structure can be investigated for the progression of stiffness. For bending-active structures, no analytical solution is available like it was used for the snap-through problem. Here, the separation of stiffness components can be achieved through subtraction of load deflection curves for the undeformed (K_e), the geometric nonlinear (K_g) and the reference geometry cases (K_u). The measure of stiffness K_i is thereby given by the relation of $\lambda \cdot F/U_z$, which is correct in unit but force dependent in magnitude. However, when applying the same load factor λ to all steps of investigation, the relations between the separated stiffness components are shown correctly; therefore, no quantities of stiffness are given in the following investigations and only relations, as well as algebraic signs, are analysed. The equations for separating stiffness based on load deflection are:

$$K_e = \frac{F}{U_z} = \text{const. } (1_f)$$

$$K_u = \frac{F}{U_{z,ref.geo.}} - K_e \quad (2_f)$$

$$K_g = \frac{F}{U_{z,geo.nonl.}} - (K_e + K_u) \quad (3_f)$$

In Figure F.2 the separated progression of stiffness is shown based on the equations (1_f-3_f) for several rise to span ratios of the elastica arc. Both elastic stiffness and total beam length are constant throughout this investigation. The compression force induced to the beam causes a negative geometric stiffness as

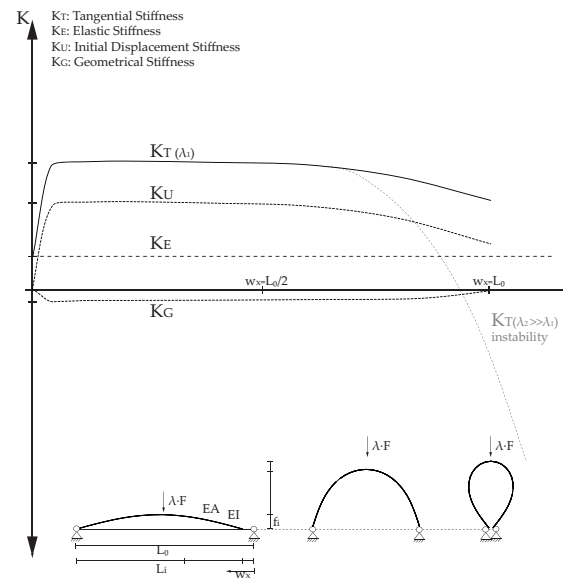


Fig. F.2

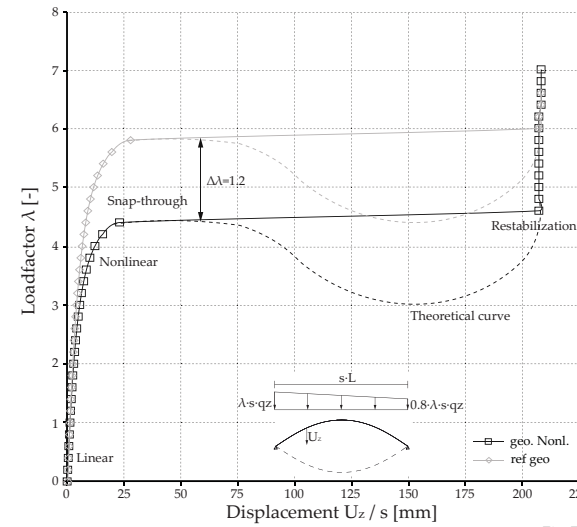
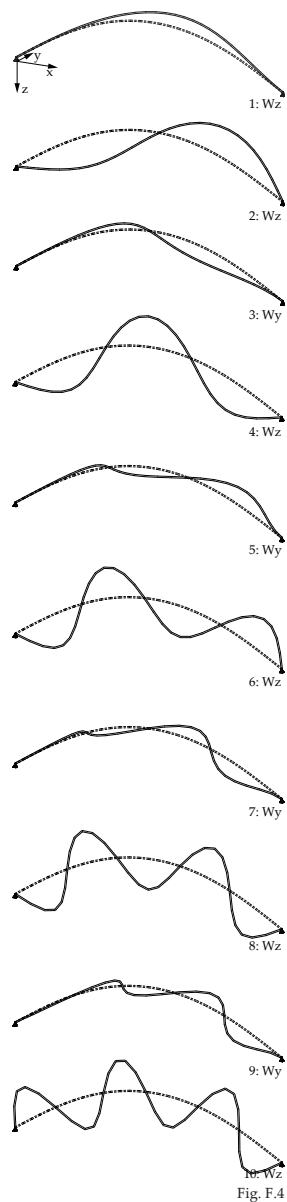


Fig. F.3



the support movement reduces the span (compare (8_B)). Once the beam forms the post-buckling elastica curve there is no significant change in normal force, leading to a constant negative geometric stiffness. Meanwhile, a change in load bearing mechanism from single span beam to an arc leads to a drastic increase in initial displacement stiffness, which decreases again at rise to span ratios larger than 0.35 (compare chapter E3.1 Figure E.17). At rise to span ratios larger than 1, the tangents of the beam ends start to lean outwards, leading to tension in the beam as the span is further reduced. This becomes visible with a slight increase of geometric stiffness, while initial displacement stiffness reduces again due to the structurally inappropriate shape of the arc.

Eigenfrequency analysis of an elastica arc

As a most general method for measuring stiffness of a structure, independent of load magnitude and direction, a comparative Eigenfrequency analysis is used (see Chapter B2.3), in which mass and stiffness are defined through a primary load case. In Figure F.4 the qualitative deformation of the first ten dynamic Eigenmodes of an elastica with rise to span ratios of 0.15 are given. In Figure F.5 the first ten Eigenfrequencies of various rise to span ratios are given, comparing the frequency spectrum of the geometric nonlinear case (primary load case dead load plus bending stress) to the reference geometry case (primary load case dead load). For the un-deformed beam, there is no difference in Eigenfrequencies, as expected. In accordance to the findings above, the Eigenfrequencies of the elastically deformed geometric nonlinear case are lower than those of the reference geometry case, indicating a lower stiffness. While the aforesaid conclusions are all based on a single vertical point load, the Eigenfrequency analysis includes various kinds of in-plane, out-of-plane and asymmetric deformations. This allows for a more general interpretation of stiffness in the structure, independent of specific loading directions. In the case of the elastica arc, all dynamic Eigenmodes exhibit a lower stiffness in the geometric nonlinear case. Again, in accordance with the findings in Figure F.2, the geometric stiffness increases for larger rise to span ratios. In this case, particularly the first and fourth dynamic Eigenmodes show even positive geometric stiffness in the extreme case of the elastica where the two supports touch each other.

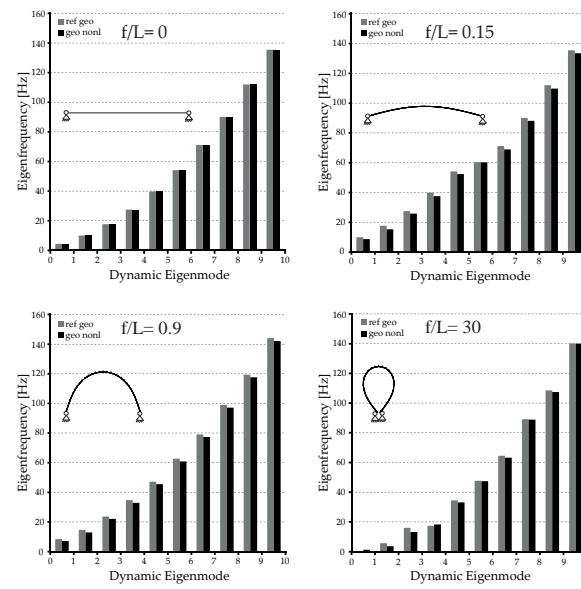


Fig. F.5

In general, it is important to compare the correct dynamic Eigenmodes for their varying Eigenfrequencies, since some particular cases in the following studies may show different dynamic Eigenmodes at a particular Eigenfrequency (eg. First second or third Eigenfrequency) when comparing the reference to the geometric nonlinear case.

Load deflection curves of an elastica arc

Having analysed and visualized the general characteristics of stiffness in various rise to span ratios of the elastica arc, a more precise investigation may be made for particular geometric instances with a load deflection curve (see Chapter B2 Figure B.4). In the Eigenfrequency analysis above, the largest difference between the geometric nonlinear and the reference case is found in the second and third dynamic Eigenmode throughout all rise to span ratios. In order to cause a similar in-plane deformation as the second dynamic Eigenmode, an asymmetric line load is applied to the elastica arc of rise to span ratio 0.15. The mechanical properties of the system are given in Appendix D. In the load deformation curve in Figure F.3, the de-stiffening effect of

Fig. F.4 Qualitative deformation of the first ten dynamic Eigenmodes of the elastica arc with symmetric cross-section and rise to span ratios of 0.15, showing deflections with various amplitudes in z and y direction.

Fig. F.5 First ten Eigenfrequencies for various rise to span ratios of the elastic arc, comparing the frequency spectrum of the geometric nonlinear case to the reference geometry case.

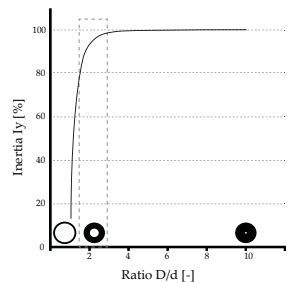


Fig. F.6

normal compression force in the geometric nonlinear case can be observed once more. As the load factor λ is increased, the system becomes unstable and snaps-through, indicated by the horizontal section of the load deformation curve. Here the calculation jumps to the next stable point on the equilibrium path, the negative stiffness as shown by the theoretical line cannot be traced by the solvers used in this investigation. Once the system has snapped-through, the arc is inverted and load is transferred by tension forces leading to a re-stiffening of the system indicated by the vertical tangent of the load deflection curves. In this largely nonlinear analysis, it becomes visible that residual compression stress in the geometric nonlinear investigation not only reduces stiffness but also considerably destabilises the system. In the investigated case in Figure F.3, the difference in load factor at the point of snap through buckling is $\Delta\lambda > 1$. This is a significant influence of residual stress on the structural performance of the system which must be considered in the analysis of bending-active structures.

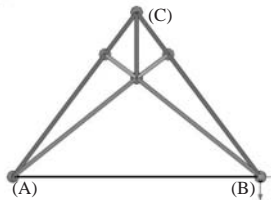


Fig. F.7

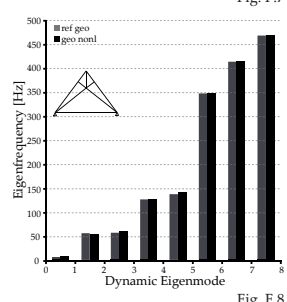


Fig. F.8

Fig. F.6 Dimensionless graph with the relation of a tube's inner and outer diameter, plotted against the moment of inertia.
Fig. F.7 Truss system with cable suspension and fully hinged support in (A) and a hinged slipping support in (B).

F 1.1.1 Balancing elastic stiffness

The choice of cross-section has a significant influence on the behaviour of an entire bending-active structure. In this special case, the cross-section is not chosen according to a given system behaviour but rather defines the behaviour. In general, a smaller cross-sectional height allows for smaller bending radii (compare (21_B)), yet also reduces elastic stiffness of the system. Therefore, the moment of inertia must be maximised while the cross-sectional height is material and bending radius dependent. As a consequence, solid and wider cross-sections are usually preferred over hollow double symmetric sections.

In Figure F.6, the relation of inner and outer diameter of a tube is plotted against the moment of inertia in a dimensionless graph. An optimal range of the D/d ratio can be appointed to ± 2 , where the stiffness is close to the maximum while the cross-sectional area is kept in an economic range, minimizing material and thereby dead load deformation. For flat sections the width has a linear influence on both moment of inertia and cross sectional area. Therefore, no optimal relation can be appointed.

Similar to the cross-section, a smaller Young's Modulus allows for smaller bending radii yet also reduces elastic stiffness. In chapter B3.1 the ratio of Young's Modulus to permissible stress is introduced to locate adequate materials for bending-active structures. In general, elastic stiffness must be low to allow for small bending radii yet large enough to ensure structural integrity.

For all of the following investigations the same set of basic mechanical parameters is used for structures in the range of 3 m span. The cross section is circular with 25 mm diameter and 5 mm wall thickness, Young's modulus is set at 25.000 N/mm². Further specifications are given in Appendix D.

F 1.2 Pre-analysis of Stress-stiffening in Basic Structural Systems

Having shown the de-stiffening effect of compression in an elastica arc, further analysis and investigations will focus on unveiling stress stiffening effects which may work in favour of a bending-active structure. Before looking into the complex behaviour of coupled bending-active structures, a simple truss structure

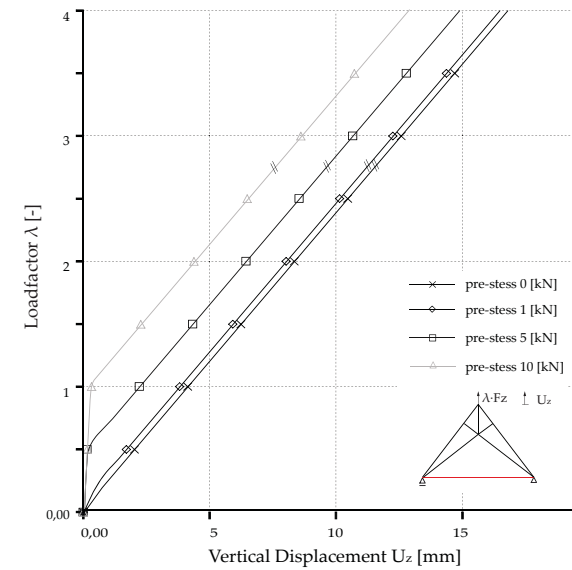
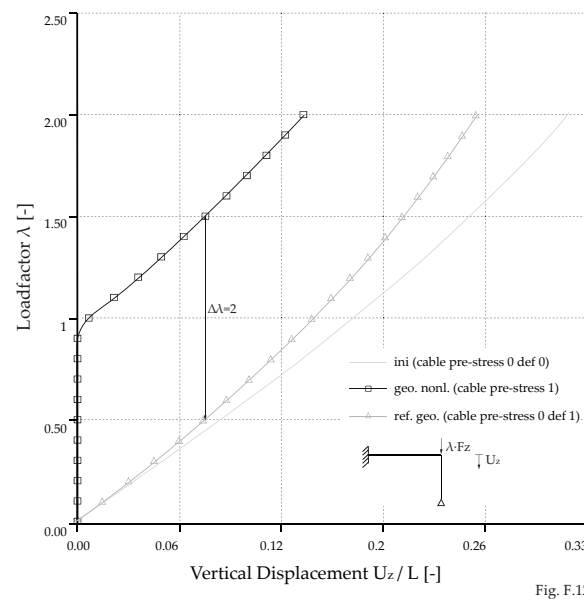
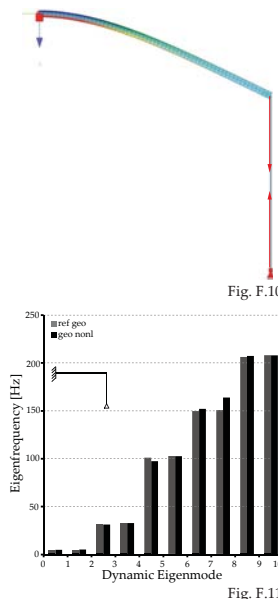


Fig. F.8 First ten Eigenfrequencies of the truss system in Fig. F.7 for various degrees of pre-stress in the bracing cable, comparing the frequency spectrum of the geometric nonlinear case to the reference geometry case.

Fig. F.9 Load deflection curves for the truss system in Fig. F.7 for various degrees of pre-stress in the bracing cable. Mechanical properties according to Appendix D.



and a cantilever beam with pre-tensioned cable suspension are analysed.

F 1.2.1 Basic truss system

In Figure F.7 a truss system is introduced with a fully hinged support in (A) and a hinged slipping support in (B). A pre-tensioned cable spans between the two supports, inducing tension in the outer cords and compression in the inner cords of the system. A vertical point load $\lambda \cdot F$ is applied to node (C) pointing upwards, which causes a decreasing of the cable-pretension. In Figure F.9 the load deflection curves of the system are compared for various degrees of cable pre-tension, showing similar behaviour to the pre-tensioned cable introduced in B2.2 where the load deflection curves are parallel once all pre-tension is overcome by compression in the system. In the example of the truss structure, this effect is only visible when load is applied in a direction that reduces pre-tension. In this case, increasing pre-tension linearly increases stiffness. This example thereby generally shows the stiffening effect of tension in a system. This is also supported

by the Eigenfrequency analysis in Figure F.8. It also shows that such effects are only noticeable when elastic stiffness K_e is relatively small and therefore in the order of magnitude of the geometric stiffness K_g , thereby large deformations activate the stress-stiffening effects. As mentioned above, a relatively small elastic stiffness is a prerequisite of bending-active structures. It can therefore be concluded that stress stiffening effects can play a noticeable role in the performance of a bending-active structure.

F 1.2.2 Cantilever beam

For a basic system of combining pre-tension with bending, a cantilever beam with a vertical pre-tensioned cable at the beam end is introduced in Figure F.10. For the stiffness analysis, three cases are compared; the undeflected system without cable pre-tension (ini), the deflected reference system without cable pre-tension (ref. geo.) and finally, the deflected system including cable pre-tension (geo. nonl.). A vertical point load $\lambda \cdot F$ is applied to node (B) pointing downwards, causing a decreasing of the cable-pretension. The Eigenfrequency analysis in Figure F.11 already indicates a strong stress stiffening effect in the 1st 7th, 8th and 9th Eigenfrequency. In Figure F.12 the load deflection curves of the system are compared for the three investigated scenarios. Again, the cable-pretension activates a stress-stiffening effect in the system. In contrast to the example of the simple pre-stressed cable and the truss system, the load deflection curves are nonlinear, but still there is a parallel shift of the geometric nonlinear line in comparison to the reference geometry. In this example the stress-stiffening effect is visible for systems where the cable pre-tension causes a significant bending deformation (initial displacement). However, the stiffening effect is not based on the bending itself, but rather becomes visible when the system undergoes large bending deformations as elastic stiffness and geometric stiffness are in the same order of magnitude. A tension element that plays an active part in the elastic from defining process therefore automatically contributes to the geometric stiffness a bending-active structure.

F 1.3 Stiffness Development in Basic Bending-active Systems

Four pairs of input reaction relationships may be distinguished:

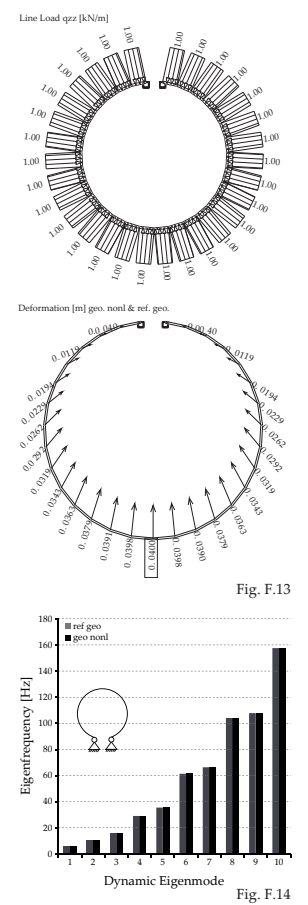
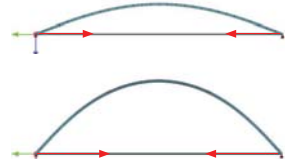


Fig. F.13 Load deformation of the pure bending system from Figure B.22, showing identical deformation for the geo. nonl. and ref. geo. cases.

Fig. F.14 First ten Eigenfrequencies of the pure-bending system in Fig. F.14, comparing the frequency spectrum of the geometric nonlinear case to the reference geometry case.



- Pure-Bending-Systems
- Bending-Compression-Systems
- Bending-Tension-Systems
- Bending-Torsion-System

F 1.3.1 Pure-Bending-Systems

Pure Bending systems are form-found by inducing a bending moment to individual elements of a structure without activating any additional tension or compression forces in the system. Such a system is used in chapter B2.4 Figure B.22 to compare bending stresses of an FE form-found circle to the analytical solution. Analysis of the first ten Eigenfrequencies in Figure F.14 shows no change in geometric stiffness when comparing the frequency spectrum of the geometric nonlinear case to the reference geometry case. An applied line load in Figure F.13 can confirm that pure bending systems are not able to activate stress stiffening effects. The fact that there are no destabilising residual compression forces in a pure-bending system can be seen as an advantage in comparison to the elastica arc discussed above. Not activating geometric stiffness does not exclude pure-bending systems from offering interesting solutions for basic bending active components; interesting basic shapes of bending-bending systems are shown in Figure E.3 and E.11.

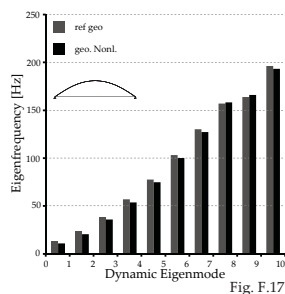


Fig. F.15 Cable tensioned arcs with two different rise to span ratios.

Fig. F.16 Dynamic Eigenmodes 8 and 9 of the cable tensioned arc

Fig. F.17 First ten Eigenfrequencies of the cable tensioned arc in Fig. F.15, comparing the frequency spectrum of the geometric nonlinear case to the reference geometry case.

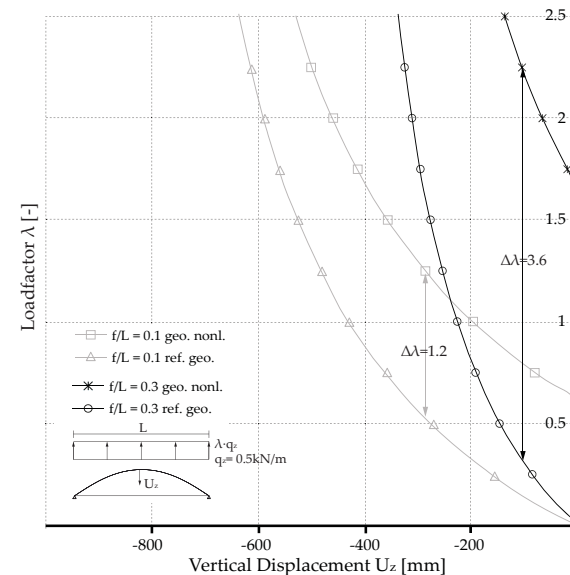
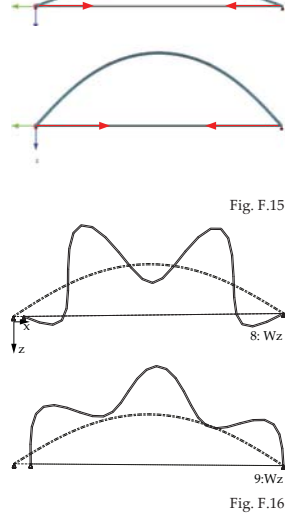


Fig. F.18

mous stiffness due to the dominant shell behaviour and the laying of multiple grids, and thereby realize large spans.

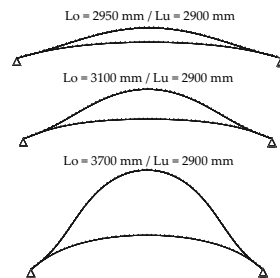
F 1.3.3 Bending-Tension-Systems

Cable Tensioned Arc

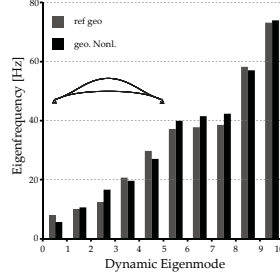
A simple coupled bending-active structure is based on the bow and string principle, in which a pre-tensioned cable (string) holds the shape of an elastica arc (bow) (Figure F.15). The elastic restoring effect of the bending-active arc is used to initiate a pre-tension force in the cable, which in turn is holding the shape of the arc. The system is thereby fully short-cut and supports are only affected by the dead load of the unloaded structure.

The Eigenfrequency analysis shows a stress stiffening effect for the 8th and 9th Eigenfrequency (Figure F.17). Looking at the respective Eigenform, it is noticeable that their deformation leads to a shortening of the span and thereby a reduction of the cable pre-tension (compare Figure F.16). This indication can be trans-

Fig. F.18 Load deflection curves for cable tensioned arcs of various rise to span ratios, comparing the geometric nonlinear case to the reference geometry case. Mechanical properties according to Appendix D.



lated to a stress stiffening effect which may be activated through a vertical load in the negative z direction or a horizontal load in the positive x direction, both of which will also lead to a deformation that reduces pre-tension in the cable.



In Figure F.18 the load deflection curves for cable tensioned arcs of various rise to span ratios are plotted. For loads in the negative z direction, a stress stiffening effect similar to that of the cantilever beam discussed above becomes visible. The stiffening can clearly be assigned to the pre-tension of the cable which is linked to the stored elastic bending energy in the arc. This example demonstrates how the bending activation of a component can be used to introduce tension normal forces in adjacent components. The residual stress of the elastica analysed by itself is de-stiffening (see above), yet it can therefore be turned into a structural advantage when the restoring effect is linked to tension elements. A built example of a bending-active arc that draws additional geometric stiffness from cables pre-tensioned against an elastically deflecting beam was used in a prototype GFRP footbridge (see Figure C.26) [Baverel et al. 2010]. Here, the pre-tensioning of a steel cable is arranged perpendicular to the actively bent arc, making the cables act as additional supports of the bridge construction.

Double arc

The double arc presents a fully coupled bending-active system in which all elements are actively bent. The system is created through the coupling and subsequent shear-resistant connection of two beam elements of different lengths. The upper beam is always longer than the lower beam. Through the different lengths of both beams, they must be elastically bent so that the two ends connect. The double arc is form-found by connecting several points of the beam ends with elastic form-finding cables (see E4.1). Once the contraction cables have been pulled fully together, the nodes are coupled into a stiff connection. The double arc is analysed as an externally statically determinate system. Through the variation of the lengths of the upper beams, various rise to span ratios of the double arc are achieved. Three of these variations of the double arc are shown in Figure F.19. The structure forms a closed equilibrium system: the upper beam exhibits compressive normal forces and the lower beam shows tensile normal

Fig. F.19 Rise to span ratios of the double arc depending on length ratio of the lower and upper beam.

Fig. F.20 First ten Eigenfrequencies of the double arc in Fig. F.18, comparing the frequency spectrum of the geometric nonlinear case to the reference geometry case.

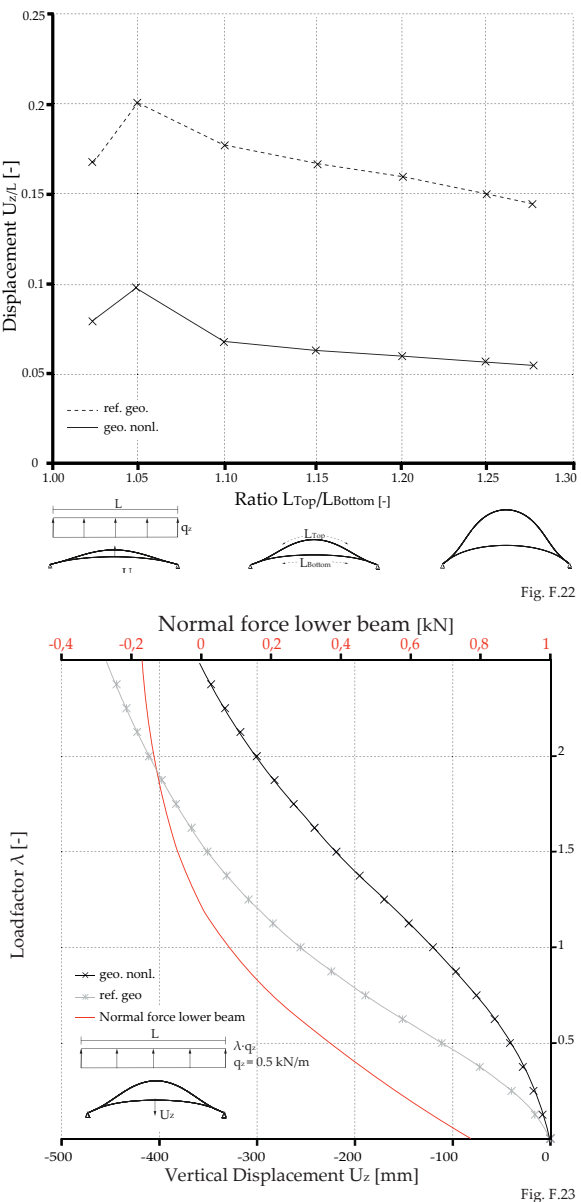
Fig. F.21 Qualitative deformation of the first two dynamic Eigenmodes of the double arc. For the first ten, see Appendix E.

forces which at any section through the system are in balance. Even though bent, for the lower arc the stresses in the centre of the section are still positive because of an over-layering tension, this leads to a stress-stiffening effect, similar to the cable-tension arc, enclosed in the bent element.

In the Eigenfrequency analysis, out-of-plane deformations (1st, 5th and 9th dynamic Eigenmode) of the upper arc show a de-stiffening for the geometric nonlinear case which can be assigned to the compression normal force (see Figure F.20 and F.21). All other dynamic Eigenmodes shown indicate a stress-stiffening effect. This is particularly visible in the 3rd dynamic Eigenmode where the lower arc deviates sideways and in the 6th, 7th, 8th and 10th dynamic Eigenmodes which all lead to compression forces in the lower arc and thereby reduction of its pre-stress due to a shortening of the span. A complete set of dynamic Eigenmodes is given in Appendix E.

In Figure F.22 the load deflections of various length ratios of lower and upper arc are shown. A vertical line load is applied to the various systems and deformation is measured as maximum deformation in global Z direction. Of the various rise to span ratios, a structurally advantageous ratio Lo/Lu can be appointed to $Lo/Lu=1.04$. The vertical deformations decrease linearly with increasing aspect ratio. To obtain small deformations, the aspect ratio should lie according to the calculations at about 1.25. In Figure F.23 the load deflection curve of a double arc with $Lo/Lu=1.04$ is given for a line load $\lambda \cdot qz$ in negative z direction.

Comparison of the geometric nonlinear curve to the reference geometry curve clearly shows a stress stiffening effect in the system. The red line in the graph indicates the normal force in the lower arc. Even though the load bearing behaviour is highly nonlinear it is clearly visible how the geometric nonlinear and the reference geometry curve run parallel as of the moment when the normal force passes from tension through zero and further into compression. If the double arc is supported statically indeterminate, forces that would decrease pre-stress in the lower beam directly go into the supports, stress-stiffening effects thereby cannot be activated. Similarly a vertical line load pointing downwards would activate arch action but no stress stiffening effects.

Fig. F.22
Fig. F.23

The study of the double arc clearly shows how the elastic restoring effect of bending-active elements can be used, to initiate tensile normal forces in adjacent components and thus activate stress-stiffening effects that increase stiffness of the entire system.

Coupled Arch

The coupled arch system is based on two adjacent strips which are interconnected in several points along their edges. Because of an alternating span between the connection points, the system forms a sequential series of arches and tension elements in the two strips (see Figure E.27). The form-finding of the coupled arch with the elastic cable approach clearly shows the advantage of this approach again, when considering the complexity of the equilibrium path the system follows during its form-finding. Through the imposed edge conditions, the beam strips are forced to bend locally, while the adjacent element is pre-stressed through the elastic restoring action of the bent element. This tension pre-stress of large sections in the beam indicates a significant stress-stiffening effect. However, this system is only of structural significance when the arches are arrayed to a larger tube or torus structure like the ICD/ITKE Pavilion 2010 (see chapter D1) so that the local hinges are randomly distributed over the surface. The study of the single coupled arch is therefore only made to highlight the stress-stiffening effects in the system. The stress-stiffening effect is simply shown by comparing the vertical deformations of a discrete load case for the geometric nonlinear case and the reference geometry case in Figure F.24. The distribution of the normal forces (Figure F.24 top) clearly shows that the curved element sections stand mainly under compressive normal forces, as known from the elastica arc. The straight element sections, however, are predominantly under tensile normal forces which increase geometric stiffness of the coupled system. Further analysis of this system will be made in the FEM model of the actual pavilion structure in Chapter F1.5.

F 1.3.4 Warping: Bending-Torsion-System

Torsion Beam

Warping couples torsion with flexion (see chapter B2.5). In this combination a pure bending system, or bending compression

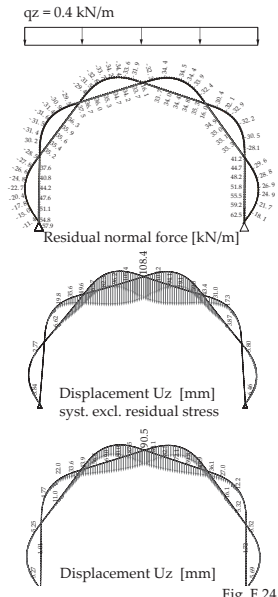
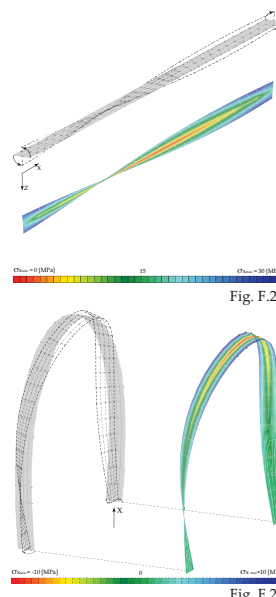
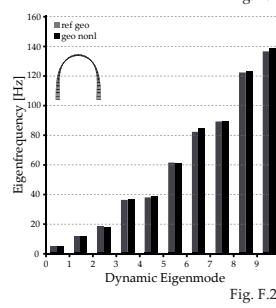


Fig. F.22 Load deflections of various length ratios of the lower and upper beam of the double arch.

Fig. F.23 Load deflection curve of a double arch with $L_0/L_u=1.04$, comparing the geometric nonlinear case to the reference geometry case, as well as showing the normal force in the lower beam. Mechanical properties according to Appendix D.Fig. F.24 Displacement U_z of a coupled arch section from the pavilion, showing 17% increase in stiffness for the system including residual stress induced by active bending.



system can develop additional geometric stiffness from torsion. In order to understand the stress-stiffening effect through torsion the single span beam from chapter B2.5 is analysed here with the afore introduced measures of stiffness.



The positive influence on geometric stiffness is only given for a beam with fully clamped supports. In such a case, for non-warping-free cross-sections, tensile stress adds to the geometric stiffness. For large rotations the elongation of the outer fibres, present for all section types, leads to a dominant tensile stress in the section. These normal stresses from non-uniform torsion only play a visible role in the overall stiffness when elastic stiffness is set relatively small. Even though structurally inappropriate, setting the Young's Modulus to 10 % of the standard GFRP values unveils the potential stress-stiffening effect in the torsion beam. In Figure F.28 the progression of stiffness for the single span torsion beam is shown with a reduction of Young's Modulus to 10 %. It can be seen how geometric stiffness increases for large torsional rotations. The stress-plot in Figure F.25 shows the principle stress in the middle of the section, clearly showing the dominant tension bands on either side of the section and no compression in the centre. The presence of stress-stiffening in a torsion beam is thereby proven. The examples below will show how spatial configurations with warping elements can draw significant stiffness reserves from this stress stiffening effect.

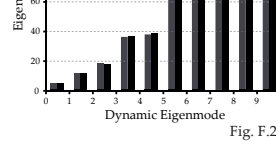


Fig. F.25 Principle stress in the middle of the section of a torsional beam.

Fig. F.26 Principle stress in the middle of the section of a torsional arc.

Fig. F.27 First ten Eigenfrequencies of the torsional arc in Fig. F.25, comparing the frequency spectrum of the geometric nonlinear case to the reference geometry case.

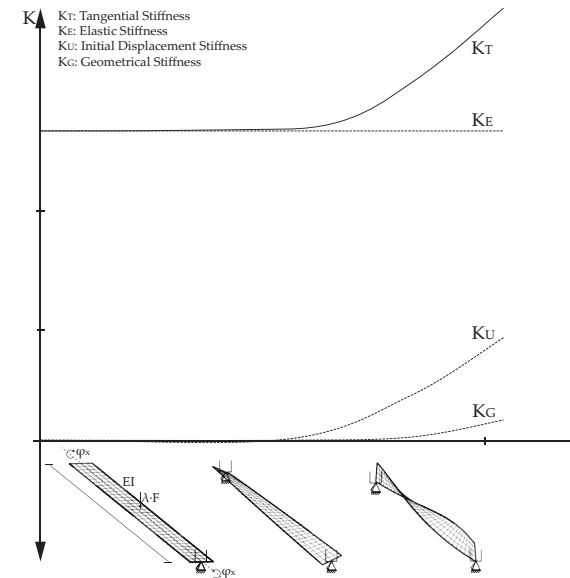


Fig. F.28

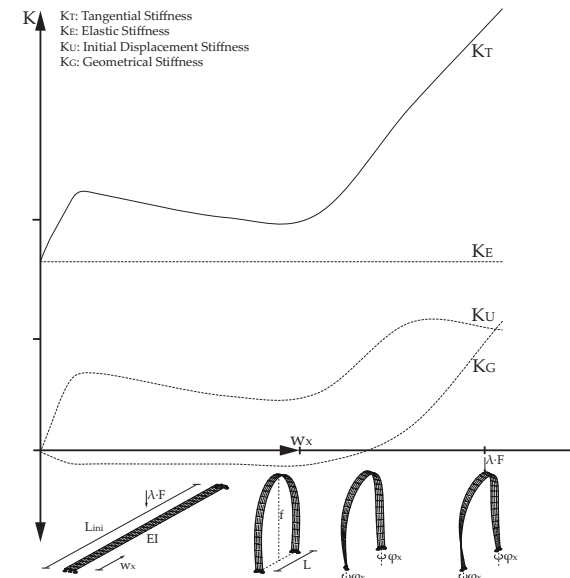


Fig. F.29

Fig. F.28 Stiffness progression for the single span torsion beam is shown with a reduction of Young's Modulus to 10 %.

Fig. F.29 Stiffness progression of the torsional arc.

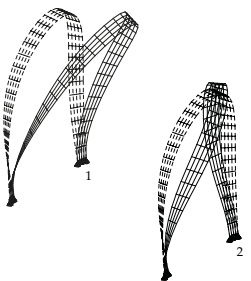


Fig. F.30

this stress-plot to the torsional beam shown in Figure F.25 it becomes apparent how the stress resulting from torsion are dominant in the system. While the forced elongation of the outer fibres in the torsional beam with fully clamped supports is easily comprehensible, the same effect being present in the torsional arc can be explained by a spatial shortening of the system through torsion which again leads to tension in the outer fibres. The tension is held in the system because the centre of the cross-section resists the shortening and is thereby under compression. A closer look at the stress-plot in Figure F.26 shows how the magnitude of the tensile stress is greater than the corresponding compression stresses in the centre of the section. Overall, this leads to the increased geometrical stiffness also shown in the Eigenfrequency analysis in Figure F.27 and F.30. The Eigenfrequency analysis in Figure F.27 shows stress stiffening effects in the 1st, 5th, 7th, 9th and 10th Eigenfrequencies. (A complete set of dynamic Eigenmodes is given in Appendix E). Comparing these to the dynamic Eigenmodes in Figure F.30 the system suggests to activate stress stiffening effects for vertical deformations. This assumption is proven by the load deflection curve in Figure F.31 where the line of geometric nonlinear case is offset by a maximum of load factor $\lambda=1$ to the reference geometry.

"Bender"

The elastic kinetic shading lamellas of the Expo 2012 One Ocean Pavilion (see Chapter C2.3 Figure C.28-29) has been referred to as "bender" by the structural engineers. The system is based on slightly pre-curved GFRP strips which are actuated by shortening the span of one of the long edges by means of support displacement. The system reacts by buckling into an asymmetric arc and in plane rotations. These rotations add on the compression side to the buckling of the system. On the fixed side the rotations lead to dominant tensile stress. Because the system cannot deviate from the imposed forces on this side, tension forces are higher than compression forces. Therefore, and intuitively unexpectedly the system develops additional geometric stiffness.

Fig. F.30 Qualitative deformation of the first two dynamic Eigenmodes of torsional arc. For the first ten, see Appendix E.

This stress stiffening effect may also be explained when looking at the definition of the geometric stiffness matrix for shell elements in Appendix B. Here all in-plane stress components, including shear, show a positive effect on geometric stiffness when positive in algebraic sign. In Figure F.36 the principal stresses in

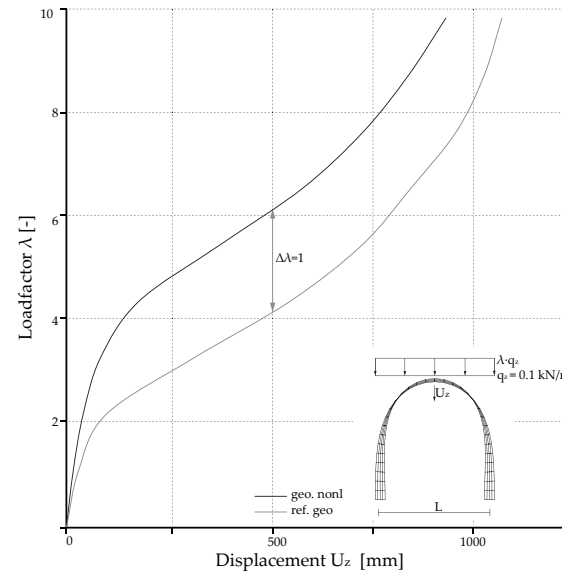


Fig. F.31

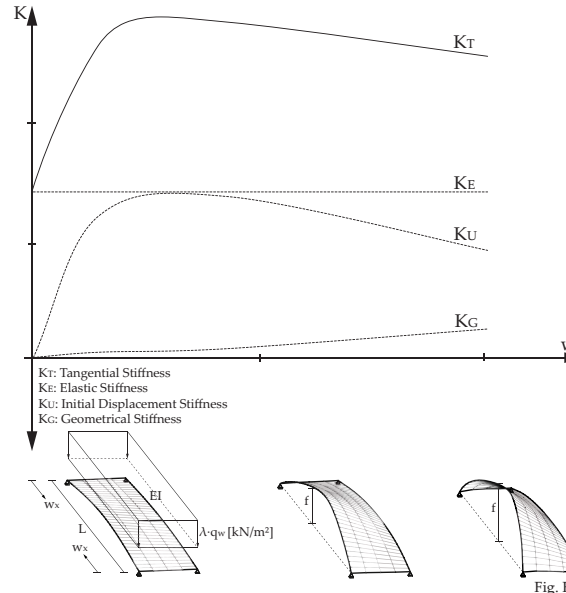
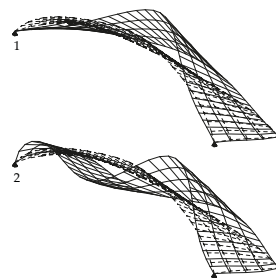


Fig. F.32

Appendix D.

Fig. F.32 Stiffness progression of the "bender".



the section middle are shown, displaying a dominance of tensile stress. The stiffness progression curves in Figure F.32 show how geometric stiffness develops upon actuation of the system. The Eigenfrequency analysis in Figure F.33 and F.34 shows stress-stiffening in all 10 of the first dynamic Eigenmodes since tension pre-stress is present in the entire element. A complete set of dynamic Eigenmodes is given in Appendix E.

F 1.4 Stiffening Effects of Case Study Structures

ICD/ITKE Research Pavilion

The pavilion structure is based on an array of the afore introduced coupled arch structure (Figure E.26 and F.24). The stress stiffening effect based on the tensile pre-stress in the straight sections can be seen in the Eigenfrequency analysis in Figure F.35. Stress-stiffening can be observed for both horizontal and vertical deformations. Because of the complexity of the system however, no clear interpretations of load directions in which stress-stiffening is activated can be concluded from the dynamic Eigenmodes. Therefore the load deflection curve in Figure 37 is based on a vertical areal load similar to the line load in Figure F.24. The load deflection curve shows a sudden stability loss due to snap-through buckling. The load factor at the point of snap-through can be increased by $\Delta\lambda=1$ for the geometric nonlinear case. This is an important indication that stress stiffening may be stabilizing to a structure. In contrast to the elastica, where compression forces provoked an early stability failure (compare Figure F.3) the positive geometric stiffness in the pavilion structure significantly adds to the stability of the system.

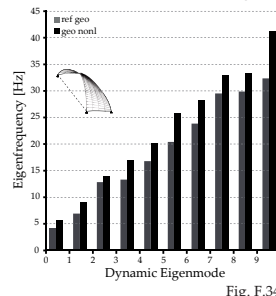


Fig. F.34

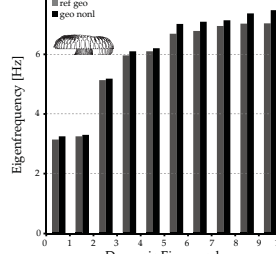


Fig. F.35

Umbrella for Marrakech

The elastically bent rods of the Marrakech umbrella are exposed to large compression forces. Therefore, negative geometric stiffness is destabilising to the system. Having the elastic beam element being positioned in the plane of the membrane will in most cases lead to critical snap-through problems at modest loads. Controlling this by adding stiffness to the beam itself is not an option if the beam is to be bent into a significantly curved geometry with sufficient remaining load bearing reserves. A practical solution has been used for several years in the design

BURFORD, N. and GENGNAGEL, C. (2004) Mobile Shelters Systems – 2 Case Studies in Innovation.

ALPERMANN, H. and GENGNAGEL, C. (2009) Membrane restrained arch.

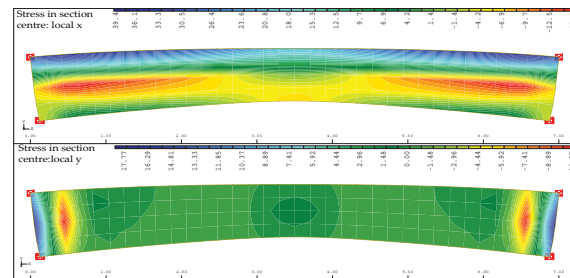


Fig. F.36

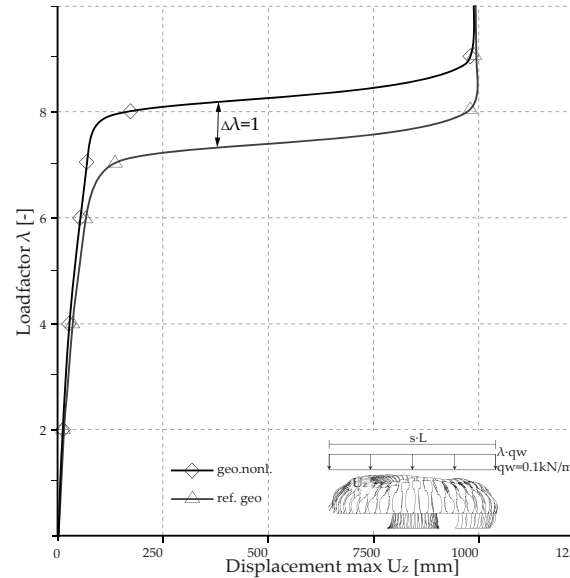


Fig. F.37

of camping tent structures; by attaching the beam eccentric to the surface a significant rise in stiffness can be observed. This effect has already been studied in temporary shelters [Burford and Gengnagel 2004] and membrane restrained arches [Alpermann and Gengnagel 2009].

Figure F.42 shows a comparison of the load deflection curves for the two investigated systems. In system 1, the beam is positioned in the plane of the membrane (Figure F.40). In system 2, the beam is attached eccentrically with a maximum distance of 12 cm in the

Fig. F.33 Qualitative deformation of the first two Eigenmodes of the "bender". For the first ten, see Appendix E.

Fig. F.34 First ten Eigenfrequencies of the "bender", comparing the frequency spectrum of the geometric nonlinear case to the reference geometry case.

Fig. F.35 First ten Eigenfrequencies of the ICD/ITKE research pavilion, comparing the frequency spectrum of the geometric nonlinear case to the reference geometry case.

Fig. F.36 Principal stresses in the section middle of the "bender", with a dominance of tensile stress.

Fig. F.37 Load deflection curves of the ICD/ITKE research pavilion, comparing the the geometric nonlinear case to the reference geometry case.

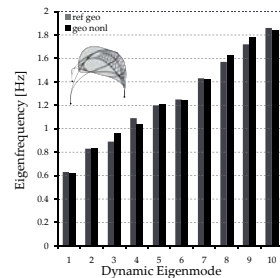


Fig. F.38

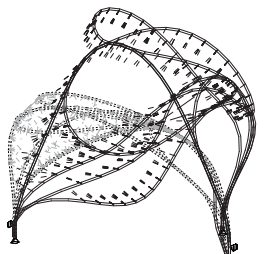


Fig. F.39

Fig. F.38 First ten Eigenfrequencies of the M1 structure without membrane, comparing the frequency spectrum of the geometric nonlinear case to the reference geometry case.

Fig. F.39 Qualitative deformation of the first dynamic Eigenmode of the M1 structure without membrane.

Fig. F.40 - 41 System 1: beam and membrane are lying in the same plane System

2: eccentric attachment of the beam.

Fig. F.42 Comparison of the load deflection curves for the two investigated systems in F.40 and F.41.

Fig. F.43 Form-finding and principal stresses in the middle section GFRP boards for the Softhouse, showing a dominance of tensile stress.

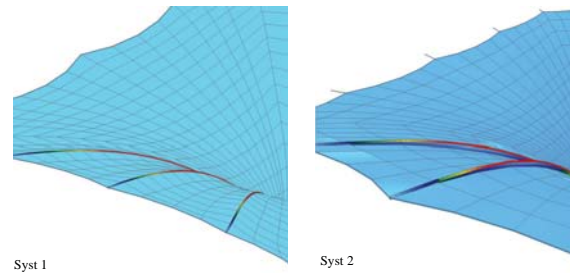
middle (Figure F.41). The eccentricity is simulated with floating coupling elements during the form-finding which are replaced by real membrane elements for the further analysis of the structure. The deflections are tracked at two positions of the beams (E: End, M: Middle) for increasing load factor λ of a wind pressure load case ($q_{zz} = 0.25 \text{ kN/m}^2$). System 1 shows very high deformations at the arm end which is abruptly stopped by a vertical tangent at $\lambda = 0.5$ once the edge cables are sagged and carry the entire vertical load. The same tangent is reached by system 2, at a load increment of $\lambda = 3.5$. Even more significant differences can be observed in the arm middle deformations. Here, System 1 has a distinct snap-through point at $\lambda = 0.75$ while system 2 shows no system failure. The final deformations in system 2 are 75 % lower than those of system 1. This gain in stiffness may be explained by the principle of a restrained arch, before a snap-through of the arched beam can occur the entire pre-stress in the membrane pocket must be outweighed.

Textile Hybrid - M1

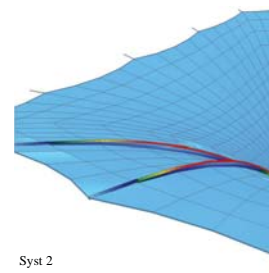
The Eigenfrequency analysis of the M1 structure without membrane shows stress-stiffening effects in the 3rd, 5th, 8th and 9th dynamic Eigenmode (see Figure F.38). Because of the complexity of the dynamic Eigenmodes deformation, as seen in Figure F.39, it is not possible to interpret further the directional dependences of these stress-stiffening effects. Since the form-finding of the bending-active primary structure is entirely based on pulling associate points of the rods with elastic cables into an interlocked system, the existence of dominant tensile stress and thereby increase in geometric stiffness can be expected. Form-finding by pulling rather than support displacements may thereby automatically lead to an increase of geometric stiffness.

Softhouse

The cantilever of the softhouse behaves similar to the afore mentioned cantilever system bent with a pre-tensioned cable. Here, the pre-stress membrane induces tensile stress in the actively bent cantilever. In this case of a system that is formed through pre-stress of a structurally integral membrane, no structurally relevant reference geometry can be defined that is free of pre-stress. Therefore, none of the afore used measures of stiffness can be used to isolate the effect of geometric stiffness. Instead, the



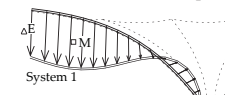
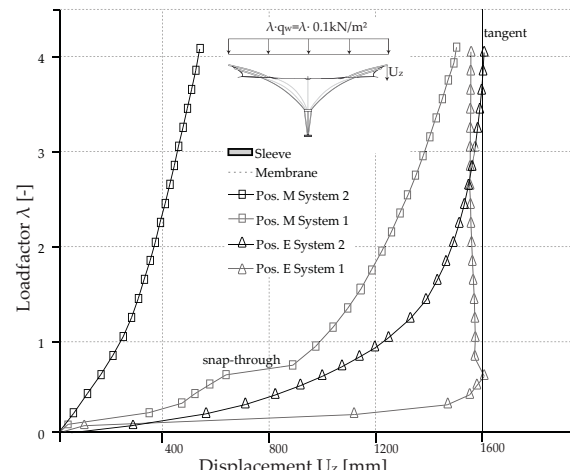
Syst 1



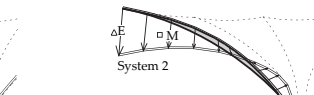
Syst 2

Fig. F.40

Fig. F.41



System 1



System 2

Fig. F.42

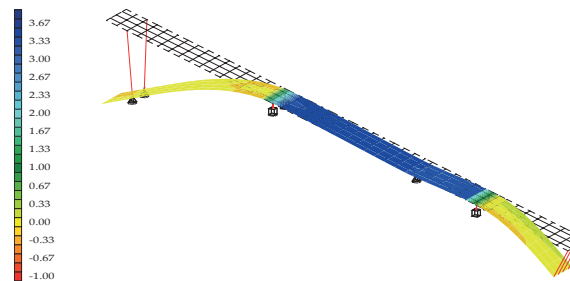


Fig. F.43

argument of positive geometric stiffness being present is based on the stress-plot of the cantilever shown in Figure F.43. The principal stresses in the section middle are positive (tensile) in the longitudinal direction, based on the findings from the previous section it can therefore be concluded that positive geometric stiffness works in favour of the structural rigidity.

Flectofin®

For this compliant mechanism the study of stiffness progression is particularly important, because all stages of deformation are structurally relevant. The progression of stiffness in Figure F.46 shows how geometric stiffness immediately builds up when the system is actuated. Once the Flectofin starts opening, tensile stress remains constant and thereby no additional geometric stiffness is built up. Due to increasing double curvature initial displacement stiffness continuously increases until both lamellas are fully opened. Similar to the aforementioned 'bender' the dominance of tensile stress in the shell elements leads to significant stress-stiffening in all of the first ten dynamic Eigenmodes (see Figure F.44 and F.45). In Figure F.47 load deflection is given for various opening positions of the Flectofin® under a constant wind load acting perpendicular to the surfaces. Comparison of the geometric nonlinear case to the reference geometry again shows the constant increase of stiffness due dominance of residual tensile stress within the actively bent lamellas.

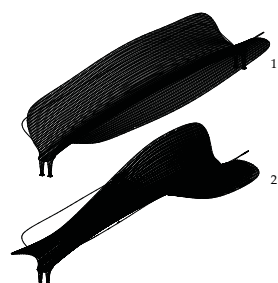


Fig. F.44

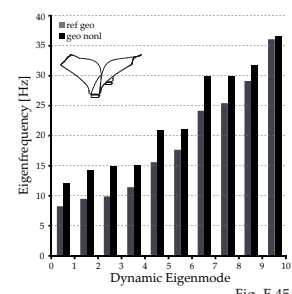


Fig. F.45

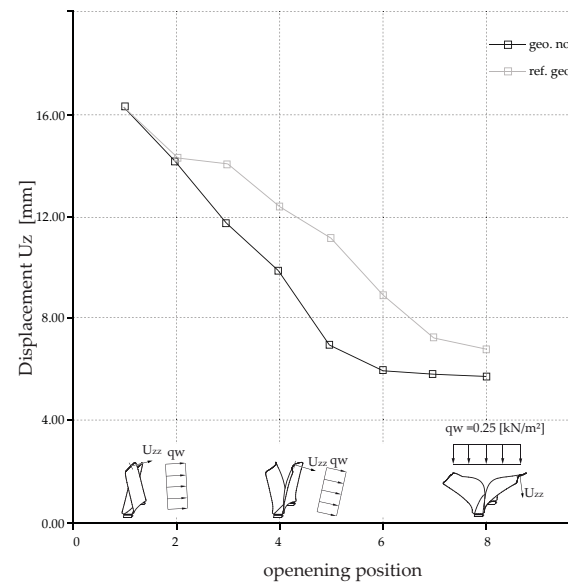
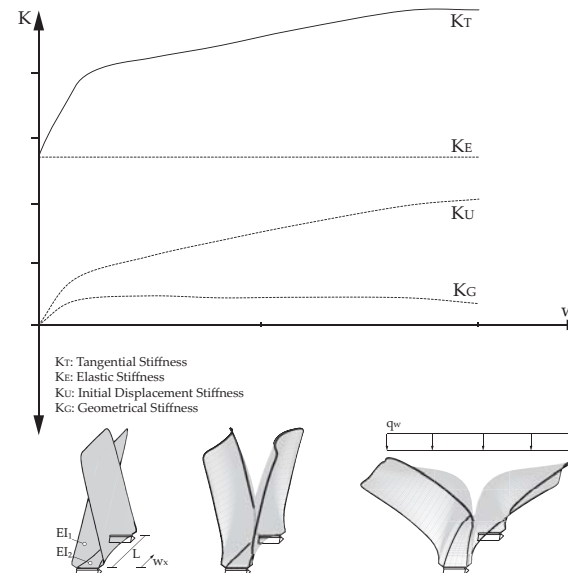


Fig. F.47

Fig. F.44 Qualitative deformation of the first two dynamic Eigenmodes of the Flectofin. For the first ten, see Appendix E.
Fig. F.45 First ten Eigenfrequencies of the Flectofin, comparing the frequency spectrum of the geometric nonlinear case to the reference geometry case.

Fig. F.46 Stiffness progression of the Flectofin.

Fig. F.47 Load deflection of the Flectofin for various opening positions, comparing the geometric nonlinear case to the reference geometry case.

F2 Scaling and Stability¹

F 2.1 General Introduction to Scaling

Since residual stresses are dependent on the bending radius and cross-sectional height, we are restricted by material strength in the sizing of structural members. This limitation means that the size of a cross-section may not be defined freely according to the requirements for strength and stiffness under external loads. Hence, scaling problems may occur when changing the scale of a bending-active structure.

In classical structural engineering we may consider three ranges of scale: the physical structural model, a reduced scale structure and a large scale structure, in which dimensional analysis and the derived scaling laws help to calibrate the proportions of test results between different scales [Harris and Sabinis 1999]. In today's engineering practice, analysis is mostly based on the Finite Element Method (FEM) in which dimensions are considered by the relation between geometrical and mechanical input variables. Structural analysis is therefore always done on a virtual 1:1 model. With these powerful computational means the necessity for structural physical models has been reduced to some dynamic problems e.g. wind tunnel testing. Reduced scale mock-up structures have similarly become dispensable.

In the development of bending-active structures the physical structural model has regained importance as a form-finding tool in the early design stages. An emergent amount of medium scale bending-active research structures is raising the question of their relevance for large scale building structures. In some cases like the gridshell, visionary projects such as the 'Multihalle Mannheim' with 64 m span have long proven their scalability. In this particular project, which was predominantly developed through physical models, scale factors for self-weight were derived to correctly simulate dead load deformation of the scaled model [Happold and Liddell 1975]. Other expressions of active bending in building structures are yet to be analysed for their scaling behaviour. The research presented in this chapter is based on the experiences from various case study structures, all

in the range of 2 to 10 m span. In all of these structures the scalar jump from a physical structural model to a medium scale structure was successfully undertaken. The question analysed now, concerns the scalar jump from a medium scale to a large scale structure and aims to fathom the scaling limits of various forms of bending-active structures.

Scaling in the most general sense is concerned with power-law relationships between two or more variables of a system. Investigating the scaling of building structures the variables concerned are deformation and stability on the one side, load and mechanical properties on the other. If the relation of these variables is independent of the system's dimensions we consider the system to be self-similar.

Some of the more common effects to consider for the scaling of building structures are:

- Dimension effect: cubic increase of mass with scale
- Load effect: quadratic increase of surface area leads to quadratic increase of surface load
- Size effect of material: probability of material defects increases with size, whereas the influence of material defects increases for small size specimens.
- Height effect: exponential growth of wind-speed with height combined with quadratic growth of wind-load with speed.
- Dynamic effects: Wind induced vibration etc.

Since the investigations in this paper are aimed to be of general nature we only consider the change in mass and load. The effects of change in material properties, wind load and dynamic behaviour with scale are very individual to each project and are therefore not taken into account in the further investigations. Their influence on scaling, however, will play a role on the construction of some large scale bending-active structures.

F 2.2 Dimensional Analysis of Elastica

In order to gain a principal understanding of the scalability of a simple bending-active system some initial studies are made on the elastica arc. From section B2.4.3 we can recall that residual

¹Based on a pre-published article: LIENHARD, J. and Knippers, J. (2013) Considerations on the scaling of bending-active structures

HARRIS, H.G. and SABINIS, G.M. (1999) Structural modelling and experimental techniques.

HAPPOLD, E. and LIDDELL, W.I. (1975) Timber lattice roof for the Mannheim Bundesgartenschau.

stress in such an elastically deformed beam can be determined with the Euler-Bernoulli law, in which the bending moment M_y is proportional to the change in curvature as shown in equation (4_F) [Fertis 2006]. With the section modulus W_y and the consideration that the width b of a cross-section has no influence on the maximum bending stress we can write the residual bending stress as an expression of the cross-sectional height h , the Modulus of Elasticity E and the Curvature $1/r$ (5_F).

$$\frac{1}{r} = \frac{M_y}{E \cdot I_y} \quad (4_F) \quad \sigma_M = \frac{E \cdot I_y}{r \cdot W_y} = \frac{E \cdot h}{2 \cdot r} \quad (5_F)$$

$$r = \frac{(s \cdot L_i)^2 + s \cdot f_i}{s \cdot 8 \cdot f_i} = s \cdot \frac{L_i^2 + 4 \cdot f_i^2}{8 \cdot f_i} \quad (6_F)$$

In (5_F) we can see that both curvature ($1/r$) and cross-sectional height h have a linear influence on the residual stress caused by active bending. The moment of inertia I_y is therefore limited by a given minimal curvature in the system and the permissible bending stress of the chosen material. The radius of curvature can be expressed as a function of the span L_i and the rise f_i . In (6_F) this relation is given with a scale factor s . Simplification of the equation shows that s can be excluded as a linear factor; thus, linear up-scaling of a structure allows for a linear up-scaling of the cross-sectional height while keeping the residual stress constant. Assuming constant material properties this leads to the overriding question, whether the influence of the span L on the deflection U_z can be compensated by the moment of inertia I_y , if the scaling of the cross-sectional height is limited to be linear for keeping the residual stress σ_M constant.

Deriving the dimensions using the Buckingham Pi Theorem:

Dimensional analysis enables a convenient investigation of physical behaviour by combining the variables of a system into dimensionless groups (Pi-terms). The Buckingham Pi-Theorem states that the relations in any physical system can be described by a group of $n \cdot r_d$ Pi-terms, in which n is the number of variables and r_d the number of basic dimensions therein (rank of the dimensional matrix) [Buckingham 1914]. In mechanics, the basic dimensions are mass, length and time. In the following consid-

erations on static structural behaviour, force is chosen as a basic dimension without further reduction into its constituent components for better comparison to known engineering equations. Based on the Pi-terms, a functional equation can be derived which shows a reduced form of the relevant variables; however, it does not give information about the nature of the solution. The exact form of the functional relationship has to be empirically obtained by a set of experiments in which the Pi-terms are systematically varied. Analytical analysis of the individual Pi-terms often is sufficient enough to describe the change of system behaviour with scale, without knowing the complete solution of the functional equation.

Investigating the deflection for a given elastica curve of span L stiffness EI and the line load q_z and excluding the influence of mass and residual axial force we may derive the following functional equation:

$$U_z = f(L, E, I_y, q_z)$$

5 Variables: U_z, L, E, I_y, q_z 5-2= 3 Pi-Terms
2 Dimensions: [mm], [N]

The dimensional Matrix is:

	U_z	L	E	I_y	q_z
[N]	0	0	1	0	1
[mm]	1	1	-2	4	-1

The dimensionless Pi-terms may be derived using various procedures, some of which are explained and discussed in detail by [Barr 1983]. Independent of the procedure it must be noticed that there is no unique set of Pi-terms that can be derived for a given problem. Pi-terms may differ in type depending on the choice of a repeating variable that eliminates dimension, additionally transformations of Pi-terms are possible. Here the results of the system deflection under a linear load were derived with the step wise procedure using L as the repeating variable. The resultant dimensionless Pi-terms are:

$$\pi_1 = \frac{U_z}{L}; \pi_2 = \frac{L^4}{I_y}; \pi_3 = \frac{q_z}{E \cdot L} \longrightarrow \frac{U_z}{L} = \phi\left(\frac{L^4}{I_y}, \frac{q_z}{E \cdot L}\right) \quad (7_F)$$

BARR, D.I.H. (1983) *A survey of procedures for dimensional analysis*.

An analysis of the given Pi-terms now enables to clarify at which power each variable is effected by scaling. In the common terminology of dimensional analysis one distinguishes between the scale of the model and that of the prototype. Investigating the scaling of I_y we can compare the Term π_2 in a model state m to an s times larger prototype state p .

$$\left(\frac{L^4}{I_y}\right)_m = \left(\frac{(s \cdot L)^4}{I_y}\right)_p \longrightarrow I_{y,p} = s^4 \cdot I_{y,m} \quad (8_F)$$

If all dimensions of the system are scaled by the same factor s we can show that the similitude in (8_F) is satisfied by a linear up scaling of the cross sectional dimensions, here shown for a flat section:

$$s^4 \cdot I_m = s^4 \frac{b_m \cdot h_m^3}{12} = \frac{s \cdot b_m \cdot (s \cdot h_m)^3}{12} = I_p \rightarrow b_p \cdot h_p = s \cdot b_m \cdot h_m \quad (9_F)$$

With (8_F) we can show that the deflection of an elastic arc is self-similar, if the effects of self-weight and residual force are excluded. Similar to (8_F) the term π_3 can be used to analyse the relation of the loading condition in model and prototype state, showing that the line load q_z scales linearly for constant material properties between model and prototype state:

$$\left(\frac{q_z}{E \cdot L}\right)_m = \left(\frac{q_z}{s \cdot E \cdot L}\right)_p \longrightarrow q_{z,p} = s_L \cdot s_E \cdot q_{z,m} \quad (10_F)$$

$$\text{with } s_L = \frac{L_p}{L_m} \text{ and } s_E = \frac{E_p}{E_m}$$

Including self-weight with the constant for density ρ and earth acceleration g adds another Pi-term, given in (11_F) where ρ and g appear as a linear factors. The cubic growth of mass with the cross-sectional area and length of an element however violates the similitude shown in (8_F).

$$\pi_4 = \frac{\rho \cdot g \cdot L}{E} \quad (11_F)$$

On the other hand, for lightweight structures such as those considered here, the cubic growth of mass with scale is per definition of minor influence, since the stiffness of a lightweight structure does not rely solely on the elastic stiffness of their members but also on their topological arrangement and geometric stiffness.

The influence of mass on scaling may therefore be negligible for small changes in scale at a medium size range; however, it will play a role when investigating large scale structures.

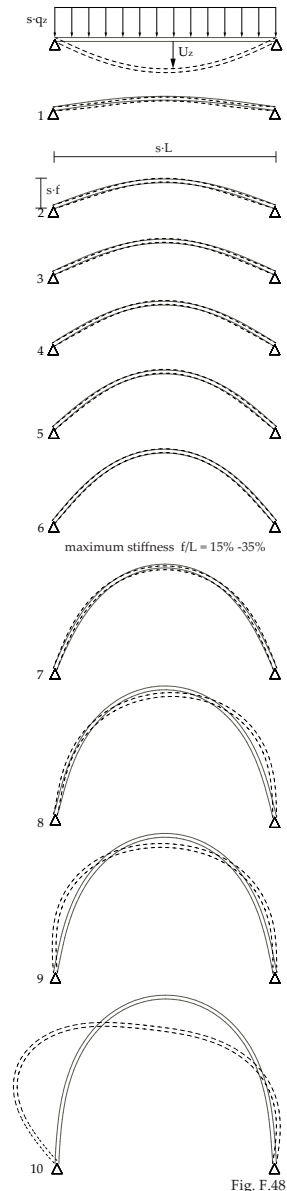
In the investigations above, only linear behaviour and elastic stiffness are taken into consideration. Next to the residual bending stress, there is also usually a considerable amount of residual axial force N in a bending-active system e.g. the nonlinearly distributed axial compression force in the post-buckling state of an elastica curve. In a nonlinear investigation axial force has an influence on the geometric stiffness which, in the case of bending-active structures is usually also nonlinear in its distribution along individual elements. Such behaviour cannot be considered by a single equation derived through dimensional analysis.

From these considerations a preliminary conclusion can be drawn: *Bending-active systems are self-similar if dead load plays a minor role and axial force is not destabilising to the system.*

F 2.3 FEM Analysis of Elastica

In the following study, the conclusions drawn above are verified for several span to rise ratios of elastica curves and then studied considering the mass and axial force N for a set geometry at varying size ranges, using nonlinear Finite Element Analysis. Each geometry was first form-found using incremental deformation and then studied for load displacement behaviour by step-wise increasing the load up to the point of system failure.

In Figure F.49 Elastica curves with various span L to rise f ratios are investigated in which L is kept constant. The system is investigated at scale factors $s = 1, 2, 4$ and 8 . In accordance to Pi-term 3 and equation (10_F) derived above, the line load q_z is also scaled by s to account for the growing loading area that may be spanning between two arcs. The system lines in Figure F.48 show the various arcs in the initial and comparative deformed position, clearly showing maximum stiffness at ratios of $f/L = 0.15$ to 0.35 . As this ratio tends towards $f/L=1.0$ the arches show increasingly low stiffness and nonlinear behaviour; compare dashed line in Figure F.48. The graphs in Figure F.49 show the displacement curves in the linear range without dead load or residual axial



force. Their linearity prove the similitude derived above for all variations of the elastica curve, in which the rise to span ratio is a constant in correspondence with the incline of the graph.

In Figure F.1 and F.3 an elastica curve with $f/L=0.15$ is investigated by plotting the load deformation with corresponding compression stress for a step wise increasing scaled line load. In order to exclude findings that are limited to symmetric systems, the line load is applied asymmetrically. In Figure F.50 investigations were compared at two different scales with $s=1$ and $s=8$ showing the nonlinear behaviour at higher loads and final snap-through buckling.

For each scale, the system is calculated in three different scenarios. First, (indicated by the continuous lines) including dead load and axial force, showing a difference in load factor $\Delta\lambda=1$ between scale $s=1$ and $s=8$ at the point of snap-through buckling. In a second scenario, (dashed line) the residual stress and thereby axial force N is disabled. This leads to a shift of both graphs by load factors $\Delta\lambda=1.0$ for $s=1$ and $\Delta\lambda=1.2$ for $s=8$ higher at the point of failure. The difference between scales is reduced from $\Delta\lambda=1$ to $\Delta\lambda=0.9$.

Finally, the dotted line shows the elastica in a calculation without dead load and residual stress. Here, the two load deflection curves almost perfectly match and snap-through buckling occurs at the same load factor, $\Delta\lambda=0$. This clearly supports the hypothesis made in section 2 that the bending-active elastica arc is self-similar if dead load and axial force are omitted. In general, the graph shows how the curves are very close in the linear range and the influence of dead load grows with size ($\Delta\lambda=0.2$ for $s=1$ and $\Delta\lambda=1$ for $s=8$).

F 2.4 Scaling of Case Study Structures

With the scaling investigations on three successfully built case study structures, the above drawn conclusions are verified. A jump in scale from a prototypical structure, in the size of an exhibition pavilion, to a large building structure is investigated. The choice of material for these bending-active structures is limited by availability of materials offering high strength with low

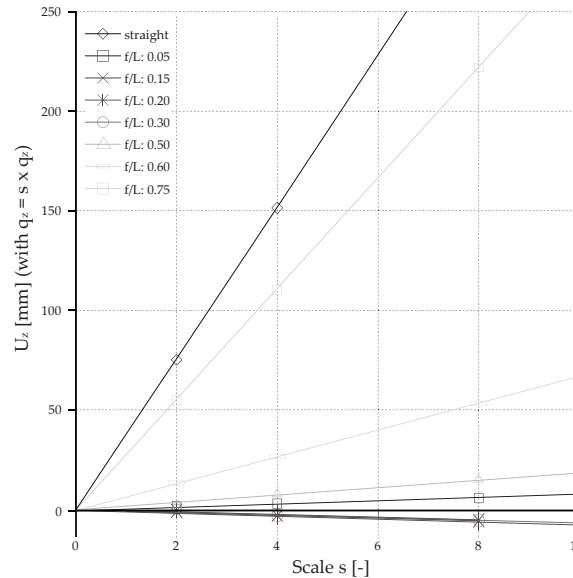


Fig. F.49

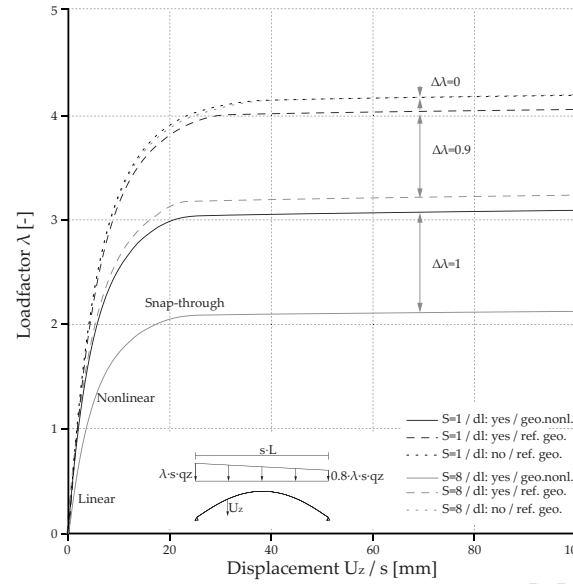


Fig. F.48 Study of Elastica curves with constant span and varying rise at different scales.

Fig. F.49 Deflection curve for different scales of the elastica arcs in F.48.

Fig. F.50 Load deflection curve of the elastica curve with 15% f/L ratio at two scales; showing linear, nonlinear and snap-through failure range.

bending stiffness such as plywood and GFRP. In addition the scalar investigation are made in a relatively small range of $s = 0.5$ to 5. Therefore, material properties are assumed constant. For all systems several wind and combined snow load cases are investigated; the graphs in Figures F.51 - F.54 are a selection that best highlight the scale dependent behaviour discussed here. In contrast to the investigations on the elastica, loads are real and therefore constant across scale. Height effects of wind are not considered because of the relatively small scalar range investigated.

Research pavilion ICD/ITKE 2010

In Figure F.36 the deformation of the pavilion under vertical load shows significant stiffening effects in the system where the residual stresses from the erecting process are included.

Figure F.51 shows the load deflection curves of the system on three different scales. The applied load q_w is a wind pressure surface load and therefore remains constant for all scalar investigations. The general behaviour is similar to that shown of the elastica curve in Figure F.50, showing snap-through buckling at decreasing load factors with increasing scale. With increasing scale, the system also shows distinct nonlinear behaviour. At scale $s=4$ snap-through already occurs under dead load which leads to a completely nonlinear behaviour with increasing load. In contrast to the elastica curve in Figure F.51 where the residual compression stress is destabilising to the system, the coupled arches in the pavilion store residual tension stress in their straight sections. The resultant increase in geometrical stiffness can be seen in the dashed line graphs of scale $s=1$ and $s=2$ where the system was calculated without its residual stress from the form-finding of the erection process (ref. geo.). Here, snap-through buckling occurs at an earlier point if the geometry only is taken into consideration ($\Delta\lambda = 0.5$ for $s=1$ and $\Delta\lambda = 1$ for $s=8$). However, the advantageous influence of residual tension stress to the system is reduced over time due to enhanced relaxation of timber.

Fig. F.51 Load deflection curve of the ICD/ITKE 2010 research pavilion at 3 different scales for a given wind pressure load case.

Fig. F.52 Load deflection curves of the Marrakech Umbrella at 3 different scales.

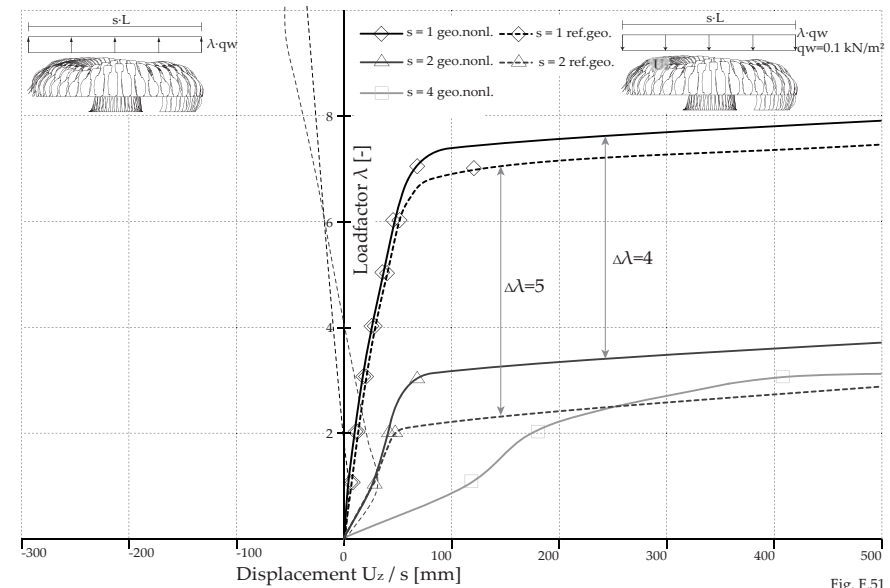


Fig. F.51

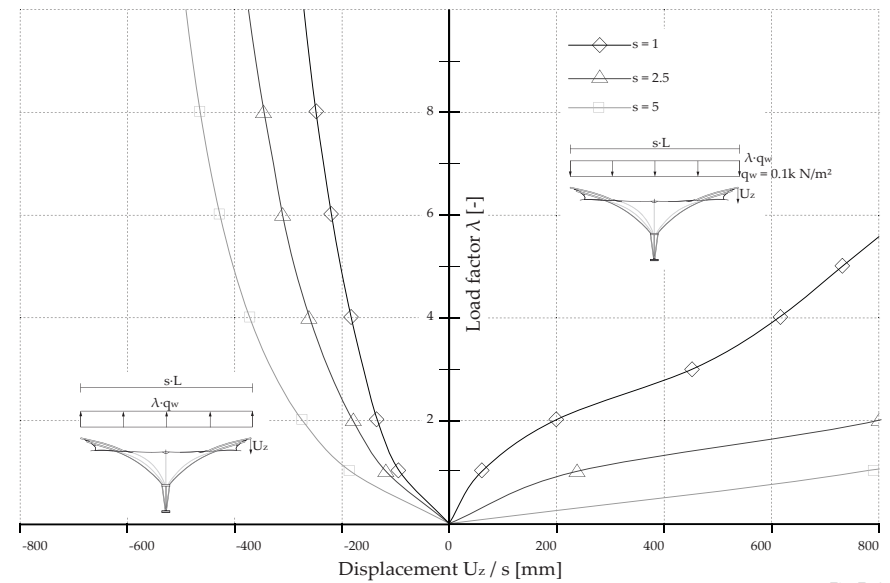


Fig. F.52

Marrakech Umbrella

For the scaling of this system, special attention must be paid to the change of membrane pre-stress. Since the pre-stress of the membrane has a direct influence on the curvature of the bending-active beam elements, it is altered in such a way that the geometry resulting from combined form-finding of bending-active beams and pre-stressed membrane is similar at all investigated scales. This results in under-proportional scaling of membrane pre-stress.

In this system, the bending-active beams are short-cutting tension forces between the edge cables and the low point. Independent of the load direction, the bending-active beam elements are therefore always under compression. These compression forces increase proportionally with scale and generally destabilise the system. In this combination of bending, shear and axial loading in the linear beam elements cannot compensate the quadratic growth in membrane surface as seen in Figure F.52. Here, the arm-end deformations U_z are shown for both wind suction (left) and wind pressure (right), showing highly nonlinear load deflection curves and significant differences in scale.

Scaling of a membrane structure with bending-active beam elements therefore necessitates a change in topology i.e. increasing the number of beam elements when scaling up in overall size. However, beyond spans of approx. 30 m, other effects may become decisive, as the membrane loses its stabilising effect on the beam elements due to flexibility increasing with size. Finally, even the availability of the necessary large size GFRP cross-sections may become limiting factors to the scale of membrane structures with integrated bending-active support systems. Similar conclusions were drawn by Adriaenssens (2008).

Textile Hybrid - M1

Scaling of the M1 structure leads to similar results as the above made findings for the Marrakech umbrella. In Figure F.53 it becomes clear that the system is already at its maximum scale. Larger scale systems could only be realised by changing the topology through adding more elements. With reference to the large scale grid shell structures introduced in chapter C, the

Fig. F.53 Load deflection curves of the M1 at 2 different scales.

Fig. F.54 Load deflection curve of the Flectofin® Lamella at 3 different scales, for a given wind suction and pressure load case.

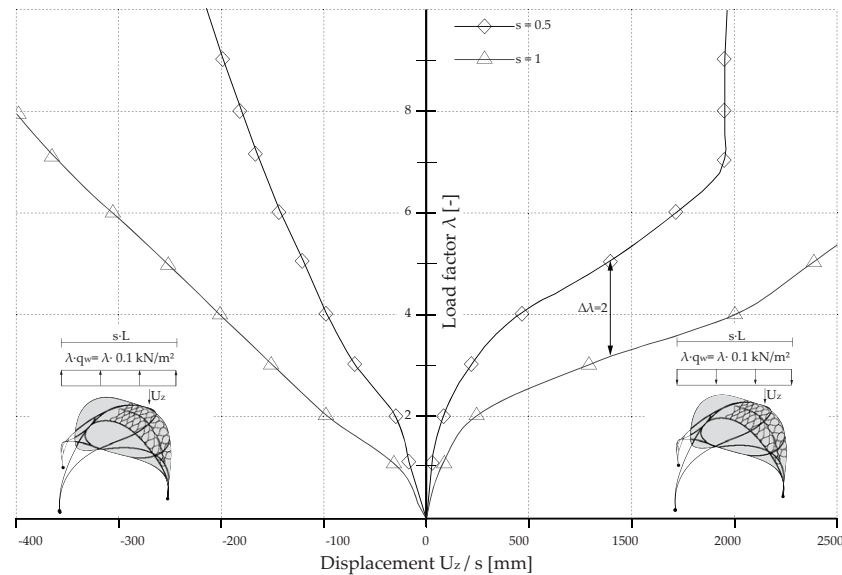


Fig. F.53

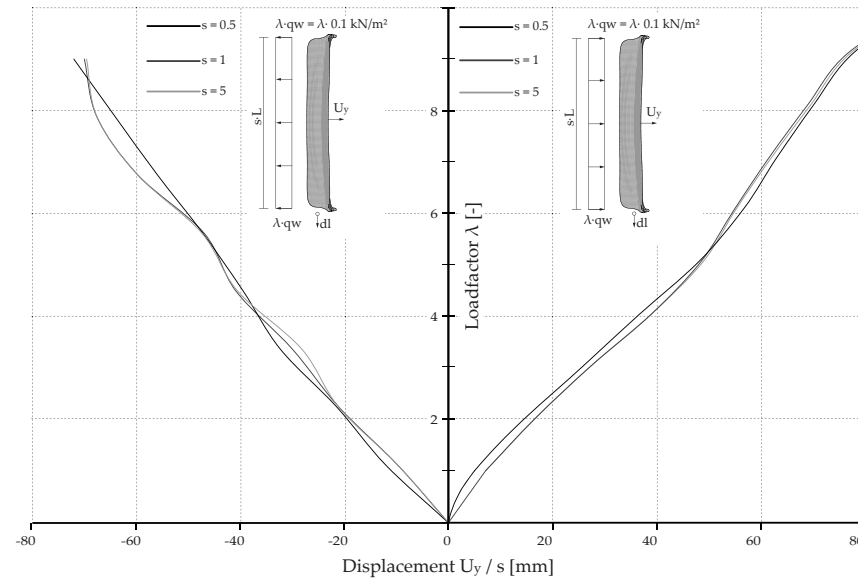


Fig. F.54

prospect of a larger M1 structure with more crossing elements seems perfectly plausible. In this case, the span between elements within the structure seems more relevant for scaling than its total dimensions.

Flectofin®, an elastic kinetic shell system

A central question of this biomimetic system was to determine whether biological inspired mechanics like the Flectofin® can be scaled up significantly to fit an architectural dimension. In Figure F.54 the load deflection curves of a Flectofin® lamella are plotted in three different scales for both wind suction and wind pressure. Besides minor nonlinearity the system shows almost perfect similitude. This behaviour may be explained by a combination of reasons:

In its deformed state, the Flectofin® lamellas predominantly hold residual tensile stress, leading to considerable stress-stiffening effects. Destabilising effects due to residual compression forces are therefore eluded. Positioned vertically on a façade, the dead load direction acts in its upright position which offers maximal elastic stiffness; dimension effects considering dead load may therefore be of minor influence to scaling. Additionally, the bending-active surface element makes up the entire load bearing surface; the quadratic growth in surface is therefore compensated by the quadratic growth of the load bearing shell element itself.

This system suggests that, for the above made assumptions of dead load and stability, only the limiting factors for scalability of bending-active structures may be generalised.

This is additionally supported by the recently built large scale adaptive façade for the theme pavilion of EXPO Yeosu, Korea 2012 designed to withstand the very high wind loads at the Korean coast [Knippers et al. 2012] (see Chapter C2.3 Figure C.28). Some early feasibility studies using the Flectofin® already suggest that scalability to a size range of 14 m high lamellas is possible. Here, the geometrical scaling factor is 7, the thickness of the shell element is only scaled by a factor 3, while the material parameters remains constant with standard GFRP values. Thus, maximum stress levels at the minimum bending radii rise

only by a factor of 1.3. These findings may differ between various systems, yet they clearly demonstrate the scalability of the investigated elastic kinetics.



G Conclusions and Future Trends

G Conclusions and Future Trends

General

The objective of this thesis was to provide general insight into form-finding and structural analysis of bending-active structures. New forms of structures were developed by an inverse, case study based approach: Engineering and building the structures without bias - generating feedback from materialised structural behaviour and bringing it back to a theoretical framework.

The work aimed to explore the potentials of understanding active bending as an approach to generating new structural forms. By initiating the work with actually built structures before in-depth analysis of a theoretical question, new territory was unveiled. The five case study structures built during this work were realised in the timespan of three and a half years. In this period of time, information was continuously fed back into this research and created the basis for the developed working methods. Gained experience thereby informed the scientific developments as well as the cross-linking of the work between the case study structures themselves.

Review

The concept of bending-active structures as an approach rather than a distinct structural type was discussed in Chapter B and C, based on engineering and historical background. The case study structures, introduced in Chapter D, opened a wide field of applications of active bending in lightweight building structures. Particular findings were highlighted and the potential of Finite Element Modelling as part of the general design process was reflected upon. This leading to the question whether the conclusions drawn from case studies are viable for bending-active structures in general. Chapter E on form-finding introduced the basic working methods and modelling environments developed for the present work. Chapter F on structural behaviour presented the scientific core of this work: By scanning a wide field of abstract models this research clarifies the influence of residual bending stress on the general structural performance of bending-active structures. These findings were verified by further in-depth anal-

ysis of the complex systems offered by the case study structures, to then draw conclusions where generalisation is validated.

Alongside the technical study of form-finding and structural behaviour, the engineer's role in the design process was challenged. Similarly to the work with form-active membrane structures, the requirement of a mechanically informed form-finding process makes engineering knowledge indispensable in the design process. By opening the engineers definition of 'form-finding' to a more general definition, the partitioning between architect and engineer was avoided. The present work thereby contributes both in-depth mechanical understanding as well as generalised design rules to the development of bending-active structures.

Form-Finding

A key to the case study structures was the setup of an uninterrupted mechanical description of bending-active structures in a general purpose FEM environment. The three main process steps of form-finding, structural analysis and unrolling/patterning could thereby be represented by a single modelling environment. This ensured that structurally substantial residual stresses could be traced throughout all stages of design. The inclusion of FEM as an integral part of the design process was made possible through several custom programmed routines inside the commercial FEM Software Sofistik®.

Specifically, the development of an elastic cable approach, which associates points in the planar configuration of a structure and through contraction joins them into an elastically deformed configuration, opened the field for new typology-free expressions of structure. This was shown through the research pavilion ICD/ITKE 2010 and the development between the Marrakech Umbrella and the Textile Hybrid M1: While the Marrakech umbrella still relies on the exhausted formal vocabulary of classical, mechanically pre-stressed membranes, the M1 managed to bridge the gaps between the clearly separated types.

The question of generating sufficient mechanically informed input data for the FEM environment was answered best by the work with physical models, supplemented by behaviour

based computational modelling environments. Physical models proved to offer expedient means for mechanically informed design sketches, because of their capacity to guide the intuition of a designer through the given instantaneous and haptic physical feedback.

Structural Behaviour

Investigations on the structural behaviour particularly dealt with the structural performance of a system designed and form-found to rely on the physical behaviour in its elastically deformed configuration. In detail, the influence of residual stress on structural behaviour was extensively analysed. The proposition, that the elements of a structure can be flexible enough to be significantly deformed into curved geometries and at the same time, in their association, create a structurally sound system was introduced as a paradox which this work aimed to solve. It was found that the niche, within which the balance of elasticity works, can only be found if all stiffness reserves in the system are carefully studied and deliberately made available. Therefore, the following generalised conclusions are an important contribution for the designing engineer and architect of bending-active structures:

Stress stiffening

The stiffness study of basic bending-active systems unveiled the existence of stress-stiffening effects, not only in elements under pure tensile residual stress, but also in elements where bending is combined with torsion and in-plane rotations. Pure bending is found to have no influence on the stiffness of a structure, whereas residual compression stresses have a critical destabilising effect. It was shown that effects connected to geometric stiffness are only of relevance to structures with relatively small elastic stiffness. This characteristic is relevant for all bending-active structures, as elastic stiffness is limited by material strength and degree of bending curvature. Intentionally activating stress-stiffening effects is therefore a key to the successful development of structurally stable bending-active structures. This was also confirmed in the case studies, through detailed analysis of stiffness development.

Scaling

Through dimensional analysis, general FEM analysis and detailed investigations of the case studies it was shown that the scaling of bending-active structures is dependent on the significance of dead load and the influence of residual stress on stability. As an important influence on the stability, it was shown that residual compression stresses are destabilising (example of elastica curve and Marrakech Umbrella) and tension stresses are stabilising due to nonlinear stress-stiffening effects (example of ICD/ITKE pavilion and Flectofin®). The consideration of axial forces in the geometrical stiffness is therefore of particular importance and may be used advantageously for the scaling of bending-active structures.

Common load bearing behaviour

Since all bending-active structures are composed of slender profiles and comparatively elastic materials, it can be concluded that the governing failure mode is that of snap-through buckling as seen in the results of all investigated systems in chapter F.2. It can therefore be generalised that stability plays a decisive role in the structural integrity of all bending-active structures. In contrast to other types of building structures these effects cannot simply be compensated by adaptation of elastic stiffness, since element thickness is limited by material strength and bending curvature.

Future Reference

The on-going development of new materials and simulation tools suggest that the presented case study projects, which exhibit active bending in various typological expressions, have by no means exhausted their field of application. There is a growing international number of scientists committing themselves to research and development of design, material and simulation questions related to bending-active structures. This opens the field for future applications of bending-active structures; however, it does not mean that they will replace established building techniques on a larger scale. Despite the apparent form freedom that the case study structures presented, all bending active structures rely on physical form-defining mechanisms which design intentions must subordinate to. On a structural level, the form-defining residual bending stress leads to a material dependent

relation of curvature and element size which restricts these structures in scale. The general field of application will therefore remain a niche in the greater picture of building and construction.

An important application was highlighted in the integration of bending-active elements in hybrid systems. As shown by the *Textile Hybrid M1*, the combination of bending-active with form-active structures, could particularly expand the otherwise limited form vocabulary in mechanically pre-stressed membrane structures. The integration of bending-active elements in pneumatically pre-stressed membranes is yet to be explored and promises to be another extensive field of application.

The greatest potential for future applications of bending-active structures may be seen in the further exploration of elastic kinetics on an architectural scale. There is no other approach that so imminently offers the prospect of adaptation without supplementary mechanisms. Forward-looking applications, such as the 2012 Expo Korea façade, prove that elastic kinetic structures can pass the reality test even in locations with extreme wind occurrences. The work on elastic shape adaptation leads to further possibilities of including auxiliary functions in the structural elements. Current research on bending-actors, integrated into the anisotropic fibre layup of bending-active elements, suggests new prospects for autonomous shape adaptation and variable stiffness on the basis of material intelligence. These particular aspects are subject of current research and will be explored further over the years to come.

- APPENDIX

Appendix A

Stiffness matrix of a TL Plane Beam according to [NFEM: 10-21]

$$\mathbf{K}_G = \frac{N}{2} \begin{bmatrix} 0 & 0 & s_m & 0 & 0 & s_m \\ 0 & 0 & -c_m & 0 & 0 & -c_m \\ s_m & -c_m & -\frac{1}{2}L_0(1+e_m) & -s_m & c_m & -\frac{1}{2}L_0(1+e_m) \\ 0 & 0 & -s_m & 0 & 0 & -s_m \\ 0 & 0 & c_m & 0 & 0 & c_m \\ s_m & -c_m & -\frac{1}{2}L_0(1+e_m) & -s_m & c_m & -\frac{1}{2}L_0(1+e_m) \end{bmatrix}$$

$$\frac{V}{2} \begin{bmatrix} 0 & 0 & c_m & 0 & 0 & c_m \\ 0 & 0 & s_m & 0 & 0 & s_m \\ c_m & s_m & -\frac{1}{2}L_0\gamma_k & -c_m & -s_m & -\frac{1}{2}L_0\gamma_m \\ 0 & 0 & -c_m & 0 & 0 & -c_m \\ 0 & 0 & -s_m & 0 & 0 & -s_m \\ c_m & s_m & -\frac{1}{2}L_0\gamma_m & -c_m & -s_m & -\frac{1}{2}L_0\gamma_m \end{bmatrix} \quad (9_B)$$

Appendix B

Stiffness simple shell element according to [Werkle 2008: 504]

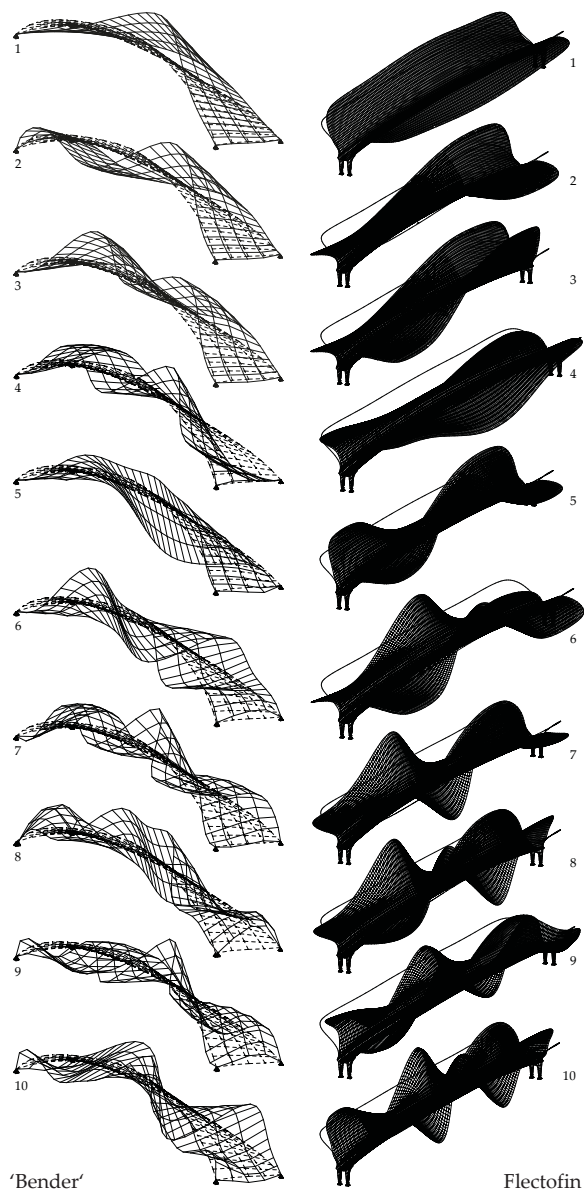
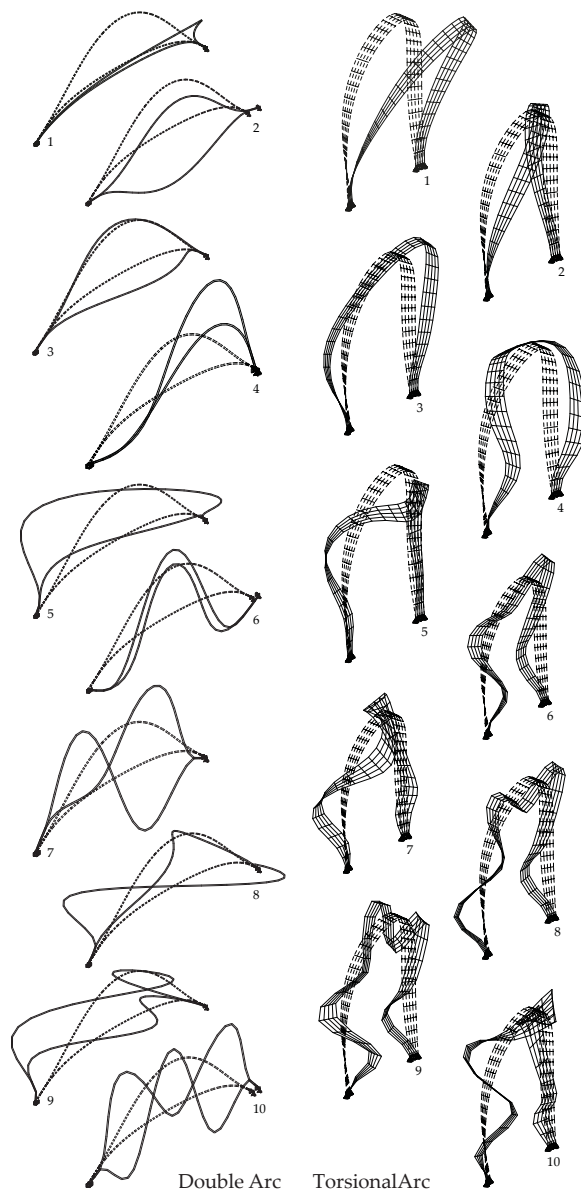
$$k_{gx} = \sigma_x \cdot \frac{h \cdot b}{1260 \cdot a} \begin{bmatrix} 552 & 66 \cdot b & -42 \cdot a & . & . & . & . & . & . \\ 66 \cdot b & 12 \cdot b^2 & . & . & . & . & . & . & . \\ -42 \cdot a & . & . & . & . & . & . & . & . \\ . & . & . & . & . & . & . & . & . \\ . & . & . & . & . & . & . & . & . \\ . & . & . & . & . & . & . & . & . \\ . & . & . & . & . & . & . & . & . \\ . & . & . & . & . & . & . & . & . \\ . & . & . & . & . & . & . & . & . \end{bmatrix} \quad (10_B)$$

$$k_{gy} = \sigma_y \cdot \frac{h \cdot b}{1260 \cdot a} \begin{bmatrix} 552 & 42 \cdot b & -66 \cdot a & . & . & . & . & . & . \\ 42 \cdot b & 56 \cdot b^2 & . & . & . & . & . & . & . \\ -66 \cdot a & . & . & . & . & . & . & . & . \\ . & . & . & . & . & . & . & . & . \\ . & . & . & . & . & . & . & . & . \\ . & . & . & . & . & . & . & . & . \\ . & . & . & . & . & . & . & . & . \\ . & . & . & . & . & . & . & . & . \\ . & . & . & . & . & . & . & . & . \end{bmatrix}$$

$$k_{gxy} = \tau_{xy} \cdot \frac{h \cdot b}{1260 \cdot a} \begin{bmatrix} 180 & 0 & 0 & . & . & . & . & . & . \\ 0 & 0 & . & . & . & . & . & . & . \\ 0 & . & . & . & . & . & . & . & . \\ . & . & . & . & . & . & . & . & . \\ . & . & . & . & . & . & . & . & . \\ . & . & . & . & . & . & . & . & . \\ . & . & . & . & . & . & . & . & . \\ . & . & . & . & . & . & . & . & . \\ . & . & . & . & . & . & . & . & . \end{bmatrix}$$

Appendix E

First 10 Eigenmodes of bending-active systems studied in Chapter F.1



-
- **Bibliography and Index**

Bibliography

- ADRIAENSENS, S. (2008) *Feasibility Study of Medium Span Spliced Spline Stressed Membranes*. International Journal of Space Structures, Vol. 23. (No. 4), pp. 243-251.
- AHLQUIST, S. and MENGES, A. (2013) *Frameworks for Computational Design of Textile Micro-Architectures and Material Behavior in Forming Complex Force-Active Structures*, Adaptive Architecture, Proceeding for ACADIA 2013 Conference, Waterloo.
- ALLEN, E. and ZALEWSKI (2009) *Form and Forces. Designing Efficient, Expressive Structures*. Hoboken, New Jersey: Wiley & Sons
- ALPERMANN, H. and GENGNAGEL, C. (2009) *Membrane restrained arch*. In: Structural Membranes 2009 International Conference on Textile Composites and Inflatable Structures. Stuttgart
- ALPERMANN, H. and GENGNAGEL, C. (2013) *Membrane restrained girder*. In: TensiNet symposium [RE] THINKING lightweight structures, Istanbul, 2013. Accepted.
- ALPERMANN, H., GENGNAGEL, C. and LAFUENTE HERNÁNDEZ, E. (2012) *Case-studies of arched structures using actively-bent elements*. In: Proceedings of the International IASS Symposium, Seoul, Korea.
- AMIRKHANI, A. et. al. (2010) *Iranian felt tents: an architectural heritage of the Turkmen*. International Journal of Academic Research, Vol. 2. (Part I/No. 6./November).
- ASHBY, M. F. (2005) *Materials selection in mechanical design*. MRS Bulletin.
- (2007) *Bamboo Bar*. The Architectural Review Magazine, (Issue 1330/December).
- BARNES, M. R., KIEFER, M. and RENNER, W. (1996) *Case Studies in the design of wide-span Expo structures*. International Symposium on Conceptual Design of Structures, 1, Stuttgart. pp. 814-824.
- BARR, D.I.H. (1983) *A survey of procedures for dimensional analysis*. Int'l J. of Mechanical Eng. Education, Vol. 11, pp 147 - 159.
- BAVEREL, O., BEAUGELIN, M. and CARON, J.-F. (2010) *Concept of a beam prestressed by bending: Application to a footbridge in composite materials*. J. IASS, Vol. 51.
- BISCHOFF (2011) Lecture on nonlinear Finite Element Analysis, University of Stuttgart
- BOLLINGER, K., GROHMANN, M. and TESSMANN, O. (2010) *Structured Becoming: Evolutionary Processes in Design Engineering*. Archit Design, 80: 34–39. doi: 10.1002/ad.1103

BRINKMANN, G. and BLUM, R. (1990) *Leicht und weit: Zur Konstruktion weit gespannter Flächentragwerke*. Weinheim Verlag, pp. 91.

BUCKINGHAM, E. (1914) *On physically similar systems; illustrations of the use of dimensional equations*. Phys. Review, 4.

BURFORD, N. and GENGNAGEL, C. (2004) *Mobile Shelters Systems – 2 Case Studies in Innovation*. In: Conference Proceedings IASS Symposium 2004, Shell and Spatial Structures from Models to Realization, Montpellier, France.

BÜV-EMPFEHLUNGEN. (2010) *Tragende Kunststoffbauteile im Bauwesen [TKB]*. Entwurf, Bemessung und Konstruktion, August 2010. Available from: http://www.buev-ev.de/images/pdf-dokumente/Kunststoff_Empf.pdf [Accessed date].

CRAWFORD, R.F. (1971) *Strength and Efficiency of Deployable Booms for Space Applications*. AIAA Paper No. 71-396, AAS/AIAA Variable Geometry and Expandable Structures Conference, Anaheim, California.

DIBT. *Allgemeine bauaufsichtliche Zulassung Z -10.9-299, Pultrudierte Profile aus glasfaserverstärkten Kunststoffen*

DOUTHE, C., BAVEREL, O. and CARON, J.-F. (2006) *Form-finding of a grid shell in composites materials*. In: Proceedings of the International Association for Shell and Spatial Structures (IASS) Symposium.

EN 13706. *Reinforced plastics composites. Specifications for pultruded profiles*; Part 1-3, CEN European Committee for Standardization, Brussels, February 2003

ENDRESS, P.K. (1994) *Diversity and evolutionary biology of tropical flowers*. Cambridge: Cambridge University Press, pp. 352-58.

ENGEL, H. (1999) *Tragsysteme – Structure Systems*. Ostfildern-Ruit.

EULER, L. (1744) *Methodus Inveniendi Lineas Curvas*.

FERTIS, D. G. (2006) *Nonlinear Structural Engineering. With Unique Theories and Methods to Solve Effectively Complex Nonlinear Problems*. Berlin, Heidelberg: Springer.

FLEISCHMANN, M., KNIPPERS, J., LIENHARD, J., MENGE, A., and SCHLEICHER, S. (2011) *Material Behaviour: Embedding Physical Properties in Computational Design Processes*. In: MENGE, A. *Material computation: higher integration in morphogenetic design*, Architectural Design (AD). London: John Wiley & Sons Ltd.

Bibliography

- FRANCKE, W. and FRIEMANN, H. (2005) *Schub und Torsion in geraden Stäben*. Vieweg+Teubner Verlag
- GAS, S., DRUESDAU, H. and HENNIKE, J. (1985) IL 31 *Bambus – Bamboo*. Stuttgart: Karl Krämer Verlag.
- GENGNAGEL, C. (2005) *Mobile Membrankonstruktionen*. Dissertation, Schriftenreihe des Lehrstuhls für Tragwerksplanung Band 12, Technische Universität München.
- GERTSMA, L. W., DUNN, J. H. and KEMPKE, E. E. (1965) *Evaluation of one type of foldable tube*. NASA Lewis research Center, Cleveland, Ohio, NASA TM-X-1187
- GORMAN, J.G. (2005) *Buckminster Fuller Designing for Mobility*. Milano: Skira Editore, pp.154-157.
- GRUBER, P. (2011) *Biomimetics in architecture [architekturbionik] architecture of life and buildings*. Berlin: Springer
- HAPPOLD, E. and LIDDELL, W.I. (1975) *Timber lattice roof for the Mannheim Bundesgartenschau*. The Structural Engineer, Vol. 53. (No.3).
- HARRIS, H.G. and SABNIS, G.M. (1999) *Structural modelling and experimental techniques*. New York: CRC Press.
- HARRIS, R. (2011) *Design of timber gridded shell structures*. In: Proceedings of the Institution of Civil Engineers-Structures and Buildings, 2011. 164 (2), pp. 105-116.
- HARRIS, R., HASKINS, S. and ROYON, J., (2008) *The Savill Garden gridshell: design and construction*. The Structural Engineer, 86 (17), pp. 27-34.
- HARRIS, R., JOHNSON, S. , KELLY, O. and ROHMER, J. (2003) *Design and construction of the Downland Gridshell*. Building Research & Information, 31(6), 2003, pp. 427-54.
- HARTMANN, F. and KATZ, C. (2004) *Structural Analysis with Finite Elements*. Berlin: Springer.
- HENNICKE, J. (1975) IL 10 *Gitterschalen – Grid Shells*. Stuttgart: Karl Krämer Verlag.
- HOEWELER and YOON (2013) Available from: www.mystudio.us/projects/12 [Accessed 02.2013].
- HOWELL, L.L. (2001) *Compliant Mechanisms*. New York John Wiley & Sons.
- HUMAR J.L. (1990): *Dynamics of Structures*. Englewood Cliffs, N.J : Prentice Hall
- HYPERBODY RESEARCH GRP. (2005) *Muscle reconfigured - Programmable Architecture*. Insight of Smart

- Environments, 2005/ 11, Archidata, pp. 105 – 124.
- JODIDIO, P. and BAN, S. (2010) *Shigeru Ban: Complete Works, 1985 – 2010*. Köln: Taschen Verlag.
- KNIPPERS, J., CREMERS, J., GABLER, M., and LIENHARD, J. (2011) *Construction Manual for Polymers + Membranes*. Institut für internationale Architektur-Dokumentation, München: Edition Detail
- KILIAN, A., OCHENDORF, J. (2005) *Particle Spring Systems for Structural Form Finding*. Journal of the International Association for Shell and Spatial Structures Vol. 46, n. 147
- KNIPPERS, J., SCHEIBLE, F., OPPE, M. and JUNGJOHANN, H. (2012) *Bio-inspired Kinetic GFRP-façade for the Thematic Pavilion of the EXPO 2012 in Yeosu*. In: Proceedings of the International IASS Symposium, Seoul, Korea.
- KNIPPERS, J. and SPECK, T. (2012) *Design and construction principles in nature and architecture*. Bioinspir. Biomim. 7
- KNIPPERS, J. (2013): *From Model Thinking to Process Design*. AD Architectural Design 02/2013, pp 74-81
- LAFUENTE, E., GENGNAGEL, C., SECHELMANN, S. and RÖRIG, T. (2011) *On the Materiality and Structural Behavior of highly-elastic Gridshell Structures*. Computational Design Modeling. 2012 Edition. In: Proceedings of the Design Modeling Symposium. Berlin: Springer.
- LEVIEN, R. (2008) *The Elastica: A Mathematical History*. University of California, Berkeley, CA
- LEVIEN, R. L. (2009) *From spiral to spline*. University of California, Berkley, CA
- LEWIS, W. J. (2003) *Tension structures*. Form and behaviour. London: Thomas Telford.
- LI, J. and KNIPPERS, J. (2011) *Form-finding of grid shells with continuous elastic rods*. In: NETHERCOT, D. et al. Proceedings of the International Symposium of the IABSE-IASS Symposium, Taller Longer Lighter, London, UK.
- LIENHARD, J., KNIPPERS, J., SCHLEICHER, S., POPPINGA, S. and SPECK, T. (2010) *Form-finding of Nature Inspired Kinematics for Pliable Structures*. In: ZHANG, Q. et al. Proceedings of the International Symposium of the International Association of Shell and Spatial Structures (IASS), Spatial Structures Temporary and Permanent, Shanghai, China, pp. 2545-2554.
- LIENHARD, J., SCHLEICHER, S. and KNIPPERS, J. (2011) *Bending-active Structures – Research Pavilion ICD/ITKE*. In: NETHERCOT, D. et al. Proceedings of the International Symposium of the IABSE-IASS Symposium, Taller Longer Lighter, London, UK.

LIENHARD, J., SCHLEICHER, S., POPPINGA, S., MASSELTER, T., MILWICH, M., SPECK, T. and KNIPPERS, J. (2011) *Flectofin: a nature based hinge-less flapping mechanism*. Bioinspiration & Biomimetics 6 , special issue on Biomimetics of Movement, 045001.

LIENHARD, J. and KNIPPERS, J. (2012) Permanent and convertible membrane structures with intricate bending-active support systems. In: Proceedings of the International IASS Symposium, Seoul, Korea

LIENHARD, J., AHLQUIST, S., MENGES, A. and KNIPPERS, J. (2013) Extending the Functional and Formal vocabulary of tensile membrane structures through the interaction with bending-active elements. In: TensiNet symposium [RE]THINKING lightweight structures, Istanbul..

LIENHARD, J., JUNGJOHANN, H., RIEDERER, J., OPPE, M. and KNIPPERS, J. (2013) Multifunctional adaptive Façade at IBA 2013; design studies for an integral energy harvesting façade shading system. In: Proceedings of Structural Membranes, München.

LIENHARD, J., KNIPPERS, J. (2013) Considerations on the Scaling of Bending-Active Structures. International Journal of Space Structures Vol. 28 No. 3&4 2013, p 137-147

LIENHARD, J., ALPERMANN H., GENGNAGEL, C., KIPPERS, J. (2013) Active Bending, a Review on structures where bending is used as a self-formation process. International Journal of Space Structures Vol. 28 No. 3&4 2013, p 187-196

LIEVEN, N. AJ. and GREENING, P. (2001) Effect of experimental pre-stress and residual stress on modal behaviour. Philosophical Transactions of the Royal Society of London. Series A: Mathematical, Physical and Engineering Sciences 359.1778 (2001): 97-111.

LUDWIG, F. et. al. (2009) Plant stems as building material for living plant constructions. In: THIBAUT, B. Sixth Plant Biomechanics Conference. Cayenne, French Guyana, France. UMR EcoFoG.

MACNEAL, R. and HARDER, L. (1985) A proposed set of problems to test finite element accuracy. Finite Elements in Analysis and Design, (1): pp. 3-20

MANJUNATHA, C.M., TAYLOR, A.C. and KINLOCH, A.J. (2009) The effect of rubber micro-particles and silica nano-particles on the tensile fatigue behavior of a glass fibre epoxy composite. J Mater Sci, 44 , pp. 342-345.

MATINI, M.R. (2007) *Biegsame Konstruktionen in der Architektur auf der Basis bionischer Prinzipien*. Institut für Tragkonstruktionen und Konstruktives Entwerfen (ITKE), University of Stuttgart.

MATTHECK, C. and BURKHARDT, S. (1990) A new method of structural shape optimization based on biological growth. International Journal of Fatigue, 12, pp. 185-190.

MENGES, A. (2004) *Emergence: Morphogenetic Design Strategies*. In: WILEY & SONS, AD - Architectural Design, (May), pp. 62 – 63.

MEYER, H.-J. (1992) Zur Bemessung von GFK-Bauteilen unter Zuhilfenahme der Linear-Elastischen Bruchmechanik und probabilistischer Versagenskriterien. Thesis (PhD), TU Hamburg-Harburg.

NATTERER, J. and MACINTYRE, J. (1993) *Polydôme: A Timber Shell, Switzerland*. Structural Engineering International, (2/93), pp. 82-83.

Nonlinear Finite Element Methods (ASEN 6107) - Spring 2012

OFF, R. (2010) *New trends on membrane and shell structures - examples of batsail and cushion-belt technologies*. In: CRUZ. Structures and Architecture. London: Taylor & Francis Group.

OLIVER, P. (Hg.) (2007) *Encyclopedia of Vernacular Architecture of the World, Vol. 1 Theories and Principles*. Cambridge: University Press.

OLIVER, P. (Hg.) (2007) *Encyclopedia of Vernacular Architecture of the World, Vol. 3 Cultures and Habitats*. Cambridge: University Press.

PHILIPPIDIS, T.P. and VASSILOPOULOS, A.P. (1999) *Fatigue Strength Prediction under Multiaxial Stress*. Journal of Composite Materials, Vol. 33 (no. 17), pp.1578–1599.

PRZEMIENIECKI, J. S. (1968) *Theory of Matrix Structural Analysis*. New York: McGraw-Hill.

PUCK, A. (1996) *Festigkeitsanalyse von Faser-Matrix-Laminaten*, VDEI-RiLi 2019

RABINDRANATH A., ROSET J. and KILAR V. (2011) *Interdisciplinary approach to numerical methods for structural dynamics*.World Applied Sciences Journal 14.8: 1046-1053.

RAMM, E. (1981) *Strategies for Tracing the Nonlinear Response Near Limit Points*. 2nd US-Europe Workshop 'Nonlinear Finite Element Analysis in Structural Mechanics' (eds. W. Wunderlich, E. Stein, K.-J. Bathe), Bochum, Germany, 1980, Springer, pp. 63-89

RAYLEIGH. (1877) *Theory of sound*. New York: Dover.

REITH, M., BAUMANN, G., CLASSEN-BOCKHOFF, R. & SPECK, T. (2007) *New insights in the functional morphology of the lever mechanism of Salvia pratensis*. Annals of Botany 100: 393-400

RITTEL, H.W.J. (1982) *Der Planungsprozess als iterativer Vorgang von Varietätserzeugung und Varietätseinschränkung*. In: JOEDICKE, J.: *Arbeitsberichte zur Planungsmethodik 4*. Stuttgart 1982

ROWAN, M. K. (1974) *Bird pollination of Strelitzia*. Ostrich 45 40

Bibliography

SALOKANGAS, L. (2003) *Wooden Observation Tower, Helsinki, Finland.* Structural Engineering International, Vol. 13. (no. 3/August), pp. 160-162.

SANTINI and TADDEI. (2006) Available from: www.architettura.it/architetture/20070319/index.htm [Accessed 02/2013]

SCHLEICHER, S., LIENHARD, J., POPPINGA, S., MASSELTER, T., SPECK, T. and KNIPPERS, J. (2011) *Adaptive facade shading systems inspired by natural elastic kinematics.* Proceedings of the International Conference on Adaptive Architecture, 2011 London, UK, (CD)

SCHLEICHER, S., LIENHARD, J., POPPINGA, S., SPECK, T., KNIPPERS, J. (2013) *A methodology for transferring principles of plant movements to elastic systems in architecture.* Computer-Aided Design, Elsevier Editorial Services, Exeter, UK, (submitted)

SIMITSES, G.J. and HODGES, D.H. (2006) *Fundamentals of structural stability.* Amsterdam, Boston: Elsevier/Butterworth-Heinemann, pp. 251.

SITTE, P., ZIEGLER, H., EHRENDORFER, F., and BRESINSKY, A. (1991) Strasburger. *Lehrbuch der Botanik.* Gustav Fischer Verlag (33. Auflage), p. 456-469

SOFISTIK (2013a) Benchmark Example No. 7: Large Deflection of Cantilever Beams I

SOFISTIK (2013b) Benchmark Example No. 8 Large Deflection of Cantilever Beams II

SPECK, T. and SPECK, O. (2008) *Process sequences in biomimetic research.* Design and Nature IV, ed. C.A. Brebbia, WIT Press: Southampton, 3-11.

TAN, L.T. and PELLEGRINO, S. (2004) *Ultra thin deployable reflector antennas.* In: Proc. 45th AIAA/ASME/ASCE/AHS/ASC Structures, Structural Dynamics and Materials Conference, Palm Springs, CA, 19-22 April 2004. AIAA 2004-1730.

TIMOSHENKO, S. and GOODIER, J. (1951) *Theory of elasticity.* 2nd Ed. McGraw-Hill Book Company.

WEBER, A. (2008) *Durability and bond durability of composite rebars.* Fourth International Conference on FRP Composites in Civil Engineering (CICE2008), Zurich, Switzerland

WEINAND, Y. (2009) *Innovative Timber Constructions.* J. IASS, Vol. 50.

WERKLE, H. (2008) *Finite Elemente in der Baustatik. Statik und Dynamik der Stab- und Flächentragwerke.* 3. Auflage. Friedr. Vieweg & Sohn Verlag, Wiesbaden

Directives and standards

BÜV-Empfehlungen (2010): Tragende Kunststoffbauteile im Bauwesen [TKB]. Entwurf, Bemessung und Konstruktion, August 2010: http://www.buev-ev.de/images/pdf-dokumente/Kunststoff_Empf.pdf

Dibt: Allgemeine bauaufsichtliche Zulassung Z -10.9-299, Pultrudierte Profile aus glasfaserverstärkten Kunststoffen

DIN 18820: Glass fibre reinforced laminates

DIN EN 13121: GRP tanks and vessels for use above ground

DIN EN 1993: Design of steel structures

DIN EN 1995: Design of timber buildings and civil engineering structures

DIN EN 1999: Design of all aluminium structures

DIN 1052:2004-08: Entwurf, Berechnung und Bemessung von Holzbauwerken

DIN 17221: Spring steel

Image Index

(Only images that are not original by author are listed)

B.13: EULER, L. (1744) *Methodus Inveniendi Lineas Curvas*.

B.26: MEYER, H.-J. (1992) *Zur Bemessung von GFK-Bauteilen unter Zuhilfenahme der Linear-Elastischen Bruchmechanik und probabilistischer Versagenskriterien*. Thesis (PhD), TU Hamburg-Harburg.

C.1: OLIVER, P. (Hg.) (2007) *Encyclopedia of Vernacular Architecture of the World*, Vol. 1 *Theories and Principles*. Cambridge: University Press.

C.2: *The Nijni-Novgorod exhibition: Water tower, room under construction, springing of 91 feet span*, The Engineer, № 19.3.1897, P.292-294, London, 1897

C.4: *Structures of Eduardo Torroja*, New York: F.W. Dodge Corporation, 1958

C.5: The MIT Museum. In: HESS, ALAN: Googie. fifties coffee shop architecture. San Francisco, 1986, p. 50

C.6: PAUL KRAMER, Berlin

C.8: OLIVER, P.: *Dwellings: The Vernacular House World Wide*, Phaidon Press (London), 2003, p 122.

C.9: FLICKR (2007) Traditional Dorze House [Online Image] Available from: <http://www.flickr.com/photos/henokw/353870298/sizes/z/in/photostream/> [Accessed 08/10/12]; PBASE (2007) Dorze Man Building Hut [Online Image] Available from: http://www.pbase.com/sergio_pes/image/60510139 [Accessed 08/10/12]

C.10: FLICKR HIVE MIND (2007) Yawalapiti Oca [Online Image] Available from: http://flickrhive-mind.net/flickr_hvmnd.cgi?method=GET&sorting=Interestingness&page=1&photo_type=250&search_domain=Tags&photo_number=50&tag_mode=all&sort=Interestingness&textinput=yawalapiti&origininput=yawalapiti&search_type=Tags [Accessed 16/10/12]

C.11: AMIRKHANI, A. et. al. (2010) *Iranian felt tents: an architectural heritage of the Turkmen*. International Journal of Academic Research, Vol. 2. (Part I/No. 6./November).

C.12: SAIGON PROPERTY CLUB (2008) Bamboo Bar [Online Image] Available from: <http://sgpclub.blogspot.de/2012/09/cong-ty-trong-nghia.html> [Accessed 08/10/12]

C.13: HÖWELER+YOON (2006) LOOP [Online Image] Available from: <http://www.mystudio.us/projects/12> [Accessed 08/10/12]

C.14: ARCHITETTURA (2005) Elastic Habitat [Online Image] Available from: <http://architettura.it/architetture/20070319/index.htm> [Accessed 08/10/12]

C.15: MODERNMECHANIX (2006) Plywood Dome [Online Image] Available from: <http://blog.modernmechanix.com/mags/PopularMechanics/1-1958/dome.jpg> [Accessed 08/10/12]; original from Plywood Dome Will Serve as Church in Korea. 1958. Popular Mechanics. January.

C.17: NATTERER, J.; MACLNTVRE, J.: Polydôme: A Timber Shell, Switzerland; Structural Engineering International 2/93, pp. 82-83

C.18: NERDINGER W. (2005): *Frei Otto. Das Gesamtwerk: Leicht bauen - natürlich gestalten*. Birkhäuser, Berlin

C.19: Photo: JIAN-MIN LI

C.20: BAVEREL, O., CARON, J.F., DOUTHE, C. (2010) Gridshell structures in glass fibre reinforced polymers. Construction and Building Materials, 24 (April), p. 1586.

C.21: BURFORD, N. and GENGNAGEL, C. (2004) *Mobile Shelters Systems – 2 Case Studies in Innovation*. In: Conference Proceedings IASS Symposium 2004, Shell and Spatial Structures from Models to Realization, Montpellier, France.

C.22: BURFORD, N. and GENGNAGEL, C. UNIVERSITY OF DUNDEE AND TECHNICAL UNIVERSITY OF MUNICH (2003) A Very Rapid Deployable Canopy System. p. 1

C.23: IMS-INSTITUTE (2006) Bat-Wing-Sail [Online Image] Available from: http://www.ims-institute.org/gallery.html?tx_chgallery_pi1%5Bdir%5D=3&cHash=91ac6d13030613534b8621e898cca245#c100 [Accessed 28/09/12]

C.24: Photo: BORRIS MIKLAUTSCH

C.25: Photo: SEAN AHLQHUIST

C.26: BAVEREL, O., ET AL. (2010) Concept of a beam prestressed by bending: application to a footbridge in composite materials. Journal of the International Association for Shell and Spatial Structures (February), p. 105.

C.27: TUDELFT (2004) Muscle ReConfigured [Online Image] Available from: <http://www.bk.tudelft.nl/en/about-faculty/departments/hyperbody/research/applied-research-projects/muscle-reconfigured/> [Accessed 08/10/12]

C.30: MENGES, A. (2003) Hyagrid [Online Image] Available from: <http://www.achimmenges.net/?p=4407> [Accessed 28/09/12]

C.31: PELLEGRINO, S, TZE TAN, L. AMERICAN INSTITUTE OF AERONAUTICS AND ASTRONAUTICS PAPER 2004-1730
(2004) Ultra Thin Deployable Reflector Antennas. London, p.2.

D.13: Photo: FRITZ ULRICH BUCHMANN

D.45: Photo: MATTHIAS GÜHNE (Textilbau GmbH)

D.47: Photo: RUSLOU CORTS

D.48: Photo: BORRIS MIKLAUTSCH

E.10: Photo: Student Group with MARCO BAUR, STEFANA PARASCHO, SEBASTIAN KRON, ELENA VLASCEANU

E.12: Photo: MANUEL VOLLRATH

E.13: Based on: Sommer, D. (2011) Zum Tragverhalten biegeaktiver Tragsysteme. Diploma thesis, ITKE University of Stuttgart, supervised by author

E32: Based on: Untrerer, K. (2012) Analysen zur Steifigkeit von Membrantragwerken mit exzentrisch angebundenen biegeaktiven Tragelementen. Diploma thesis, ITKE University of Stuttgart, supervised by author

E.18: Based on: HOWELL, L.L. (2001) *Compliant Mechanisms*. New York John Wiley & Sons.

E.41: SOFISTIK (2013a) Benchmark Example No. 7: Large Deflection of Cantilever Beams I

E.42: SOFISTIK (2013b) Benchmark Example No. 8 Large Deflection of Cantilever Beams II

F.22: Based on: Sommer, D. (2011) Zum Tragverhalten biegeaktiver Tragsysteme. Diploma thesis, ITKE University of Stuttgart, supervised by author

Lebenslauf

seit 2010	Lehrauftrag TU Wien, MEng-Programm
2010	Koautor im „Atlas Kunststoffe und Membranen“, Kapitel zu Tragwerk und Form sowie Materialien und Konstruktionsweisen mit Folien und textilen Membranen
2008	Gründung des Ingenieurbüros str.ucture (ehemals studioLD)
2007-2013	Mitarbeiter und Doktorand am Institut für Tragkonstruktionen und Konstruktives Entwerfen, bei Prof. Dr.-Ing. Jan Knippers.
2004 - 2008	Tragwerksplaner im Architekturbüro Rasch + Bradatsch: Formfindung, Konstruktion und Statik von Membrantragwerken,
2007	Diplom: ‘Der wandelbare Trichterschirm: Parametrisierung und Optimierung von Kinematiken für Großschirme’. Prof. Moro, Prof. Dr.Ing. Jan Knippers, Jürgen Bradatsch.
2002 - 2004	Wissenschaftliche Hilfskraft am Institut für Entwerfen und Konstruieren, Prof. Moro, Universität Stuttgart
2001 - 2006	Studium: Konstruktiver Ingenieurbau an der Universität Stuttgart
2000 - 2001	Zivildienst in Lausanne, Schweiz
1997 - 1999	Schulaufenthalt in Johannesburg, Südafrika
1987 – 2000	Waldorfschule Hamburg Nienstedten
1980	Geb. in Hamburg

Vita

Julian Lienhard was born in Hamburg 1980. He received his Diploma in Civil Engineering at the University of Stuttgart in 2007. In April 2014 he completed his doctorate at the Institute of Building Structures and Structural Design (ITKE). At the ITKE he played an active part in the academic environment between 2007 and 2013, engaging in research and teaching, where he was leading the German ministry funded research project ‘Pliable Surface Structures on the basis of biomimetic principles’ awarded the Techtextil Innovation Prize 2011, the Bionic Award 2012 and the Gips-Schüle-Forschungspreis 2013. He was also involved in the ‘ICD/ITKE Research Pavilion’ rewarded with the DETAIL Prize 2011. Along with a number of different design studios, he is teaching the ‘Principles of Membrane Structures’ course at the University of Stuttgart. Since 2011 he has been a visiting lecturer for the Masters of Engineering Program at the Technical University of Vienna. He is a co-author of the ‘Construction Manual on Polymers and Membranes’, having written the chapters on form-active structures as well as material properties and construction methods with foils and membranes.

In 2008, Julian founded the engineering and design practice studioLD now str.ucture GmbH, where he is working today. Previously, he worked as a Structural Engineer at SL-Rasch in Stuttgart, focusing on the structural design and form-finding of large membrane structures, such as the convertible umbrellas of the Madinah Piazza Shading Project.